The Process Fundamentals and Parameters of Electro-Spark Deposition

by

Siu Kei Tang

A thesis
presented to the University of Waterloo
in fulfillment of the
thesis requirement for the degree of
Master of Applied Science
in
Mechanical Engineering

Waterloo, Ontario, Canada, 2009

I hereby declare that I am the sole author of this thesis. This is a true copy of the thesis, including any required final revisions, as accepted by my examiners.

Siu Kei Tang

I understand that my thesis may be made electronically available to the public.

Siu Kei Tang

Abstract

Electrospark Deposition (ESD) is a micro-bonding process that is capable of depositing wear and corrosion resistance coating to repair, to improve and to extend the service life of the components and tools. During the coating process, short duration of electrical pulses ranging from a few microseconds to milliseconds are used to deposit the electrode material to the component's surface producing a protective layer. The low net heat input and the ability to form metallurgical bonding of coating to substrate are some of the noticeable advantages of ESD coating process. However, the influences of the controlling process parameters on the resulting coating are not well understood and documented. As a result, cracking and delaminating between the coating and substrate often occur.

The objectives of this study were to enhance the current understanding of the ESD process, of the material transfer mechanism, of the influence of major process parameters on the resulting coating and of the bond between the electrode and the substrate. To accomplish these tasks, the ESD process was set up to produce one deposition each time. In the study, sintered Titanium Carbide particles/Nickel (TiC_p/Ni) metal matrix composite (MMC) was used as the electrode to coat copper (Cu) substrate. The movement of the depositing TiC_p/Ni electrode was strictly controlled in static mode experiments. Meanwhile, in dynamic mode experiments, the electrode movement was governed by a spring mechanism. In addition, Nickel was also used as both coating electrode and receiving substrate to gain insight into the bonding mechanism. The current, voltage and the electrode displacement were measured by a PC computer-based data acquisition system.

Based on direct observations of the experiments, a phenomenological model was developed to detail the events taking place during a single deposition in both static and dynamic modes. The process began with the ESD power supply switching to the discharging mode. A spark was initiated as the electrode came into contact with the substrate. This initial spark partially melted both the substrate and electrode. The spark also expelled any molten substrate outward to form a crater. The expelled molten substrate re-solidified on the edge of the newly formed crater. The

electrical power stored inside the capacitors of the ESD power supply was only partially discharged due to the formation of a narrow gap between the electrode and copper substrate. At this stage, no material was transferred from the electrode to copper substrate. The continuous forward motion brought the electrode into contact with the substrate again. This facilitated the material transfer from the electrode to the substrate. The experimental results indicate that the material transferred between the coating electrode and the receiving substrate is primarily through direct molten metal – molten metal contact. At this second contact, the ESD power supply completely discharged the remaining electrical power. The sparking and the molten metal expulsion are responsible for removing contaminated materials from the contacting surfaces. This would result in a defect-free bonding interface.

The set voltage is a major controlling parameter of the ESD process. The effects of voltage on the ESD coating were studied using 25V, 35V, 45V and 65V. A high voltage provided higher heat input and better cleaning action since more of the receiving substrate was melted and expelled further away from the depositing location. As a result, the high voltage reduced the overall number of cracks and shortened the crack lengths that were typically found at the coating and substrate interface. This would improve the bonding strength between the coating and the substrate. Although high voltage eroded and expelled more of the receiving substrate, it also increased the amount of electrode material depositing onto the substrate.

To gain insight into the bonding mechanism between TiC_p/Ni metal matrix composite and copper substrate, three different coating electrode – substrate combinations were used. They were TiC_p/Ni electrode and Cu substrate, TiC_p/Ni electrode and Ni substrate and Ni electrode and Cu substrate. In the Ni-Cu combination, a metallurgical bond was formed with the existence of an intermixing layer as predicted by the nickel and copper phase diagram. In the TiC_p/Ni and Ni combination, the nickel diffused from the substrate into the TiC_p/Ni coating. There was no intermetallic phase at the bonding interface between TiC_p/Ni electrode and Cu substrate. The experimental results suggest that Ni in the TiC_p/Ni metal matrix composite has low mobility since nickel is used primarily as binding agent. The bond is formed by the diffusion of the copper into the metal matrix composite without any intermetallic formation.

iv

Acknowledgements

Dedication

I dedicate this thesis to my family and Elaine, who have always supported my endeavors.

Table of Contents

List of Figures

xiii

List of Tables

Chapter 1

1   Introduction

1.1   Background

Resistance spot welding (RSW) is a fast and effective method of joining sheet steel components in the automotive industries [1]. However, the requirement of improved corrosion resistance in auto body led to a significant increase in the application of zinc coated steel. The increase in usage of zinc coated steels in the auto body has drastically reduced the copper electrode tip life during RSW process because of the low electrical resistance and melting temperature of zinc coating on steels [1-2]. The low electrical resistance and low melting temperature of zinc coating on steels increases the welding current and time required to maintain the heat input for minimum weld nugget size formation [1]. Furthermore, the molten zinc interacts with the copper electrodes during RSW to form brass alloy at the electrode tip. The formed brass alloy is softer than the copper alloy, and high temperature and pressure are developed due to increased welding current and time during welding. As a result, the combined effects accelerate the wear rate and deformation of the copper electrode during the RSW process [1-2]. In addition, the formation of brass alloy during RSW causes electrode sticking, and local bonding between the electrode and workpiece. Fracture of the local bond leads to progressive erosion or pitting of electrode tips. Eventually, undersized resistance spot welds are produced [3]. The electrode is said to have failed when undersized welds are produced. Thus, welding zinc coated steel can significantly reduce the electrode life. This problem is prolific in automotive assembly since a large fraction of all steel sheets is zinc-coated. Decreased in electrode life increases the cost-per-weld and decreases productivity since the electrode can only be changed during down time of the assembly line.

RSW electrode degradation mechanism of welding zinc coated steels has been subjected to many studies in developing new electrode materials and electrode design to improve electrode life. It has been identified that the interaction of zinc coating with copper electrode is the key factor in electrode degradation [1-3]. The formation of brass alloy layers requires the diffusion of zinc

into the copper. The interaction can be prevented by introducing a diffusion barrier. This could be achieved by coating the surface of the electrode. In addition, the coating material must not interact with zinc coating and protect the electrode without affecting the weldability. Industrial processes such as physical vapour deposition (PVD), chemical vapour deposition (CVD), and high velocity oxygen fuel spray (HVOF) can be used to deposit coating on the electrode surface. However, these processes typically require the base material to be heated to higher temperature [4-5]. Due to the sensitivity to overaging of the precipitation hardened RSW copper electrode, the usable temperature of these coating processes is severely limited.

Huys Industries Ltd. has developed and patented a TiC_p/Ni metal matrix composite (MMC) coating on the RSW copper electrode by electrospark deposition (ESD) process to prolong the electrode tip life of welding zinc coated steels. When compared to the non-coated Cu electrode, the TiC_p/Ni MMC coating is effective in reducing electrode degradation. The TiC_p/Ni MMC coating acts as a barrier to zinc alloying thereby resisting erosion wear. Chan *et al* [6] have reported that coated electrodes double the tip life of uncoated electrodes when welding hot-dip-galvanized high strength low alloy (HSLA) steel. However, the electrode life for coated electrodes welding zinc-coated steel is still shorter than uncoated electrodes welding bare steel. This is due to defects in the TiC_p/Ni layer found to exist immediately after the coating process. Serious cracking and delamination in the coating is believed to the result of thermal stress build up during cooling and solidification of the deposit (see Figure 1.1) [7]. Furthermore, a softened heat-affected-zone (HAZ) was observed in the electrode tip along the coating interface [7]. During welding, molten zinc can penetrate the cracks, flow along the delaminated interface, and diffuse into the electrode at the already softened heat-affected-zone. This is accelerated by spalling of the coating due to cracks and poor adhesion. Clearly, TiC_p/Ni coatings extent electrode life in resistance spot welding of zinc-coated steels, but deficiencies in coating quality need to addressed to match the performance of electrodes in bare steel welding.
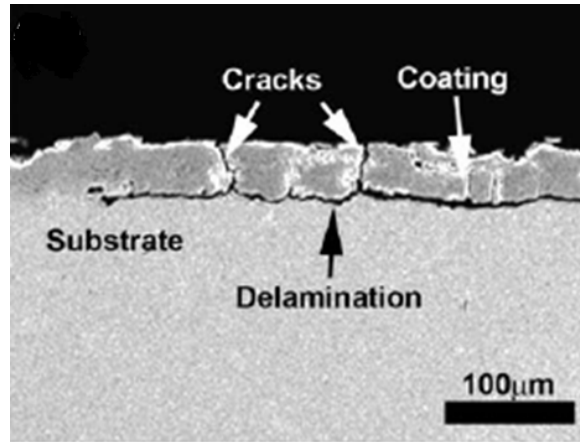
Figure 1.1: SEM cross-section images of monolithic TiC_p/Ni coating [7].

1.2 ESD TiC_p/Ni MMC Coating on Resistance Spot Welding Electrode

Electrospark Deposition (ESD) is a micro-bonding process that is capable of depositing wear and corrosion resistance coating to repair, to improve and to extend the service life of the components and tools. During the coating process, short duration of electrical pulses ranging from a few microseconds to milliseconds are used to deposit the electrode material to the component's surface producing a protective layer [8]. The spark is produced through the moving electrode as it is momentarily short-circuited and hence pulse discharged with the base material. The low net heat input and the ability to form metallurgical bonding of coating to substrate make it ideal to coat the copper electrode surface for the RSW application.

Titanium carbide (TiC) is a strong and wear resistance ceramic that has been used in the tooling and machining applications for years [9]. Since the repeated RSW process requires the coating material to withstand numerous mechanical impact and thermal cycles. The good electrical and thermal conductivity combined with the high strength make TiC ideal for the coating material in resistance spot welding electrode.

The TiC_p/Ni MMC coating is manually applied to copper electrode by the conventional ESD coating machine as shown on Figure 1.2. The sintered TiC_p/Ni depositing electrode (see Figure 1.3) is held in the vibrating handheld applicator. It is momentarily short-circuited with the

3

rotating copper electrode. The TiC_p/Ni electrode is energized by a series of capacitors. During deposition process, part of the tip of the TiC_p/Ni electrode is melted, meanwhile, spark is generated. The molten TiC_p/Ni is transferred and rapidly solidified on the surface of the copper substrate. However, only a micro size of splat is deposited at each deposition cycle. As a result, the build-up of the TiC_p/Ni coating occurs incrementally by overlapping multiple micro deposits. Figure 1.4 shows the TiC_p/Ni MMC coated RSW Cu electrode and the SEM view of electrode tip surface by the ESD process.
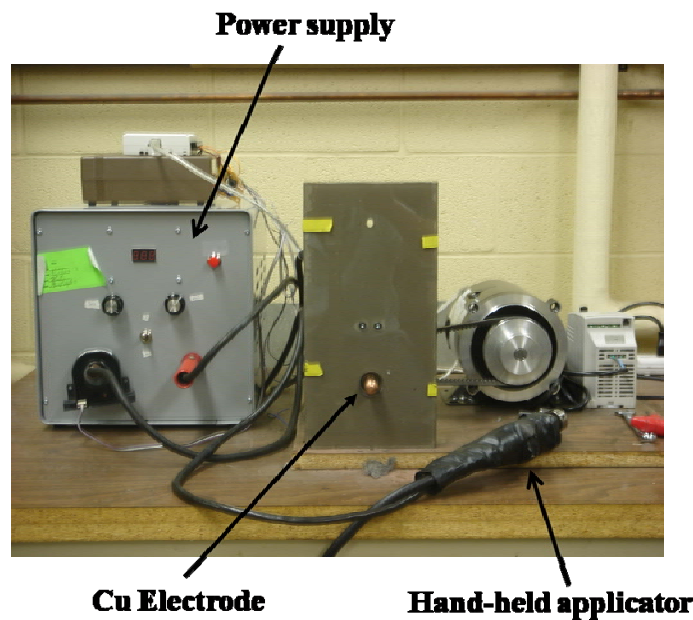
Figure 1.2: ESD experimental equipment for TiC_p/Ni MMC coating on RSW Cu electrode.
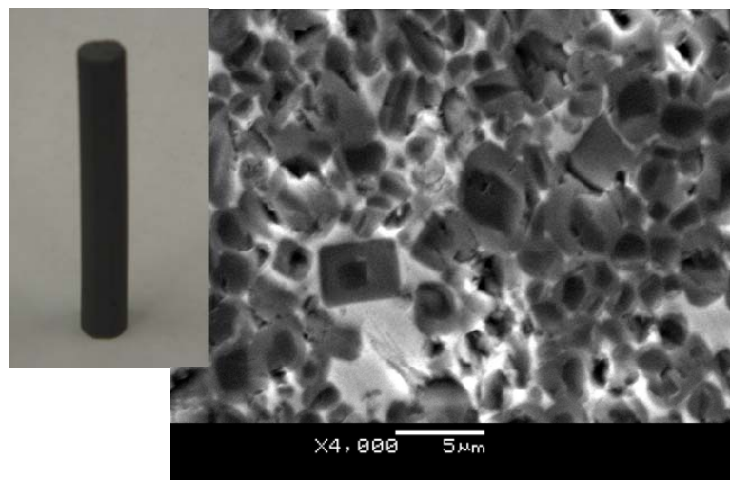
Figure 1.3: Sintered TiC_p/Ni electrode and the SEM cross-sectional view.
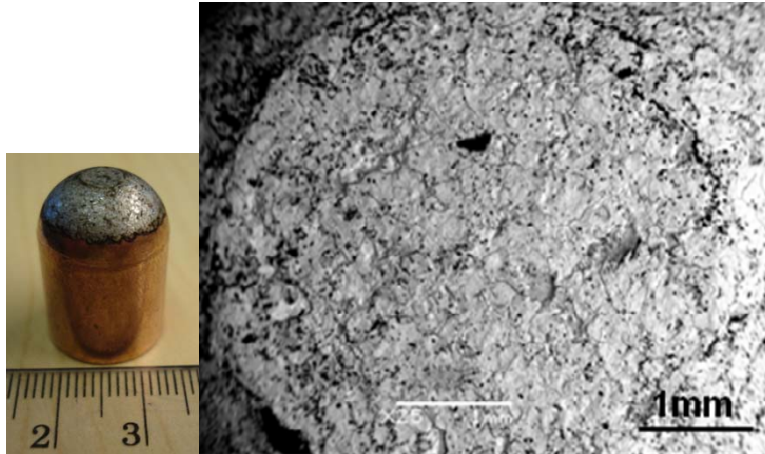
Figure 1.4: TiC$_p$/Ni MMC coated RSW Cu electrode by ESD and SEM image of coated Cu electrode tip surface.

To date, the effects of ESD parameter interactions on coating quality are not well known. It is believed that the lack of understanding of ESD parameter interactions is the result of the inferior to the coating quality. In addition, limited work has been done to detail the ESD material transfer mechanism. Understanding the material transfer mechanism is essential to optimize the process and achieve high quality coatings.

1.3   Objective

The objective of this thesis is to enhance the current understanding to the ESD process by using a single deposition study. The specific objectives include:

1) A detail examination of the events taken place during a single ESD deposition of the electrode to the substrate.

2) The material transfer mechanism between the electrode and the substrate during ESD process.

3) The effects of voltage on the ESD coating quality.

4) The ESD coating build-up by successively depositing of the coating material on the same location.

5) The bonding mechanism between the coating material and the substrate of the ESD process.

1.4   Thesis Outline

Chapter 2 of this thesis presents a literature review of the ESD process, the effects of the ESD process parameters on the resulting coating, applications and performances, and the new developments of the ESD process. Chapter 3 provides the ESD equipment, the materials, the experimental setup, experimental conditions for the depositions, and performance testing. In Chapter 4, the formation of the ESD single deposition by static and dynamic modes and the material transfer mechanism are presented and discussed. In Chapter 5, the effect of voltage on ESD single deposition and coating, and the coating evolution of the ESD process are investigated. Finally, chapter 6 summarized the key results attained from this study and proposes future work.

Chapter 2

2   Literature Review

2.1   Historical Background of Electro-spark deposition (ESD)

Electro-spark deposition (ESD) uses short duration pulses of current to deposit the electrode material to a metallic substrate to improve wear, corrosion resistance and dimensional restoration [10]. Since early 1900s, ESD was also known by other names including spark hardening, electric spark toughening, and electrospark alloying [8].

In 1924 by H. S. Rawdon noticed that hardness on the surface of iron increased when sparked with a nickel or copper electrode [8]. He further proved that the increase in hardness of iron was the result of martensite formation as rapid quenching of the spark heated surface. Similar phenomenon was also observed by Welsh in 1957 [11] when sparking the steel surface with electricity. In addition, he found that the surface hardness could be influenced by the sparking atmosphere, since absorption of atmospheric elements such as nitrogen and oxygen could affect the hardness changes [11, 12]. Rawdon *et al* [8] have shown that sparking of titanium surfaces under oil resulted in high surface concentrations of titanium carbide, which changed a very poor-wearing surface to a hard and durable surface. Further research works have shown that tungsten carbide and titanium carbide electrodes could be used to deposit wear resistance coating to steel, and found to be 6 to 30 times more wear resistance than case carburizing or cobalt base or Ni-Cr-B base hardfacings [12 – 15].

In the 1944, several aspects of the hardfacing ESD method were studied and implemented in the Union of Soviet Socialist Republics (U.S.S.R.) to increase service life of many parts that subject to wear, such as lathe tools, drills, milling cutters, dies, files, hacksaw blades, camshafts, tappets, wheel rims, and turbine blades [16 – 17]. In 1974, Johnson *et al* [8] reported on the research of ESD coatings in corrosion performance on nuclear reactor applications. However, further development was required before the satisfaction of coatings were deposited, such as better

coating uniformity, smoother surface finishes, and improved reproducibility and control of the process.

In the next section, the ESD equipment, ESD process characteristics such as process variables, coatings performance and applications will be detailed in the following sections.

2.2   ESD Equipment

The typical ESD equipment consists of two main components: the power supply and the electrode holder as shown in Figure 2.1.
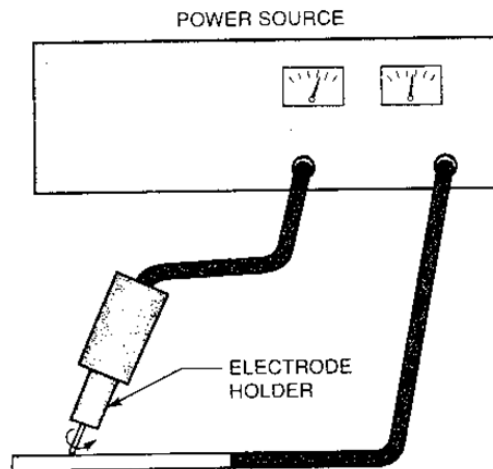
Figure 2.1: Electro-Spark Deposition Equipment [10].

The most common power source for ESD process consists of a direct current (DC) rectifier and discharge circuit [10]. The purpose of DC rectifier is to convert alternate current (AC) input to direct current (DC) which is used to charge up a series of capacitors. The electrical process parameters for the EDS process such as charging voltage and discharge frequency are often set on the power supply. To discharge the capacitors, the power supply utilizes either a resistor-capacitor (R-C) or a microprocessor-controlled discharging circuit.

The typical hand held electrode holder for the ESD consists of a non-conductive case, an inner metallic lining, and an electric motor [10]. The main purpose of the non-conductive case is to provide both electrical and thermal insulation between the energized electrode and the operator.

Meanwhile the inner metallic lining is to provide mechanical stability. The electric motor is to provide the electrode movement that requires breaking the contact between the electrode and workpiece.

There are 3 types of most common electrode movements, vibration, rotation, and oscillation. The electrical current is transferred through the power cable from the power supply by several methods, such as using a braided cable to wrap around the rotating shaft and using a rotary contractor [8, 10, 18]. In addition to the protective case and the mechanical fixture, the electrode holder can also be used to deliver shielding gas to the deposition area to provide a protective atmosphere. A gas nozzle similar to the one used for gas tungsten arc welding (GTAW) can be attached to the end of the electrode [10].

2.3   ESD Process and Coating Characteristics

The Electro-Spark Deposition has often been described as a micro arc-welding process [8]. For instance, during the ESD process, the depositing electrode is momentarily contacting the substrate surface with light pressure [8, 10, 18]. It is necessary to maintain the electrode motion to prevent the depositing electrode sticking to the substrate surface. In addition, there are important process parameters listed in Table 2.1 that are unique to the ESD process. These variables include electrode, substrate, environment, and electrical characteristics. Changing in any of these parameters will result in changing of the properties and quality of the resultant deposition. The following sub-section will detail the effect of the process parameters.

Table 2.1 ESD process parameters [8].

Electrode	Substrate	Protective Environment	Electrical	Others
Material	Material	Shielding gas type	Power input	System efficiency
Geometry	Surface Finish	Flow rate	Voltage	Number of passes
Motion	Cleanliness	Temperature	Capacitance	Overlap of passes
Speed	Temperature	Flow geometry	Spark rate	Spark duration
Contact Pressure	Geometry			
Orientation				
Application direction				

2.3.1 ESD Electrical Characteristics

The electrical characteristics of ESD process illustrate the most influence on the deposition quality and the deposition rate [18]. An increase in spark energies will increase the deposition rate. The spark energy, E_p, is defined as:-

$$E_p = \int_0^{t_p} V(t) \cdot I(t) dt \tag{2.1}$$

where V(t) is a function of voltage during discharge, I(t) is a function of current during discharge, and t_p is the pulse duration.

The variables that control the spark energy include capacitance, charging voltage, inductance, and resistivity of the circuit [18]. The capacitance and charging voltage change the spark energy by altering the discharge duration and the peak current, respectively. The charging voltage controls the amount of current flow into the capacitor. The higher the capacitance, the longer the discharge duration for a given voltage potential will be. The resistivity of the circuit has the negative influence on the spark energy by limiting the current flow of the circuitry, and it is controlled primarily by the power cable. Shortening the distance of the cables can simply minimize the effect of resistivity [18].

The spark durations of the ESD process are usually ranging from few microseconds to milliseconds, which are about three orders of magnitude shorter than other pulsed welding processes. The deposition frequency can vary from 60 Hz to 4 kHz [8, 10, 18, 19]. Heating of the substrate occurs during about 1% of the duty cycle [10], while heat dissipation occurs during the balance of time. The spark energy can range from 0.1 J to 10 J [18]. As a result of the short pulse duration and low fraction of heating time, the substrate remains at or near ambient temperature during coating. This low net heat input process can greatly eliminate or reduce the heat affected zone, metallurgical change and dimensional change of the substrate. However, an auxiliary cooling system or additional heat sink may be required for very thin sections, small parts, or parts that usually needed for longer sparking time.

The cooling rate of the ESD process can be as high as 10^5 to 10^6 degree C per second [8, 10, 18, 19]. This low net heat input and rapid solidification process is beneficial to the mechanical properties of the deposition. The rapid solidification of the deposits often results in nano-structured or even amorphous form for some materials [19]. These types of deposit demonstrate excellent wear and corrosion performance compared to the same materials at its original form due to the Hall-Petch effect. The Hall-Petch relation predicts that as the grain size decreases the yield strength increases [21]. Johnson *et al* [19] have illustrated that the Stellite 6[TM] (a cobalt-based hardfacing alloy) exhibits a hardness value of 40 Rockwell C, while the ESD Stellite 6[TM] coating shows a hardness value of 60 Rockwell C. The observed phenomenon is attributed to fine grained structure obtained from the rapid solidification of the ESD process.

2.3.2   Materials

A wide variety of electrode and substrate materials combinations have been explored in the literature [19]. All electrically conductive materials that can be melted in an arc are suitable deposition material on metallic substrates [6, 10, 18, 19]. For examples, hard alloys, carbides, borides, intermetallics or cermets have been applied for wear resistance to a wide range of substrates including steel, Al-alloys, Ni-alloys, Cu-alloys, Ti-alloys, Zr alloys and refractory metals as listed in Table 2.2 and Table 2.3. In addition, the ESD process can be used to obtain bonding with the materials combination that are considered incompatible by other welding process [19]. It is believed that rapid solidification of the deposit on the substrate is the major contribution to the compatibility of the materials combination. For example, Banovic *et al* [20] studied that iron and aluminum cannot be welded without cracks with aluminum content above 10 wt%, conversely crack-free deposits of aluminum to stainless steels with aluminum content up to 35 wt% by ESD process as studied by Johnson *et al* [19].

However, some electrically conductive materials are not suitable for the ESD application. Johnson *et al* [19] were unable to deposit bismuth telluride or chromium silicide. Both bismuth telluride and chromium silicide were presumably vaporized or decomposed in the arc. Similarly, graphite has been used as the depositing electrode, it was found that no graphite was actually transferred. It is believed that graphite does not have a molten phase at atmospheric pressures, as a result, there isn't any molten materials available to transfer [19].

Table 2.2: ESD Coatings Applied to Date [19].

Wear Resistance Coating	Corrosion Resistance Coating	Build-up or Special Surface Modification
Hard carbides[a] of: W, Cr, Ti, Ta, Hf, Mo, Zr, V, Nb	Stainless steels, Hastelloys[b], Inconels[b], Monels[b]	Ni-base and Co-base super alloys
Hardfacing alloys: Stellites[b], Tribaloys[b], Colmonoys[b], etc.	Aluminides of: Fe, Ni, and Ti	Refractory Alloys (W, Ta, Mo, Nb, Re, Hf)
Borides of: Cr, Ti, Zr, and Ta	FeCrAlY, NiCrAlY, CoCrAlY	Noble metals (Au, Pt, Ag, Pd, Ir)
Intermetallics and Cermets	Al and Al Bronze Alloys	Other Alloys (Fe, Ni, Cr, Co, Al, Cu, Ti, V, Sn, Er, Zr, Zn)

[a] With metal binders, usually 5-15% Ni or Co
[b] Trademarks: Hastelloy – Haynes International, Kokomo, IN
                  Inconel & Monel – International Nickel Co, Huntington, WV
                  Stellite & Tribaloy – Deloro-Stellite Co., Goshen, IN
                  Colmonoy – Wall Colmonoy Corp., Detroit, MI

Table 2.3: Substrate alloys coated by ESD to date [19].

High and Low Alloy Steels	Nickel and Cobalt Alloys	Refractory Metals (W, Re, Ta, Mo, Nb)
Stainless Steels	Titanium Alloys	Chromium
Tool Steels	Aluminum Alloys	Uranium
Zirconium Alloys	Copper Alloys	Erbium

2.3.3   Deposition Rate

As mentioned previously, the deposition rate of the ESD process depends primarily on both the materials and the electrical characteristic. In the most practical ESD coating, the deposition rate can be achieved at 20cm^2/min for a 25μm thick coating [19]. This deposition rate is relatively rapid when compared to physical vapor deposition and chemical vapor deposition processes. However, this deposition rate is still slow as compared to various thermal spray processes. The deposition rate can be increased by increasing the spark energy and spark frequency [8, 10, 18, 19]. However, the increase in both spark energy and spark frequency will also increase the surface roughness of the coating and the heat input to the substrate. Thus, increase the size of the heat affected zone and further allow the buildup of thermal tensile stress.

2.3.4 Coating Thickness

The ESD coating thickness can range from 3µm to over 3mm based on the material combination. For example, the coating thickness of some hard and brittle materials, such as the refractory metal carbides and the hardfacing alloys, is generally limited to 50µm. Meanwhile, for many ductile alloys, 100µm or greater coating thickness can be achieved [10, 19]. Additionally, the coating thickness is also dependent on the deposition area. Ductile materials can achieve the coating thickness of several millimeters in small areas repairing or buildup. On the other hand, a uniform coating thickness of less than 100µm may be achieved with the same materials in larger areas [19]. This is due to the fact that the deposited coating tends to buildup preferentially on the spots that the depositing electrode contacts first. Hence, any high points on the coating will be built up in the expense of surrounding areas after a certain thickness is achieved [8, 19].

Despite the variations in the coating thickness that can be achieved by the ESD process, in most of the ESD applications, the coating thicknesses of 25 to 100 µm is the most desirable. Johnson *et al* have reported that a 25µm of Tribaloy 800[TM] ESD coating lasted nearly six times longer than a 100µm coating in a rubbing test under the same conditions [19]. The thicker coating of brittle material often has higher thermal tensile stresses and can be easily fractured.

2.4   Materials Transfer Mechanism During ESD Process

During the ESD process, electrical sparks are generated as the electrode is short circuited momentarily with the substrate. These sparks can generate sufficient heat to melt a part of the electrode and a part of the substrate. The molten electrode and substrate materials are rapidly solidified to form a coating. However, the mechanism of material transferred from the depositing electrode to the substrate during ESD process is generally not well understood.

There are several hypotheses to the material transfer mechanism during the ESD process. The first hypothesis was suggested by Galinov *et al* [22]. A part of the electrode material detaches and transferred to the substrate via solid, liquid, or gaseous state. In solid state, the particles from the electrode collide and adhere to the substrate surface. However, the substrate can be eroded during the impact. In liquid state, the molten material on the electrode surface is detached, transferred and solidified on the substrate surface. Furthermore, there is almost no material

transfer during the ESD process in the gaseous state. Since the vaporized electrode material partially condenses on the substrate, and mostly dissipates to the environment. It should be noted that the solid, liquid, or gaseous state of material transfer are difficult to monitor because of the very short pulse duration and distance between the electrode and substrate.

Johnson *et al* [19] have suggested that material transfer mechanism during ESD is similar to the either the globular or spray transfer modes in gas metal arc welding (GMAW). The molten droplet from the electrode is propelled towards and impinged on the substrate as shown on Figure 2.2. The globular mode of material transfer exits in the presence of air or nitrogen environment. Meanwhile, the spray mode of materials transfer occurs in the ionized argon (Ar) gas environment. The plasma produced by Ar has low thermal conductivity [23]. In addition, the Ar gas provides shielding and cleaning effect to the substrate surface. As a result, smooth coating surface is often obtained with argon gas.

(a)   (b)
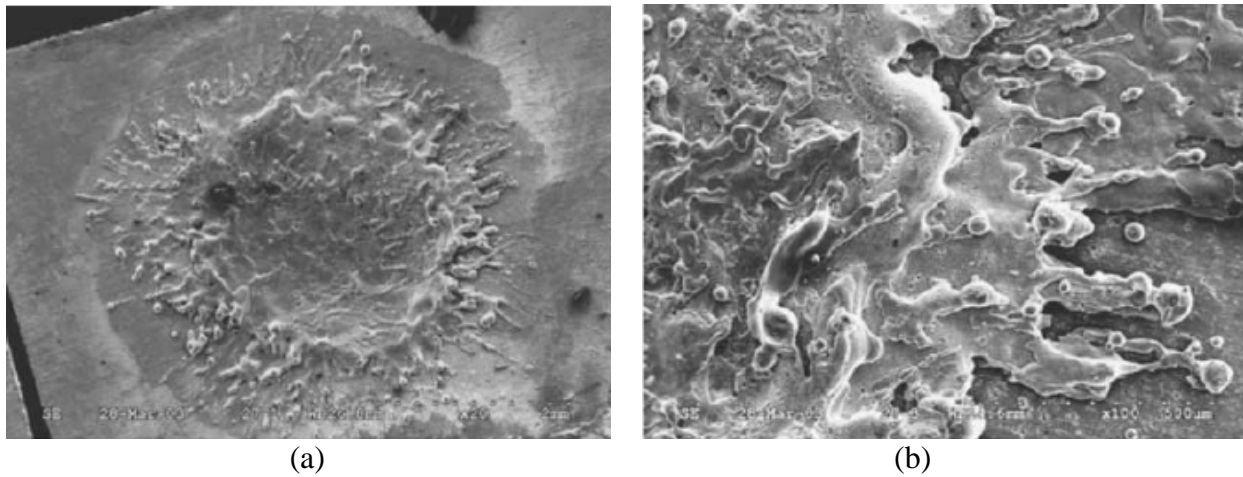
Figure 2.2: SEM micrograph of: a) Morphology of multi-pulse single spot deposition at 20X; b) Enlarged image of the spot fringe at 450X [23].

Lesnjak *et al* [24] used a high speed camera of 220 shots per second to monitor the ESD process of Tungsten Carbide (WC) coating on stainless steel substrate. Based on observation, Lesnjak *et al* [24] concluded that the materials transfer of ESD is a spark guidance transfer and can be divided into 4 phases. First, the electrode is brought to contact the substrate. Joule heating is generated owing to the high contact resistance, and the substrate and the electrode tip are heated

strongly at the local contact points. Second, the electrode is removed from the substrate. Because of the rapid movement of the electrode, the capacitors are not discharged completely. An arc is ignited (see Figure 2.3a) as the electrode is no longer in contact with the substrate. The arc can generate sufficient energy to melt the electrode tip and result in the formation of a droplet (see Figure 2.3b). Finally, the droplet is propelled and adhered to the substrate. This is very similar to the filler metal transfer mode of GMAW process. The molten droplet detaches and impinges on the substrate surface under the effect of Lorentz force [25].

(a)   (b)
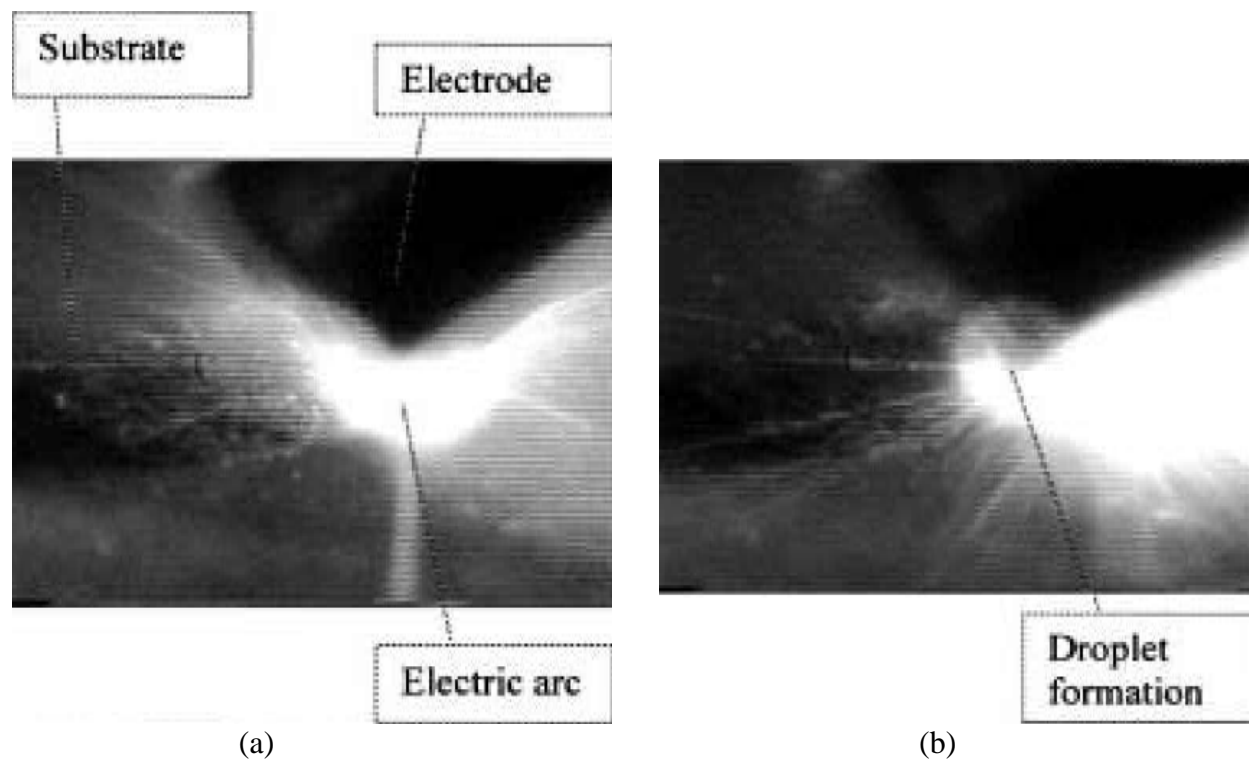
Figure 2.3: High speed camera optical images: a) arc ignition; b) droplet formation [25].

Liu *et al* [26] developed a heuristic physical model to explain the material deposition in rotating ESD process. The proposed physical model is divided into 4 stages as shown on Figure 2.4. In the first stage, the electrode is moved to contact the substrate locally. In the second stage, the pulsed electrospark discharge occurs. Due to the large current and large amount of energy supplies, the materials melt and gasified rapidly. This results in the formation of molten droplet on the electrode and a melt pool on the substrate. In addition, the thermal input enhances the gas

15

ionization between the electrode and substrate. The molten droplet is rapidly rushed to the melt pool and impinged on the substrate, and solidified. In the last stage, the electrode and substrate will contact again and a new discharging cycle is started.
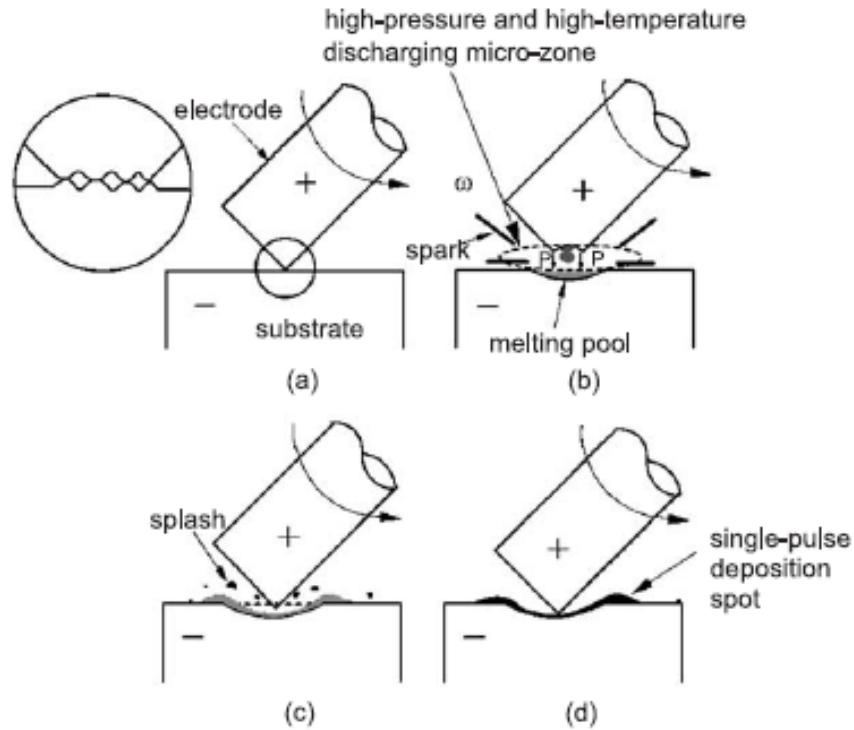
Figure 2.4: The physical model of the formation of a single-pulse deposition spot [26].

In the above studies, it is shown that the materials transfer mechanism during the ESD process is similar to the hypothesis that suggested by Johnson *et al* [19] in which the materials transfer mechanism is a combination of globular and spraying transfers. However, there is not enough evidence to support the suggested hypothesis from the above studies. As a result, in this present study the materials transfer mechanism of the ESD process will be studied in detail and presented in the following chapters.

2.5   ESD Application and Performance

The first application of the ESD process was the formation of martensite by sparking between a steel electrode and a steel substrate to form a hard facing coating [8]. The most common applications of the ESD process are to apply wear resistance and corrosion resistance coating. The continuous development of the ESD process has led to many other industrial applications. In the following, some of the industrial applications and the performance of the ESD coating will be reviewed.

In the nuclear application, the ESD coating has been developed to meet the rigorous demands of the nuclear components for wear, friction, corrosion, thermal cycling, and irradiation damage resistance [27]. As reported by Johnson [19], with the exception of ESD, almost all of the 120 commercially available coating processes failed to meet the acceptance criteria. ESD has replaced the detonation-gun (D-gun) coatings owing to its superior performance in damage and wear resistance. Figure 2.5 illustrates the comparison in damage resistance of chromium carbide coatings applied by D-gun and ESD at the same thickness. The ESD coating showed no spalling or material lost in a 180° bend test, while the D-gun coating spalled on both the concave and convex sides in less than 30° of bending. Figure 2.6 shows the comparison wear tests on chromium carbide coatings applied by D-gun and ESD. Test results showed that at low contact stresses, both coatings demonstrated very low wear rate, as the contact stresses increased, the wear rate of D-gun coating rapidly increased while the wear rate of the ESD coating remained unaffected.
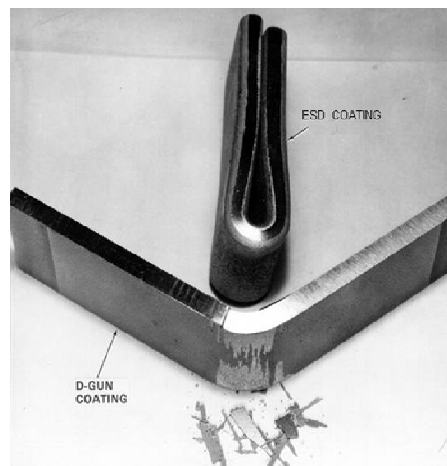
Figure 2.5: Bend test of chromium carbide coating applied by D-gun and ESD [19].
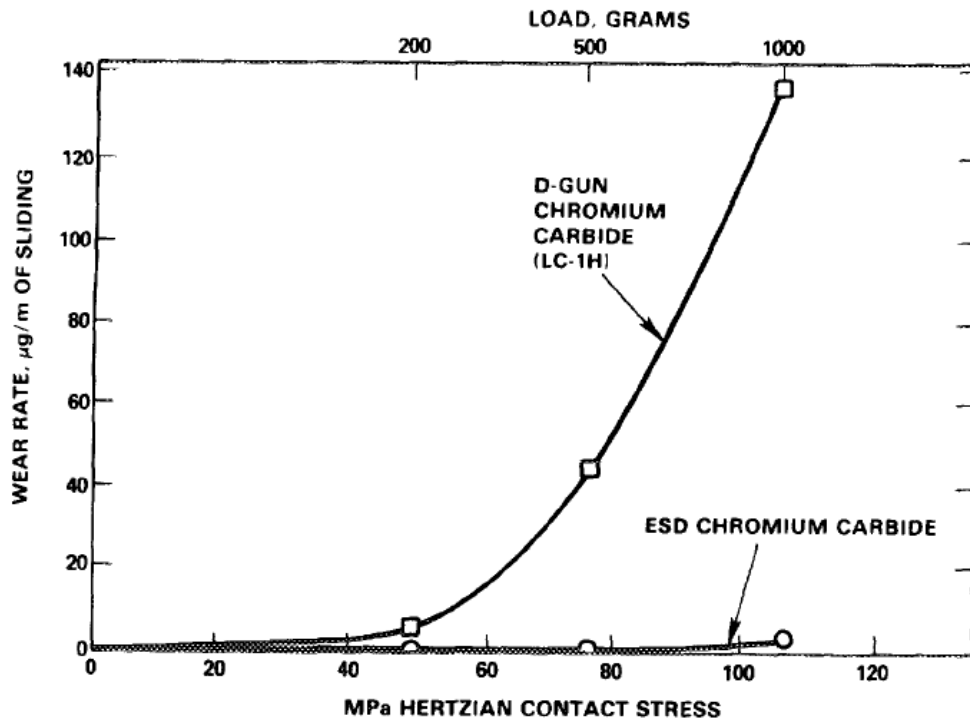
Figure 2.6: Effect of contact stress on wear of D-gun and ESD chromium carbide coating [19].
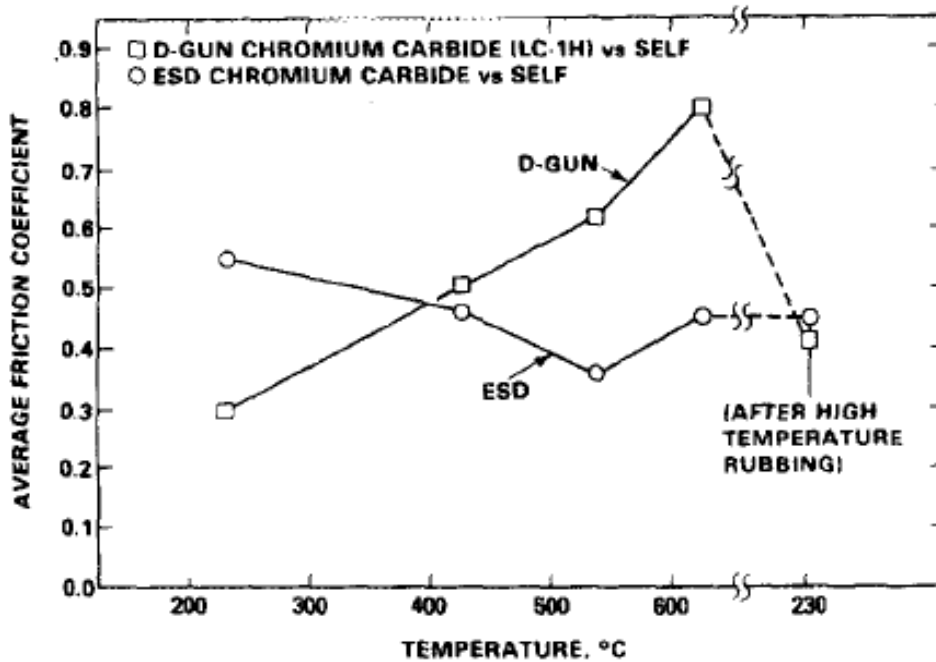
Figure 2.7: Friction of ESD and D-gun coatings in sodium [19].

The superior in both damage and wear resistance of the ESD coating is related to the structure and bonding of the coating. ESD coating has much finer grain and homogeneous structure than the D-gun coating because of the rapid solidification of ESD. Also, the ESD coating is metallugically bonded to the substrate, while the D-gun coating is primarily mechanical bond [19]. Furthermore, the ESD coating showed better performance in both friction and corrosion performance as shown on Figure 2.7 and 2.8.
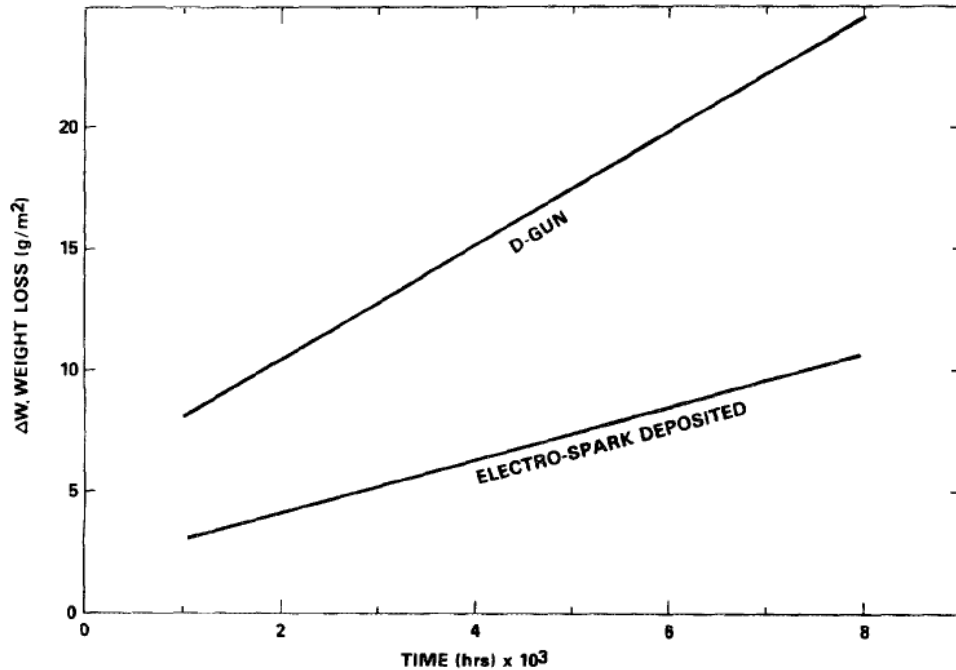
Figure 2.8: Corrosion performance of chromium carbide coatings in sodium at 625°C [19].

The ESD process is also widely used in the aerospace applications. ESD process provides surface treatments for wear, erosion, and corrosion resistance as well as repair and recovery of high values parts such as turbine components [19]. Examples of ESD in the aerospace applications include hardsurfacing of blade tips and notches for wear control in ablative seals, pre-placement of platinum on blades prior to platinum aluminide diffusion coating, repair of casting defects, pre-placement of braze alloys on difficult-to-wet superalloys for precision assembly of components, repair of diffusion coatings, build up and repair of worn or undersize parts, coatings to resist particle erosion from ingestion of sand in military turbines and repair of thermal fatigue cracks in single crystal turbine blades. Figure 2.9 shows the repairing of single crystal turbine blade by ESD, where the low net heat input and free from distortion were requirements for repairing singe crystal alloys [28].

19
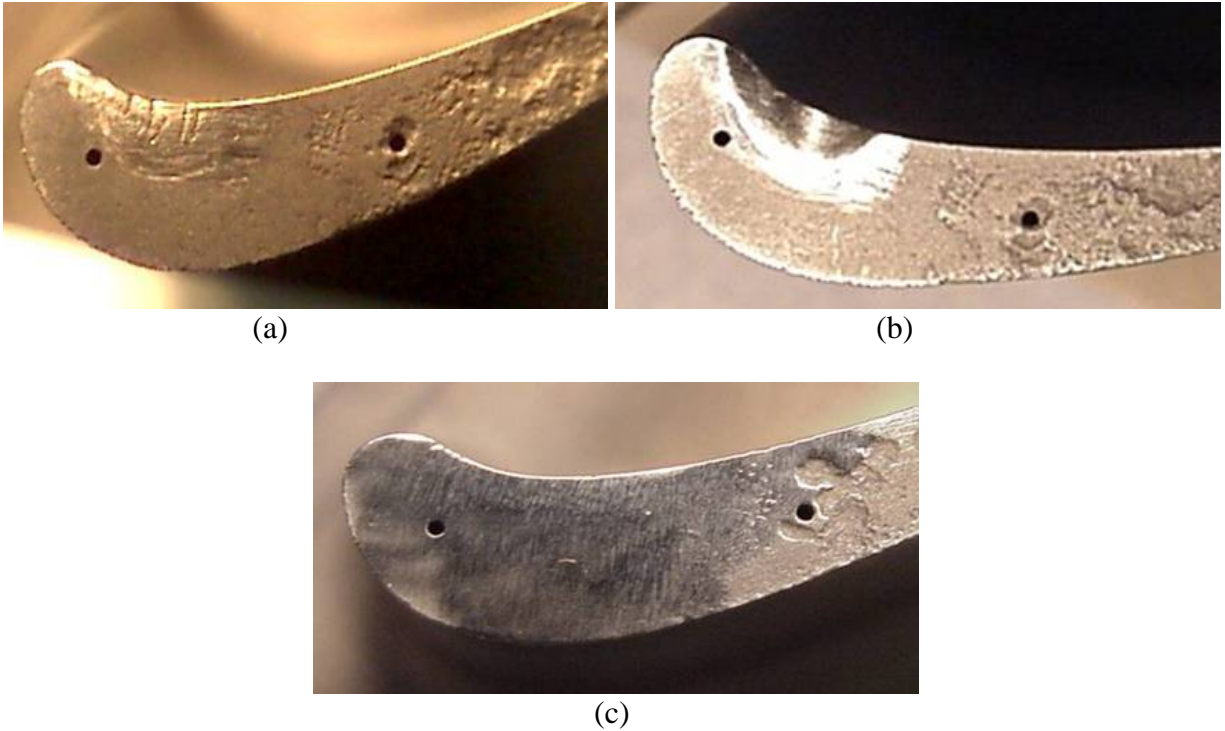
Figure 2.9: Repair of single crystal turbine blade by ESD: a) as-received blade with thermal fatigue cracks, b) cracks removed by grinding, c) restored by ESD using original materials as filler and finished. [28].

In addition, the ESD has also been used in automotive applications, where titanium carbide coatings are deposited on the titanium valve stems and valve guides in the high performance internal combustion engines [19]. Huys Industries Ltd. has developed and patented the TiC_p/Ni metal-matrix-composite (MMC) coating on resistance spot welding (RSW) copper electrode to improve the electrode tip life in RSW of Zn-coated sheet steel. As Zn coating react with the Cu electrode to form brass alloys during RSW, causing the local bonding between the electrode and the sheet steel. Fracture of these local bonds will lead to material loss on the electrode surface and causing the growth of the electrode tips diameter and eventually failure of the electrode. Figure 2.10 illustrated that the electrode tip diameter growth rate is slower with the TiC_p/Ni coating when number of welds exceeded 100. Chen et al [3, 9] studied the TiC_p/Ni MMC coating deposited on the surface of the RSW Cu electrode by the ESD process. The coating successfully acted as a barrier to prevent Cu from reacting with the Zn coating thereby improved the electrode tip life [3].
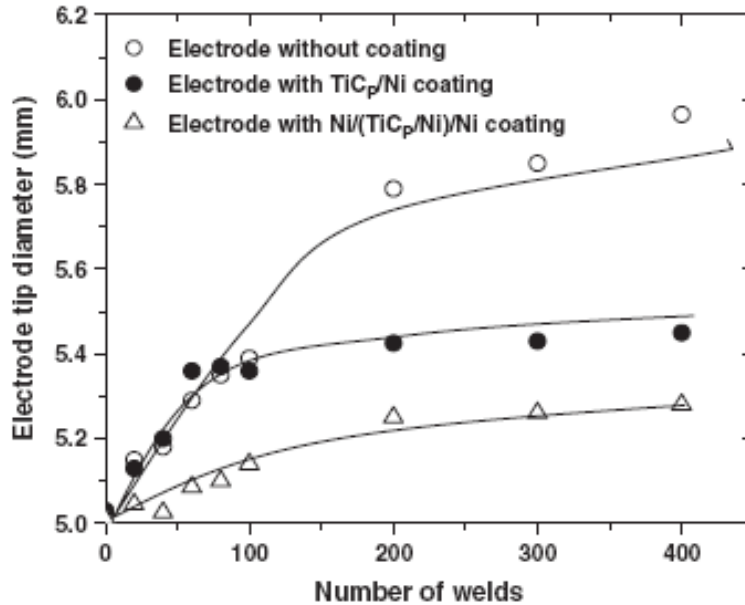
Figure 2.10: Electrode tip growth diameter as a function of weld number [3].

Other industrial applications include replacing the expensive tungsten carbide brazed inserts tips of surgical tools and needle holders with ESD chromium carbide coating. Coatings on the orthopedic drills, dental tools, hemostats, and orthotic leg and ankle brace components for the medical applications. For the high tech sports equipments, ESD coating is applied on knife edges, knife sharpeners, golf clubs, ski edges, ice axes, and crampons [19].

2.6   ESD Process Improvement

As stated above, the ESD process demonstrates some unique advantages over other coating processes. However, there is a fundamental dilemma with ESD, which the process can only be optimized for either quality or efficiency. As a result, improvement in deposition rate without sacrificing the quality of the coating must be achieved through optimization of the process parameters. There are several factors control the coating efficiency, such as the electrode properties (melting point and heat capacities), environment, and the electrical characteristic (spark energy and spark frequency) [8, 10, 18, 19]. The most important factor is the charge-discharge frequency.

Several improvements in deposition rate are achieved through the advances in the design of power supply. A capacitor discharge design is used by most of the conventional ESD power supply (see Figure 2.11) and the discharge of the capacitor is often initiated by the contact of the electrode and substrate [10]. For a vibrating applicator, the charge-discharge frequency is determined by the vibration frequency of the electrode and the restriction of the mechanical movement tends to have low deposition rate. If a rotational applicator is used, the irregular contact between the electrode and substrate varies the discharge frequency and voltage, which results in slow and unstable coating process. The discharge voltage can be increased by using a silicon controlled rectifier (SCR). However, the inductor used to regulate short-circuiting currents will extend the discharge duration and affect the discharge frequency [29].
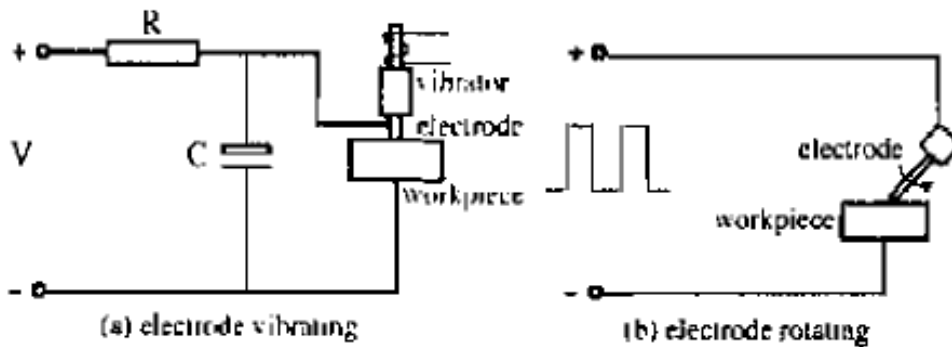
Figure 2.11: Block diagram of conventional ESD equipments [29].
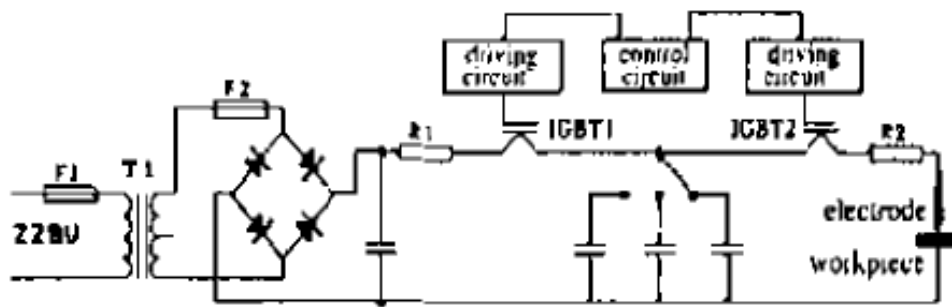
Figure 2.12: Block diagram of newly designed accelerated ESD power supply [29].

The new power supply design has taken the advantages of inverter-based electronic and microprocessor control. Wang et al [29] have studied the ESD process by using the newly designed power supply as shown on Figure 2.12. This new design utilizes the isolated gate

bipolar transistor (IGBT) switches coupled with controlling and the driving circuits. The electrical pulse is obtained by utilizing one switch, IGBT1, to the charge circuit, and the other switch, IGBT2, to the discharge circuit. The controlling and the driving circuits control the ON/OFF states of the two switches. When the voltage reaches a reset level, IGBT1 will be off and IGBT2 will be on and the capacitors will discharge. When the voltage drops to a lower level, IGBT1 will be on and IGBT2 will be off and the capacitors charging cycle begins. The advantages of IGBT switch are its flexibility and adjustability to the wide range of voltage and current. This allows higher charging voltage with short pulse period and increase in spark frequency [29]. It is shown in Table 2.4 that the both the coating thickness and deposition rate are increased by using the newly designed ESD power supply.

Table 2.4: Comparison between the conventional and newly designed ESD power supply [29].

	Conventional	New
Power supply, V	220, single phase	220, single phase
Higest output Voltage, V	40 – 50	30 – 75
Operating current, A	1 – 3	<10
Maximum coating thickness, µm	50 – 60	100
Roughness, µm	1.6 – 6.3	2.6 – 6.3
Coating rate[a], mm^2/s	0.5 – 0.8	1.6 – 3.2

(a) For highest coating thickness

2.7   Summary

In this chapter, the ESD historical background, process characteristic, applications, performance and process improvement development have been reviewed. The Electro-Spark Deposition is a micro-bonding process, in which short duration pulses of current are used to bond the electrode material to a metallic substrate. The process was first discovered in 1924 by H. S. Rawdon and subsequently found many usages in various industries.

ESD possesses some unique advantages. The coating material is metallurgically bonded to the substrate. The low net heat input allows the substrate to remain at ambient temperature during the process, and the rapid solidification of the deposits produces a nano-structured or amorphous structured coating. As a result, the most common application of the ESD process is to apply wear resistance coating. However, there are some limitations to the ESD process, such as the low

coating efficiency, and the stress relief cracking inherent in some materials. The advantages and limitations of the ESD process are summarized in Table 2.5.

The mechanism of material transfer from the electrode to the substrate during ESD process is generally not well understood. It has been suggested that the coating material is transferred through solid, liquid, or gaseous state. Others suggest that the transfer mechanism is similar to those found in GMAW process. Generally, further experimental study is required to understand the material transfer mechanism during the ESD process.

There is a fundamental dilemma with the ESD process, which it can only be optimized for either quality or efficiency. Improvements in deposition rate have been achieved by advances in power supply design. The new power supplies use SCR control for higher discharge voltage and IGBT switching for higher discharge frequencies. And it is found that the both coating thickness and coating efficiency are improved by using the new power supply design.

The literature studies presented above showed that limited works have been done on studying the effects of ESD parameter interactions on coating quality. Also, there is not enough evident to support and detail the materials transfer mechanism during the ESD process. As a result, the objective of the present study is to enhance the current understanding to the ESD process by using a single deposition study. The ESD parameter interactions on coating quality, materials transfer and bonding mechanism will be addressed and discussed in the following chapters.

Table 2.5 Summary of the advantages and limitation of the ESD process [8].

Advantages	Limitations
Metallurgically bonded coating	Maximum coating thickness of currently 50 to 250 µm, depending on material
Low heat input, eliminates distortion or metallurgical changes in substrate	Stress relief cracking inherent in some materials
Nano-structured or amorphous layers possible through rapid solidification	Both substrate and coating material much be electrically conductive
Little or no substrate preparation or post-coating surface finishing required	Maximum effective coating rate of $20cm^2/min$
Reproducible process, easily automated	Extensive optimization of coating parameters may be required for some application
Operators easily trained	
Portable equipment and process	
Applicable to complex shapes	
Can apply nearly all metals and cermets	

Chapter 3

3 Experimental Methods

In this chapter, the experimental equipment, materials and experimental methods are presented. First, the major components and their functions of the electrospark deposition setup are explained. Second, the materials used including the compositions and surface condition are presented. Then, the experimental methods including sample preparation and material characterization are detailed in the remaining sections of this chapter.

3.1 Equipment

3.1.1 Electro-Spark Deposition (ESD) Setup

The ESD setup was designed and built at Center of Advance Materials Joining (CAMJ) at the University of Waterloo. Figure 3.1 shows the ESD setup which consists of 3 major components; Spring-loaded mechanical apparatus, ESD circuit, and Data acquisition (DAQ) system.
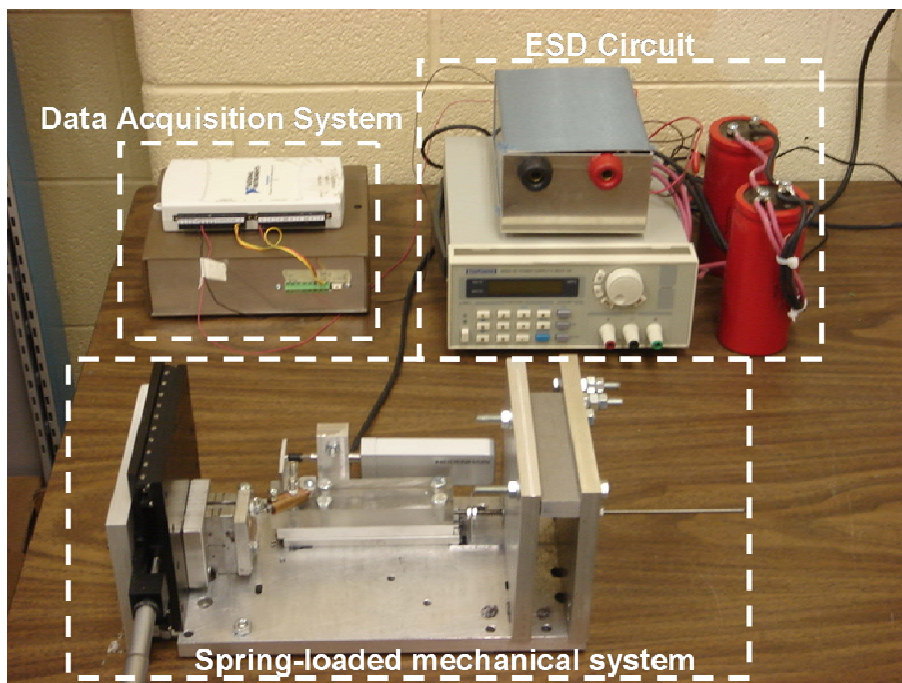
Figure 3.1: Electro-Spark Deposition setup

3.1.2   Spring-Loaded Mechanical Apparatus

Figure 3.2 shows the schematic diagram of the spring-loaded mechanical apparatus. The spring-loaded mechanical apparatus is consisted of a single axis stage, an electrode holder mounted on linear bearing, and springs and threaded rod assembly. The single axis stage was used to hold the Cu substrate which was connected to the negative terminal of the circuit. Also, the single axis stage controlled the movement of the Cu substrate in the Y-direction. The electrode holder was used to hold the TiC_p/Ni rod during the deposition process. It was connected to the positive terminal of the circuit and mounted on a linear bearing assembly. The linear bearing allowed the electrode holder to be freely moved back and forward in the X-direction.   This movement brought the TiC_p/Ni electrode into contact with the Cu substrate during deposition process. The springs and threaded rod assembly was the driving mechanism to bring the TiC_p/Ni electrode into contact and back away from the Cu substrate during the deposition process. The back away movement prevented the TiC_p/Ni electrode from sticking to the Cu substrate. Both the forward and back away travel limits were set on the springs and threaded rod assembly.
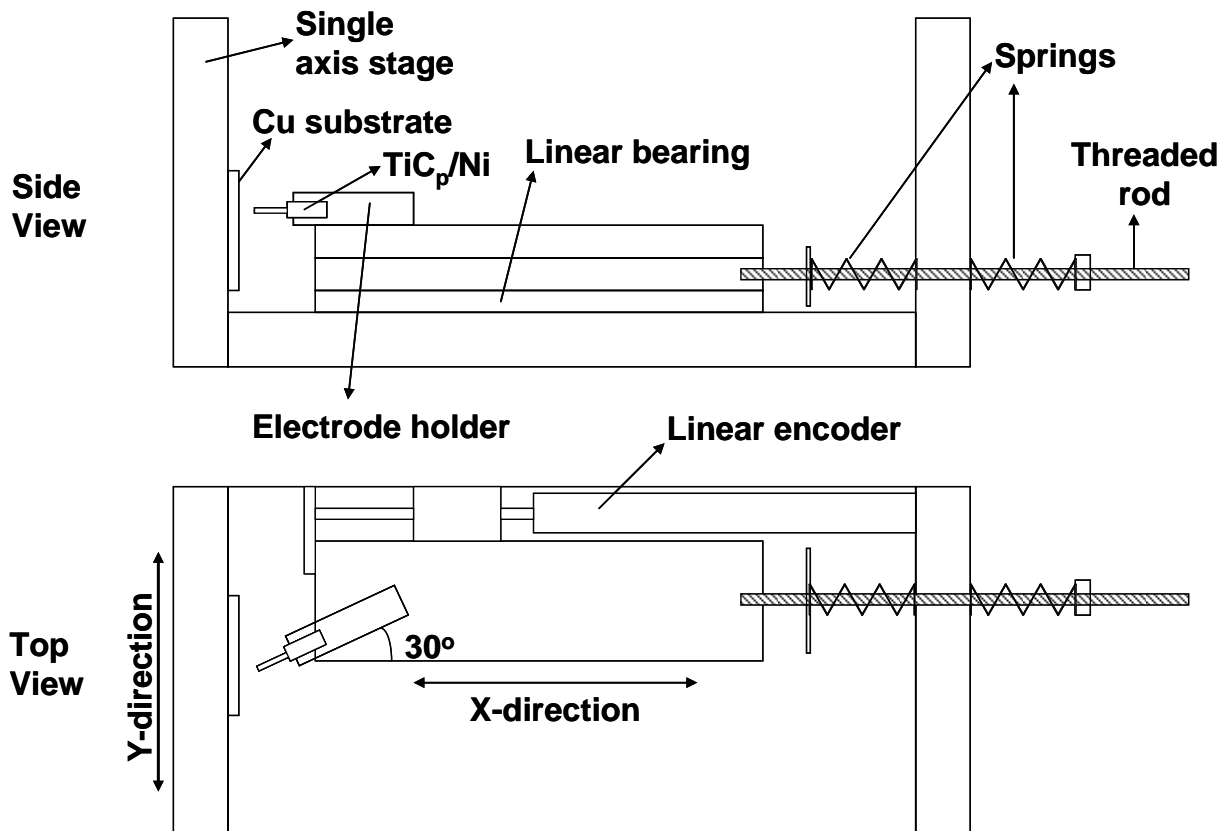
Figure 3.2: Spring-loaded mechanical apparatus.

27
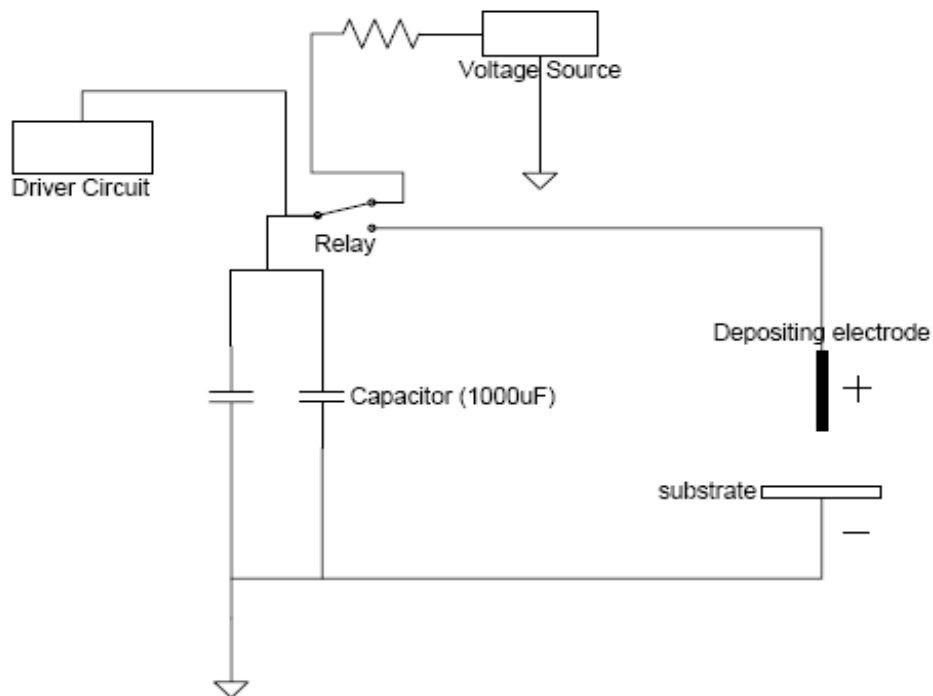
Figure 3.3: An electrical schematic diagram showing the ESD circuit.

3.1.3   ESD Circuit

Figure 3.3 shows a schematic electrical diagram of the ESD circuit. The ESD circuit is consisted of two 1000μF capacitors, power supply or voltage source, a relay and a computer-controlled driver circuit. The capacitors were used to store and to discharge the electrical power during the deposition process. The power supply was an adjustable constant voltage power supply that could charge up the capacitors to a preset voltage level. The relay was used to control whether the ESD circuit would be in charge or discharge modes. This relay was controlled by a computer-controlled driver circuit. In the present study, the ESD circuit was always set to charge mode by default setting of the program. When ready, a command would be inserted into the program to switch the relay into discharge mode.
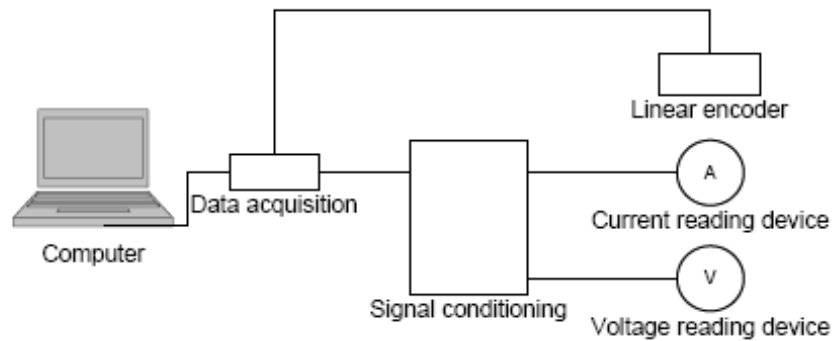
Figure 3.4: Data acquisition system for the ESD.

3.1.4 Data Acquisition System (DAQ)

Figure 3.4 shows a schematic diagram of the data acquisition system (DAQ) used in the present study. Connected to a laptop, the DAQ system was consisted of a current and a voltage sensors, a linear displacement encoder, a signal conditioning circuit board and a DAQ box. The system was controlled using a program written in LabView. The current sensor was a magnetic coil design that had ±0.001A resolution. The current sensor had a through hole which allowed the power cable to pass through from the deposition electrode to the positive terminal on the ESD power supply. The voltage reading device was a microchip that had ±0.1V resolution. The voltage reading device was connected to both ends of the positive and negative terminals by copper wires to measure the potential difference during the deposition process. The linear displacement encoder was a Heidenhain MT 2571 length gauge with 100kS/s sampling rate and ±0.1um resolution. It was mounted to the moving stage of spring-loaded mechanical system as shown on Figure 3.2 to measure displacement during the deposition process. The current and voltage reading sensors were connected to the signal conditioning board to convert the signal into appropriate format for the DAQ system. The DAQ box used in this study was a National Instrument USB-6211 M Series Multifunction DAQ with 250 kS/s sampling rate. The computer software used to collect all the measurement data was National Instrument LabView 8.6 (see Appendix). The sampling rate was set to be 100kS/s per channel in this study.

29

Figure 3.5 shows the current, voltage and displacement data of a single ESD process. The linear encoder was first set to the zero reference position along with the TiC_p/Ni electrode. Then, it was pull backward to a set position. As a result, the displacement data became negative. Initially, the ESD circuit was set to the charge mode. As the TiC_p/Ni electrode was traveling towards the Cu substrate, however, the computer program switched the ESD circuit to discharge mode. This was evident by the increase of the measured voltage to 35 V. Finally, the TiC_p/Ni contacted with Cu substrate and initiated the discharge.
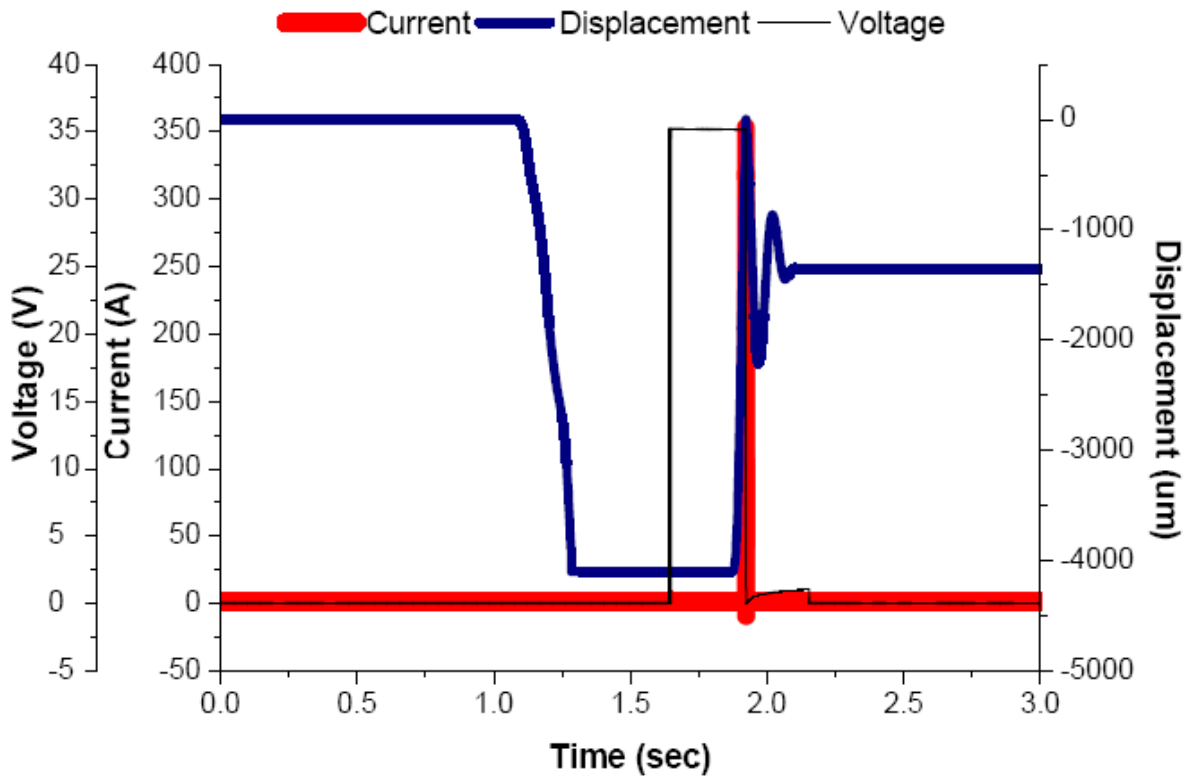
Figure 3.5: DAQ output of a single ESD deposition

3.2 Material Characterization Apparatus

In the present study, different material characterization apparatuses were used and they will be described in the following sub-sections.

3.2.1 Microscopy

Optical Microscope and Scanning Electron Microscope (SEM) were used to observe the surface and the cross-section of the ESD deposition. The optical microscope used in this study was

30

Olympus BX51M System Metallurgical Microscope. On the other hand, SEM was performed using a Jeol JSM 6460 with an attached Oxford Instruments INCA-350 for energy dispersive spectroscopy (EDS) analysis.

3.2.2   Surface Analysis and Depth Measurement

Surface analysis and depth measurement of the ESD single deposition were performed using a WYKO NT1100 Optical Profiler. Data analysis was conducted using the Wyko Vision® analysis software which accompanies with the Optical Profiler equipment. After scanning the surface of the deposition spot, a 3D contour map was generated, and the data of the centre line of X and Y profile were exported and plotted on Figures 3.6 a and b.

3.3.3   XRD Analysis

XRD analysis was facilitated using a Rigaku MSC micro-XRD. For this particular XRD the Cu k-alpha x-ray source is generated consisting of a 1.54 angstrom wavelength. A 0.8mm collimater is used to focus on the surface of the ESD deposition spot. Data conditioning was conducted using the JADE software which accompanies with the XRD equipment.
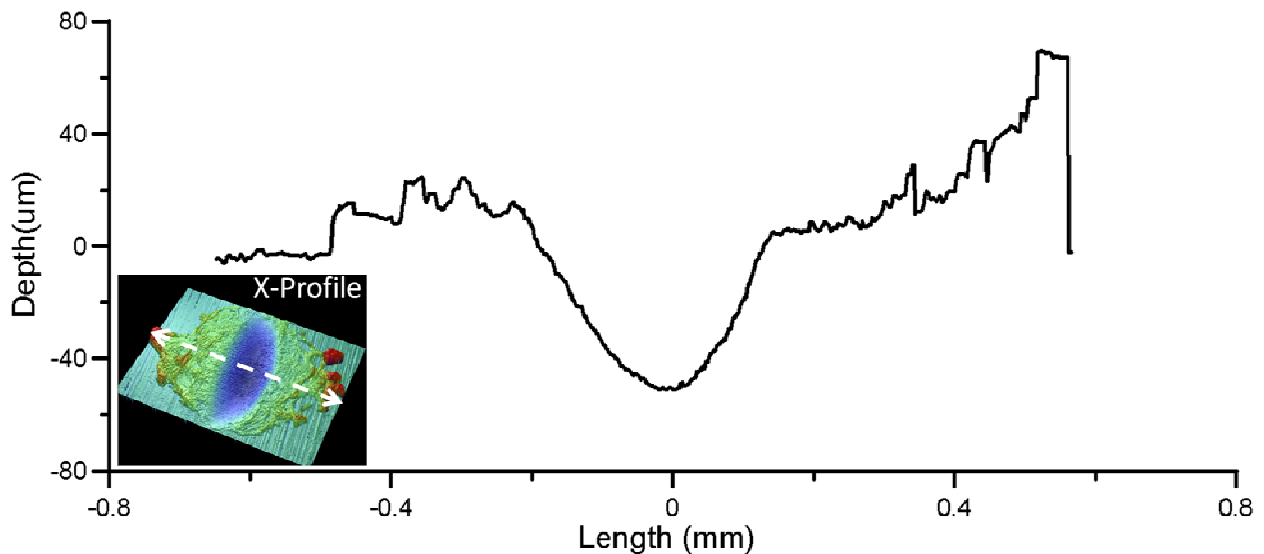
Figure 3.6a: X – profile surface scanning of single deposition.
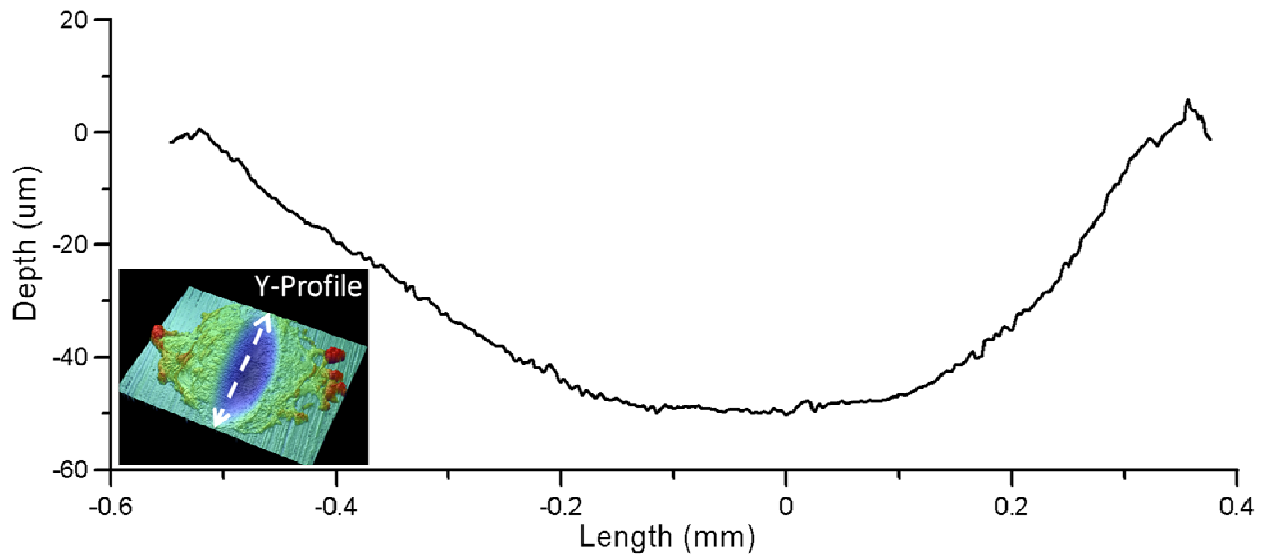
Figure 3.6b: Y – profile surface scanning of single deposition.

3.3 Materials

In the present study, the depositing materials were Titanium Carbide particles/Nickel metal-matrix composite (TiC$_p$/Ni MMC) and Nickel 200 (Ni 200) metal alloy. The TiC$_p$/Ni MMC electrode was the sintered of Titanium Carbide ceramic particles (approx. 5μm in diameter) with Nickel (Ni) and Molybdenum (Mo) as binding agents. The composition of the TiC$_p$/Ni MMC electrode is shown in Table 3.1. Molybdenum was used to enhance the wetting of Ni to TiC particles [9]. The TiC$_p$/Ni MMC electrode was 6mm in diameter and its upper portion was grinded to 1.5mm diameter for deposition purpose as shown in Figure 3.7a. In an attempt to gain insight into the bonding mechanism, Nickel 200 metal alloy (see Table 3-1 for compositions) was also used as depositing material. The Ni 200 metal alloy was cut into a 1.5mm x 1.5mm x 25mm square bar.

The substrates used in the present study were copper (Cu) and Nickel (Ni) alloys, respectively. The Cu alloy was a precipitation strengthened and work hardened class 2 alloy with the ASTM specification of C18150. Table 3.1 contains the chemical composition of this particular ASTM specification of the copper alloy. The dimension of the Cu substrate was a 25.4mm diameter and 1.5mm plate thickness as shown in Figure 3.7b. The copper plate was mechanically grinded with

320-grit SiC paper to remove oxide layer and washed with acetone before deposition. The Ni 200 substrate was cut into a 10mm x 10mm x 1.5 mm square plate. It was mechanically grinded with 320-grit SiC paper to remove oxide layer and washed with acetone prior deposition.

a)	b)
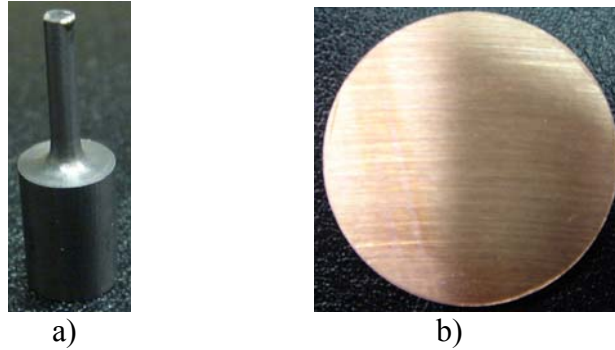
Figure 3.7: Material used for ESD: a) TiC_p/Ni depositing electrode b) Copper substrate.

Table 3.1: Compositions of depositing and substrate materials.

Materials	Composition (wt%)											
	Ti	Ni	Mo	W	Cu	Cr	Zr	C	Mn	S	Si	Fe
TiC_p/Ni MMC	68.36	15.44	13.40	2.80	-	-	-	-	-	-	-	-
Cu (C18150)	-	-	-	-	99.11	0.84	0.05	-	-	-	-	-
Ni 200	-	99.00	-	-	0.01	-	-	0.35	0.25	0.01	0.35	0.4

3.4   Experimental Procedure

In the following sub-sections, the experimental procedure for different studies will be provided.

3.4.1   One ESD Deposition Study

3.4.1.1   Static Deposition Mode Testing

Figure 3.8a shows the experimental setup used during the static deposition mode testing. The TiC_p/Ni MMC electrode was mounted on a second single axis stage which replaced the original linear bearing and springs-threaded rod assembly. As a result, the TiC_p/Ni MMC electrode was manually moved toward the Cu substrate. The depositing electrode was set with an offset angle of 30 degree. Figure 3.8b shows the close up image of the static deposition mode testing apparatus. This setup allowed the formation of one ESD deposition while the location and the movement of the electrode were strictly controlled.

To determine the occurrence of sparking between the electrode and the substrate, the TiC$_p$/Ni MMC electrode was incrementally moved towards the Cu substrate. After each move, the relay was turned to discharge mode. If there was no spark, the relay was then switched back to charge mode and the electrode was moved one more increment toward the Cu substrate. The distance, at which a spark occurred, was recorded. It should be noted that no spark was formed until the TiC$_p$/Ni electrode touched the Cu substrate. The ESD deposition spot was then examined under the SEM/EDS to observe the surface morphology and chemical analysis. Three samples were made to prevent scattering of the result.
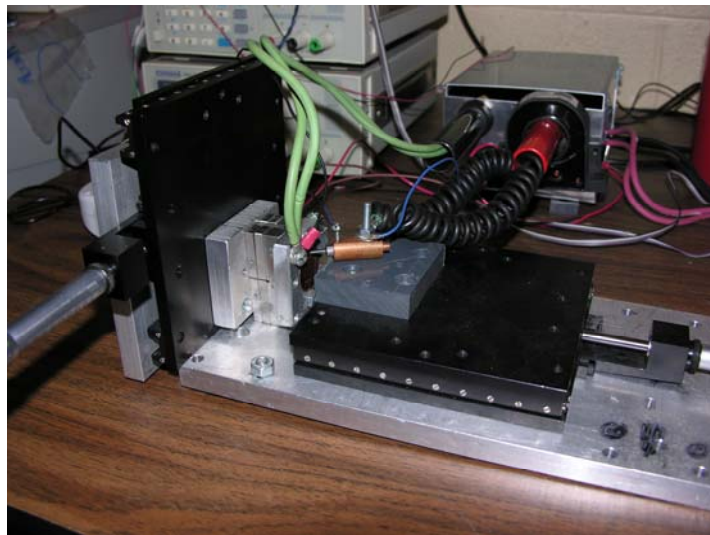
Figure 3.8a: ESD setup in Static mode.
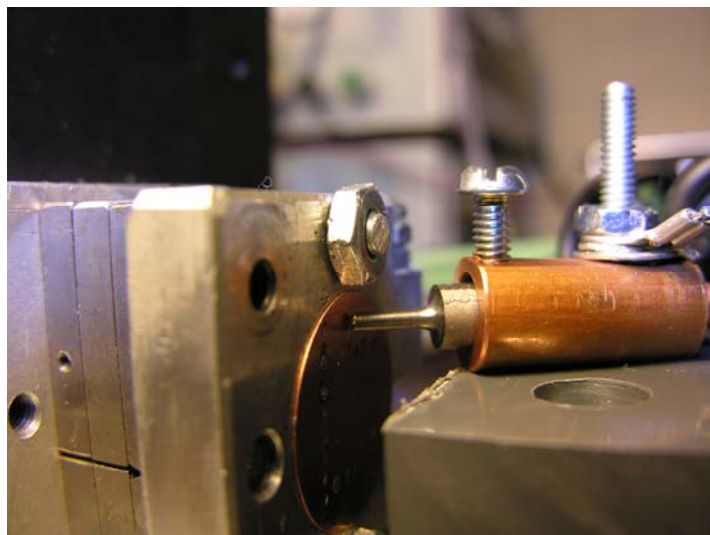
Figure 3.8b: Close up image of the TiC$_p$/Ni electrode and the Cu substrate.

34

3.4.1.2 Dynamic Deposition Mode Testing

In dynamic deposition mode testing, the TiC_p/Ni MMC electrode was mounted on the linear bearing which was connected to springs-threaded rod assembly as shown in Figure 3.2. Unlike the static mode, the springs-threaded rod assembly controlled the forward and back away movement of the TiC_p/Ni electrode.

Figure 3.9 shows the schematic diagram of the dynamic deposition mode process. The electrode was initially pushed against Cu substrate. This location was referred to as the zero reference point. Then, the TiC_p/Ni electrode was pulled backward to a location previously set on the springs-threaded rod assembly. At this time, the relay was switched to discharge mode and the springs-threaded rod assembly was released. The previously compressed spring on one side of the springs-threaded rod assembly sprang forward and brought the TiC_p/Ni electrode into contact with the Cu substrate. This initiated one ESD deposition. While the TiC_p/Ni electrode was moving toward the Cu substrate, a spring on the other side of the springs-threaded rod assembly underwent a compression. This spring would be responsible for moving the TiC_P/Ni electrode back away from the Cu substrate after the discharge, to prevent the TiC_p/Ni electrode from bonding to the Cu substrate. Finally, the TiC_p/Ni electrode returned to the original position. The ESD deposition spot was then examined under the SEM/EDS to observe the surface morphology and chemical analysis. Three samples were made to prevent scattering of the result.
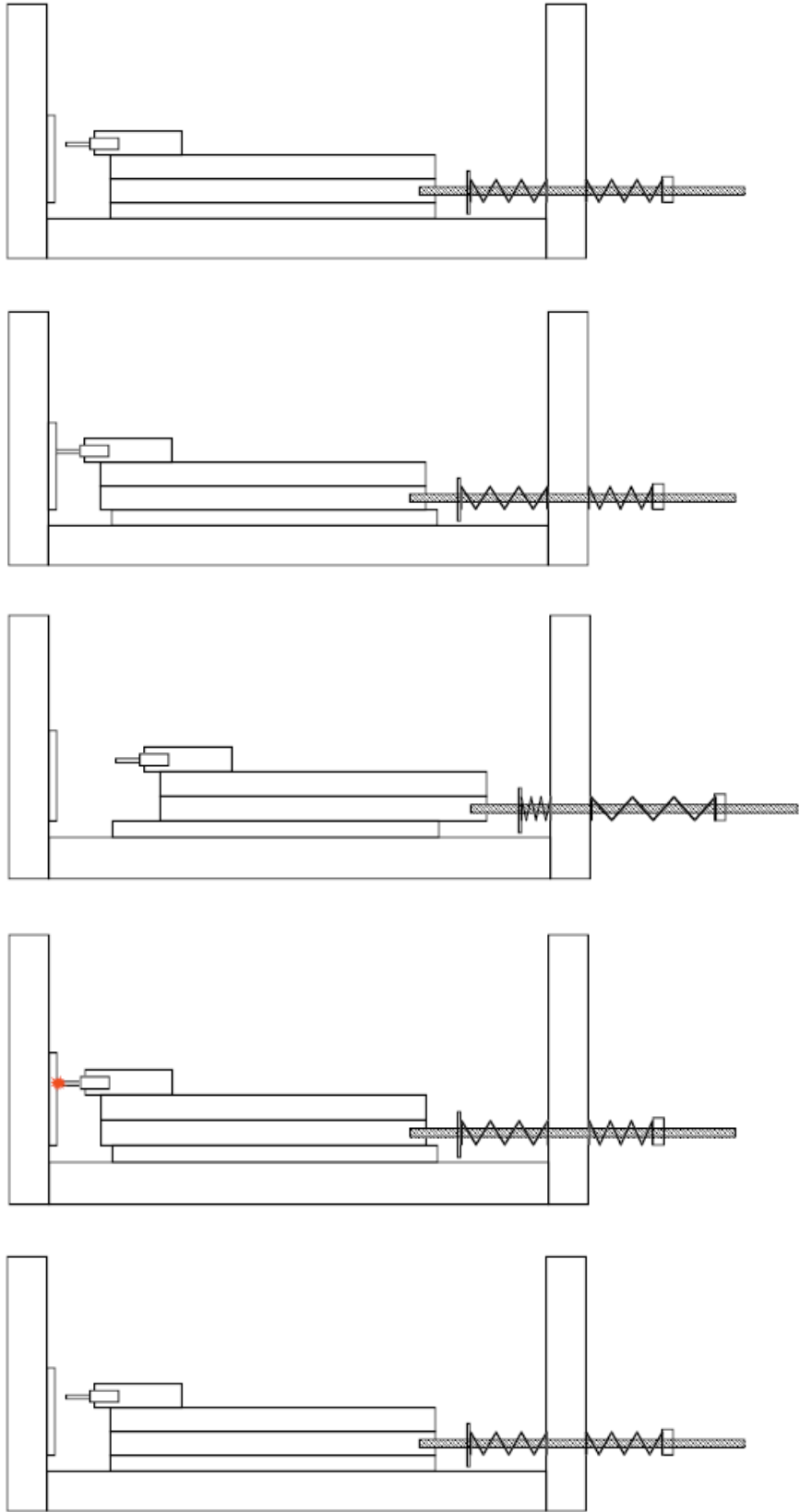
Figure 3.9: Schematic diagram of the Dynamic Deposition Mode process.

3.4.2   The ESD Coating Interface Study

Three different combinations of the coating and substrate materials were used to investigate the ESD bonding mechanism, which are $TiC_p/Ni - Cu$, $TiC_p/Ni - Ni$, and $Ni - Cu$. The ESD coatings were deposited using the spring-loaded mechanical apparatus.   The ESD coatings process was similar to the dynamic deposition mode testing, except the depositing electrode was not pushed again the substrate initially. Eighty deposits on the same spot with each electrode-substrate combination were made at 35V. The ESD coatings of each combination were examined using XRD, and the cross-sections of coating-substrate were subjected to SEM/EDS analysis. Three samples of each electrode-substrate combination were made to prevent scattering of the result.

3.4.3   The ESD Coating Build-Up Study

To document and to advance the current understanding of the coating build up during an ESD process, an ESD coating build-up study was carried out.   In this study, ESD coating was performed on the substrate using the spring-loaded mechanical apparatus.   The deposition process was the same as described in the ESD bonding mechanism study. Figure 3.10 shows the schematic diagram of the specimen. The ESD coating build-up study began with 1 ESD deposit on the substrate. Then the ESD deposit was performed again at different locations on the substrate, with the step increment of 1 deposit at a time on the same deposition spot, and up to 10 single deposits. It should be noted that the new edge of the TiC_p/Ni electrode was used for the ESD deposition at each deposition spot.   The specimen was then examined under the SEM.
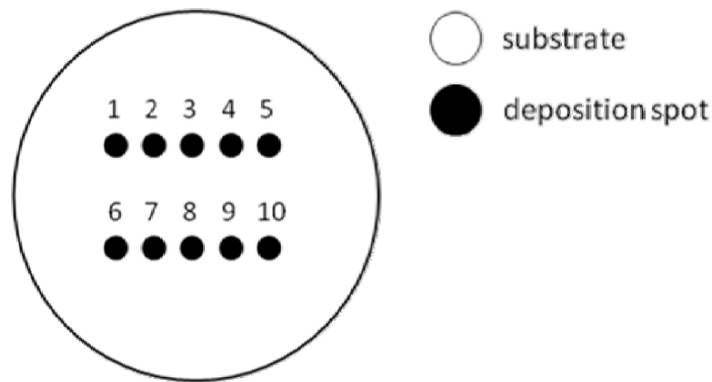
Figure 3.10: Schematic diagram of the specimen in coating build-up study. The numbers indicate the number of ESD deposit.

3.4.4   The Effects of Voltage on ESD Process Study

Single deposition was performed at 25V, 35V, 45V and 65V using the spring-loaded mechanical apparatus to investigate the effects of voltage on ESD process. The deposition process was the same as described in dynamic deposition mode testing. At each voltage level, ten samples were made to provide statistically significance to the results. The samples were examined under the SEM and Optical Profiler for surface analysis and depth measurement. To further evaluate the effect of voltage on ESD coating, ten deposits were made on the same spot of Cu substrate using the spring-loaded mechanical apparatus at each of the voltage levels. The specimens were cross-sectioned and observed under the SEM.

3.4.5   Mass Gain and Loss Quantification Study

In the mass gain and loss quantification study, the copper substrate was cut into 10mm × 10mm × 0.8mm thin plate. Four different voltage levels (25V, 35V, 45V, 65V) were used to quantify the mass gain and loss on both the TiC_p/Ni electrode and Cu substrate. At each of the voltage levels, 20, 40, 60, 80, and 100 ESD deposits were made using the spring-loaded mechanical apparatus. The deposition process was the same as described in the ESD bonding mechanism study. Both the TiC_p/Ni electrode and copper substrate were weighted before and after depositions using a Scientech SM124D analytical balance. This particular analytical balance has the resolution up to 0.1mg. In order to achieve higher accuracy, the test samples were replicated three times at each testing condition.

Chapter 4

4   ESD Process and Materials Transfer Mechanism

As stated in the literature review, several hypotheses to the material transfer mechanism during the ESD process were proposed. However, not much work has been done to validate the proposed hypotheses. As a result, the first step of the current study is to observe and document the material transfer mechanism using experiments in which a single deposition was made. In this chapter, the current, voltage and displacement data and the materials transferred during a single deposition are presented and discussed. From the experimental observations, a phenomenological model detailing the events taking place was developed. In addition, the experimental observations were compared to similar phenomenon of other welding processes.

4.1   Static Deposition Mode

In static mode, the ESD single deposition was made by mounting the TiC_p/Ni electrode on a single axis stage as detailed in Chapter 3. The electrode was manually moved towards the copper (Cu) substrate. In static mode, the electrode was held in place once it was moved to position. After the TiC_p/Ni electrode touched the Cu substrate, the ESD circuit was switched to discharge mode to create one single deposition spot.

Figure 4.1 shows the SEM image of topographic morphology and accompanying EDS elemental mapping of the ESD single deposition of TiC_p/Ni on Cu substrate in static mode. In this instance, 35V was used. As evidenced in Figure 4.1, an elliptical crater was created at the centre of the deposition area. The molten metal was expelled outward and re-solidified on the periphery of the crater. Since the crater was elliptical, the expelled material was not distributed evenly around the periphery. Also, a white region (indicated with the white dashed line) surrounding the crater of the deposition is observed. This is possibly caused by the cathode pulverization that is often observed in reversed polarity Gas Tungsten Arc Welding (GTAW) process to remove the surface oxide film on the substrate during welding [26]. This observation indicates that ESD is a self-cleaning process. In addition, the SEM/EDS elemental mapping shows that there is little materials transfer between the TiC_p/Ni electrode and the Cu substrate.
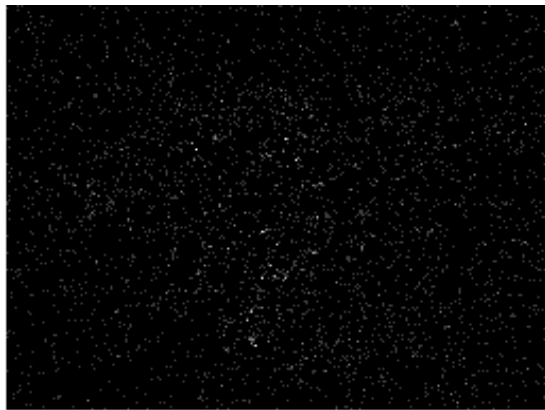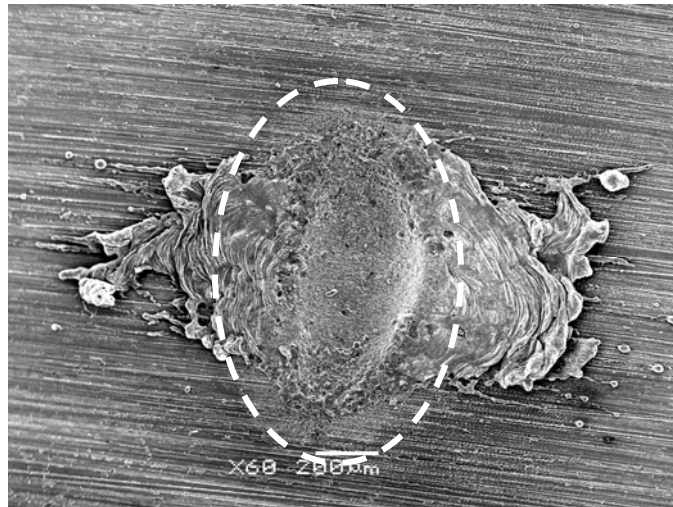
Ti Ka1
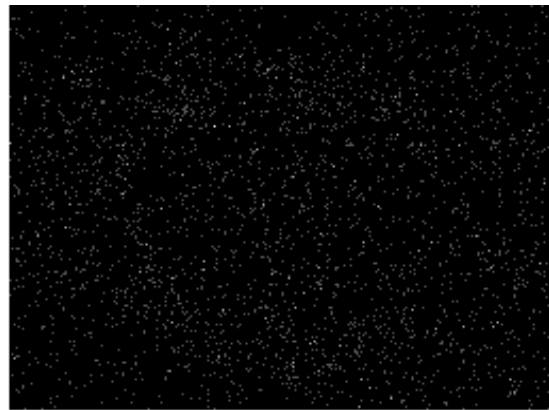
Ni Ka1
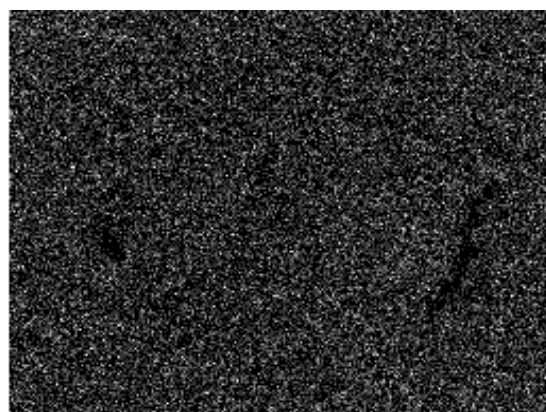
Cu Ka1

Figure 4.1: SEM image and EDS elemental mapping of ESD TiC$_p$/Ni single deposition in static mode.

Figure 4.2 shows the SEM images of the corresponding TiC_p/Ni depositing electrode after single deposition in static mode. Solidification structure at the edge of the TiC_p/Ni depositing electrode suggests that melting of the TiC_P/Ni electrode occurred during the deposition process. Although the electrode was molten, as indicated in Figure 4.1, there is no evidence of TiC_p/Ni deposited on the Cu substrate.
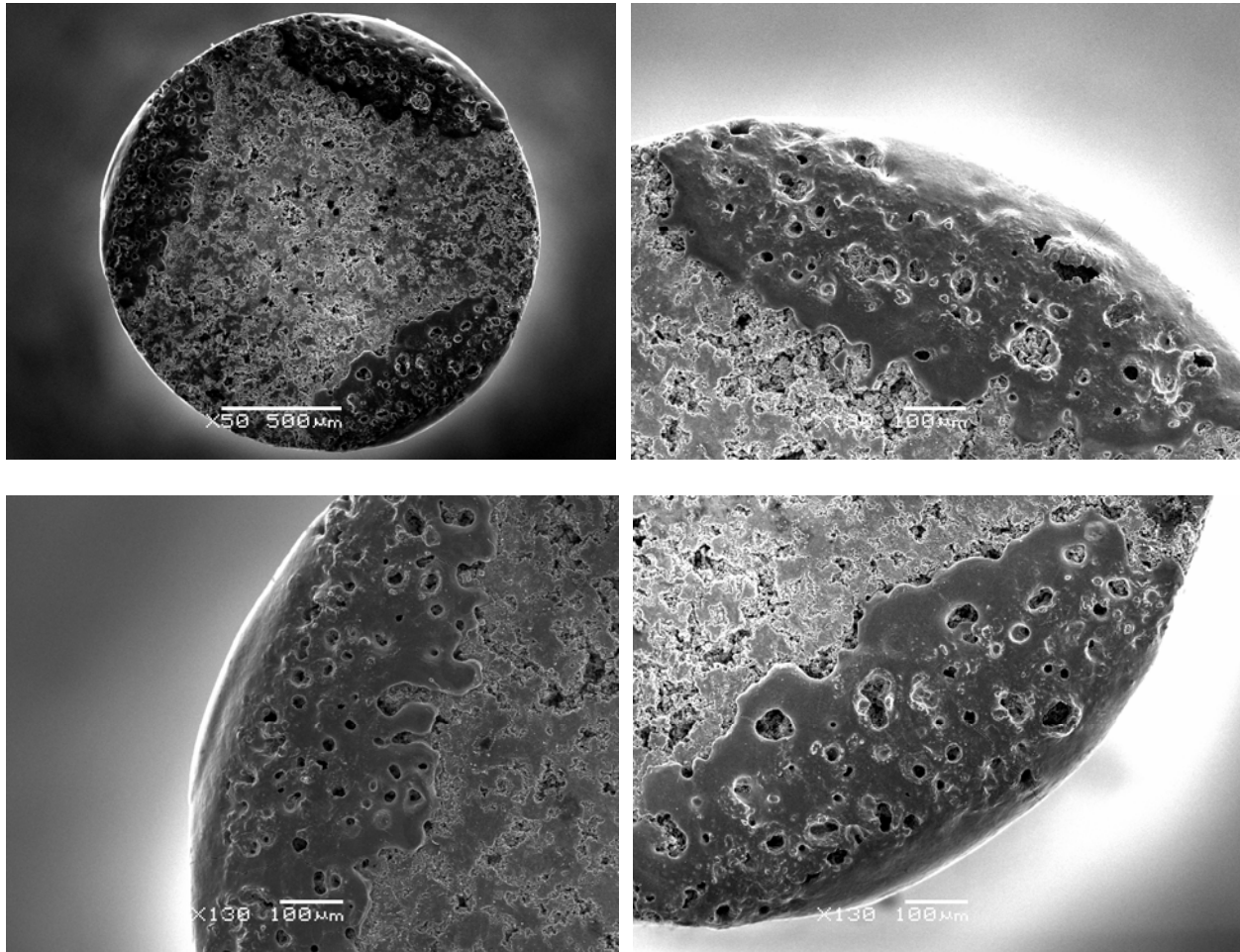
Figure 4.2: SEM image of TiC_p/Ni depositing electrode after single deposition in static mode.

Figure 4.3 shows the variations of current and voltage as functions of time during single deposition in static mode. The plot illustrates that the capacitors was partially discharged. The voltage level dropped from the initial value of 35V to 18V. Meanwhile, the current suddenly increased to 225A. After reaching the peak of 225A, the current rapidly declined back to 0A and the voltage leveled out at 18V.
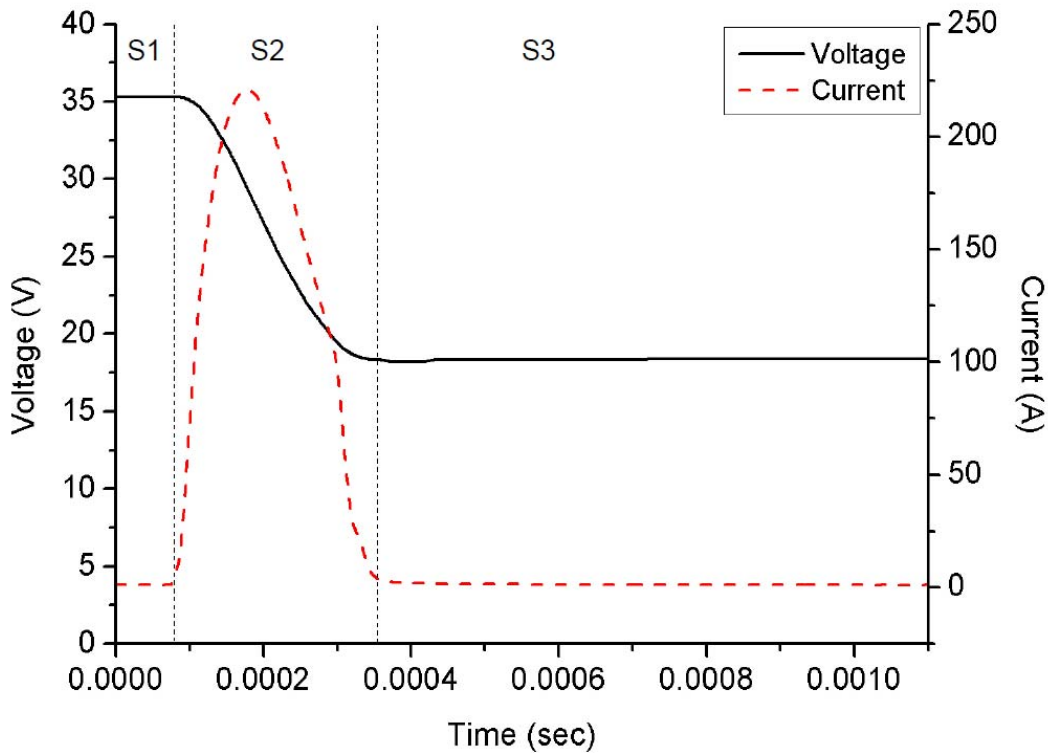
Figure 4.3: Current and Voltage waveform of ESD single deposition in static mode.

Based on observations of the surface morphology of Cu substrate, the surface of TiC_p/Ni electrode, SEM/EDS analysis results and the resultant current and voltage data, a model detailing the events taking place during the formation of a single deposition in static mode was developed. Figure 4.4 shows schematically the phenomenological model of the formation of one deposition in static mode. The model can be divided into 3 stages. In stage 1 (S1), the TiC_p/Ni electrode was manually brought into contact with the Cu substrate using the single axis stage. There was no further movement after the TiC_p/Ni electrode touched the Cu substrate. During this stage, the mechanical switch was opened and thus the ESD power supply was still in the charging mode. As a result, as illustrated in Figure 4.3, the voltage stayed in the pre-set level with 0A current.

The second stage began with the closing of the mechanical switch to initiate the discharge of the capacitors. At the beginning of stage 2 (S2), current quickly increased as the voltage dropped. It should be noted that at the microscopic level, there are no two surfaces that are completely flat [24]. When the electrode and the substrate were brought into contact, only the asperities on the two surfaces were actually touched (see Figure 4.4). As a result, the current was allowed to pass

42

through these local contact points during discharge. The resistant heating (I^2R) at these local contact areas caused melting and vaporizing of the electrode and the substrate materials (see Figure 4.2). In addition, because of the high current density at these local contact points, a spark was initiated between the electrode and the substrate. The spark expelled the molten Cu substrate forming a crater at the depositing location. A narrow gap was formed between the electrode and substrate preventing further discharge of the capacitors in stage 3 (S3).
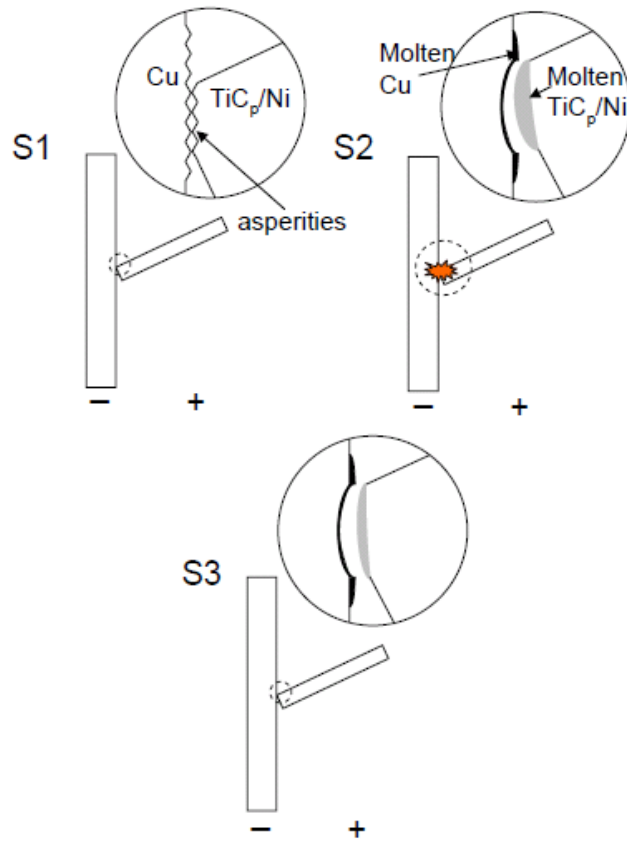
Figure 4.4: Phenomenological model of the formation of single deposition in static mode.

From Figure 4.1, the surface appearance of deposition spot is different from the observations reported by Liu *et al* [26]. In the latter case, the splash of the coating material was reported. This splash appearance of the coating material was the result of the spraying and impinging of molten coating droplets on the substrate surface [24, 28]. However, the crater appearance of the deposition spot in the present study was caused by the ejection of molten substrate material [33 – 35]. Furthermore, there was little materials transfer between the TiC$_p$/Ni electrode and the Cu substrate. The materials transfer was caused by the condensation of the vaporized TiC$_p$/Ni

electrode material on the Cu substrate. Based on this experimental observation, the spraying of coating material to the substrate did not occur.

In conventional ESD process, the electrode is momentarily sticking to the substrate [26, 30]. In the present study, the static mode did not mimic the ESD process entirely as the TiC_p/Ni electrode movement was restricted. As a result, to further examine the materials transfer mechanism, the electrode movement was not restricted as detailed in the next section.

4.2 Dynamic Deposition Mode

In dynamic mode, the deposition was made using the spring-loaded mechanical system as detailed in Chapter 3. The electrode was pulled back to a set position by the threaded rod. Upon releasing of the threaded rod, TiC_p/Ni electrode was brought into contact with the copper substrate to initiate the discharge and one deposition was made. Unlike the static deposition mode, the electrode was able to move further forward after the initial contact with the Cu substrate.

Figure 4.5 shows the SEM image of topographic morphology and accompanying EDS elemental mapping of one deposition of TiC_P/Ni onto Cu substrate in dynamic mode. The deposition spot had the same surface appearance as the static mode. An elliptical crater was created at the centre of the deposition area and the expelled molten Cu substrate solidified along the minor axis of the elliptical crater. A white region surrounding the crater was also observed. Unlike the static mode, there was quantitative evidence of TiC_p/Ni material transferred to the Cu substrate as shown on the EDS elemental mappings of Figure 4.5. The single deposition consisted of the Cu substrate and small amount of TiC and Ni. The electrode material was concentrated at the centre of the deposition spot. Liu *et al* [26] measured the chemical composition across the single-pulse deposition spots of four different coating – substrate couples. However, it is reported that the content of the electrode materials was higher at the edge of the deposition spot than the centre of the spot. Liu *et al* [26] believed that the lower electrode materials content at the centre of the deposition spot is due to dilution by the substrate (see Figure 4.6). The discrepancy between the literature and the present study will be explained in the later part of this section.
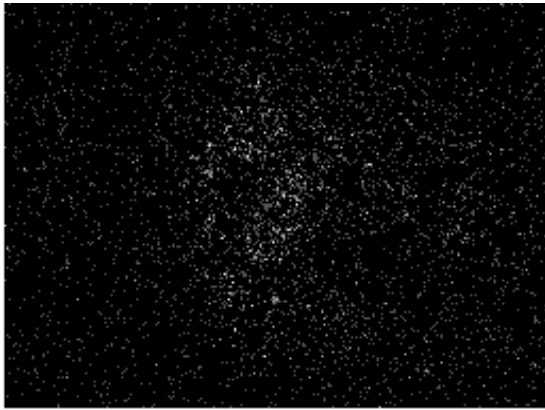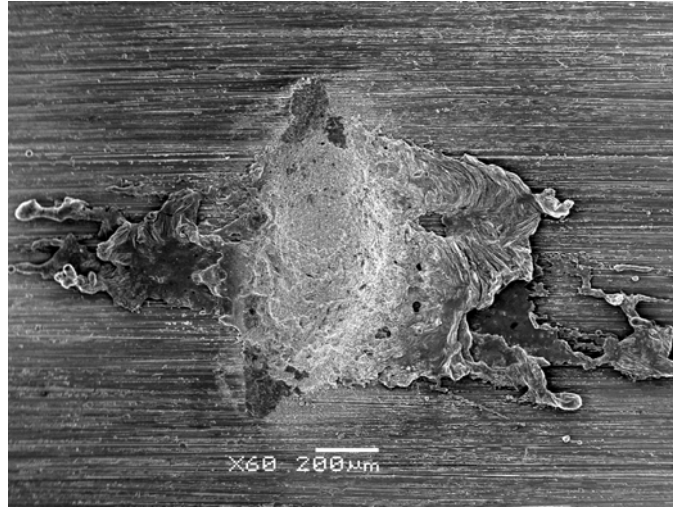
Ti Ka1
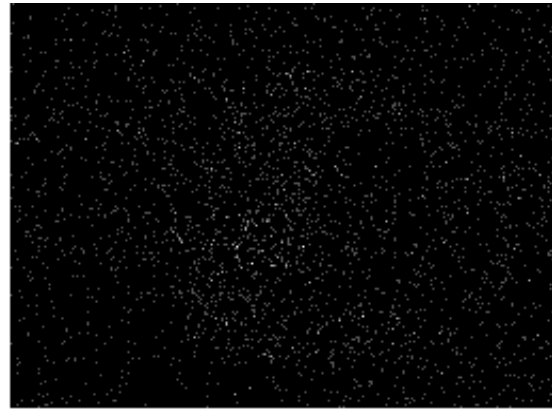
Ni Ka1

Figure 4.5: SEM image and EDS elemental mapping of ESD TiC$_p$/Ni single deposition in dynamic mode.
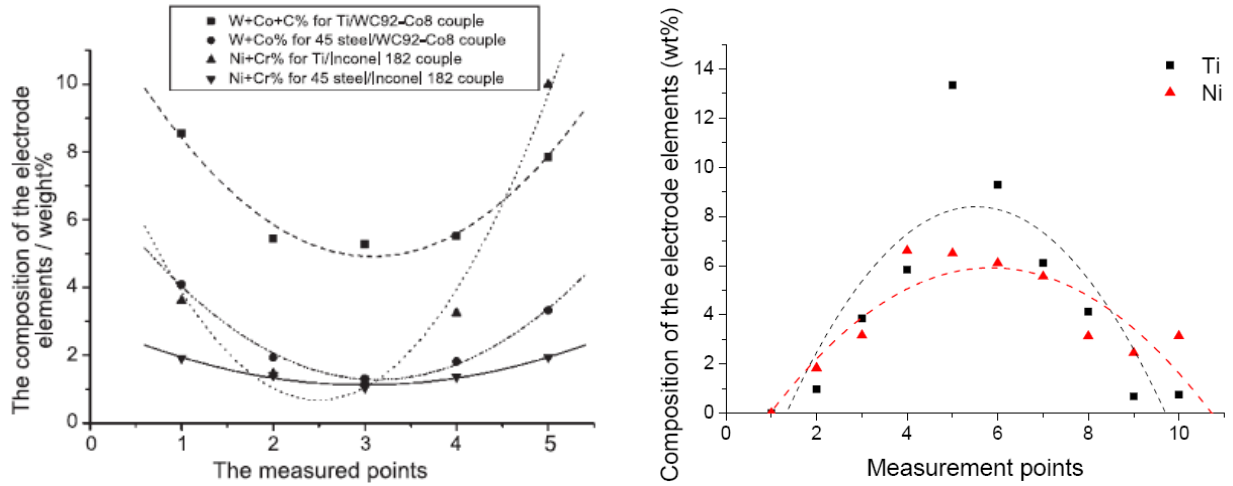
Figure 4.6: The composition of the electrode elements at different locations. On the left is the data of Liu *et al* [26] and on the right is the data from the present study.

Figure 4.7 shows the SEM images of the TiC$_p$/Ni electrode after one deposition in dynamic mode. A molten structure was evident at the edge of the TiC$_p$/Ni depositing electrode. In addition, copper was found at the edge of the molten area on TiC$_p$/Ni electrode. In fact, SEM/EDS elemental mapping shows the presence of copper at both the top and bottom of the depositing area on the TiC$_p$/Ni electrode. The observation indicates that copper was picked up during the deposition process.
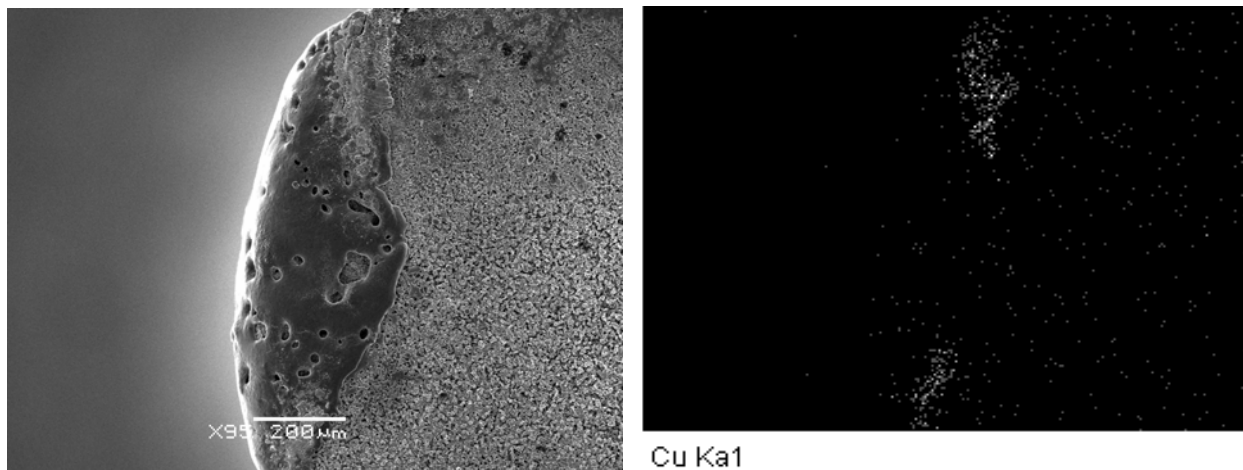
Figure 4.7: SEM image and EDS elemental mapping of TiC$_p$/Ni depositing electrode after single deposition in dynamic mode.

Figure 4.8 shows the current, voltage, and displacement as function of time during single deposition in dynamic mode. In this case, the capacitors were completely discharged during the deposition process. The voltage level dropped from 35V to 0V and two current peaks were observed. The discharge cycle can be divided into two halves. First, the voltage level dropped from the initial value of 35V to 16V. Meanwhile, the current suddenly increased to 350A and the displacement kept rising. After the current reaching the peak of 350A, the current rapidly declined to 50A and the voltage declined linearly to 13V. At this stage, the displacement curve reached its peak at 4µm. In the second half of the discharge cycle, the voltage decreased rapidly from 13V to 1V. At the same time, the current quickly increased to 225A and the displacement declined slowly. After the current reaching the second peak of 225A, the current rapidly declined to 0A and the voltage leveled at 0V.
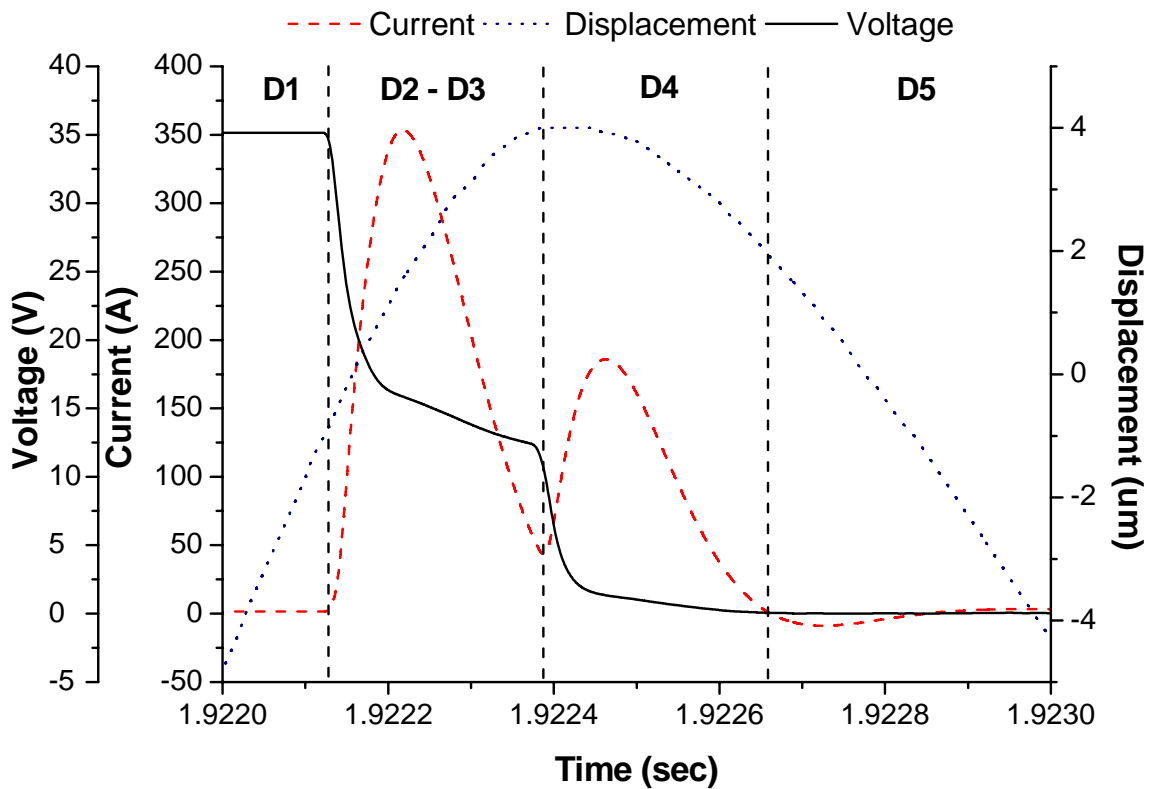
Figure 4.8: Current, Voltage, and Displacement waveform of ESD single deposition in dynamic mode.

A phenomenological model was developed for the dynamic deposition mode based on the above observations. Figure 4.9 shows the model of the formation of one deposition in dynamic mode. This model can be divided into 4 stages.

In stage 1 (D1), the depositing electrode was traveling towards to the substrate as indicated by the increase in the displacement curve on Figure 4.8. At this point, no physical contact was made between the electrode and the substrate. Thus, there was no current flow at this moment and the voltage stayed at the pre-set level of 35V. In stage 2 (D2 – D3), the depositing electrode was brought to contact with the substrate initiating the discharge. Voltage started to drop rapidly and gave rise to the first current peak. Similar to the static mode, both the electrode and substrate material were rapidly heated and melt at the local contact area. This leaded to the formation of melt pool on the substrate and the thin film of molten materials on the electrode surface. After a violent ejection of the molten substrate material, there was a momentarily gap between the electrode and the substrate. As a result, current started to decline. However, the continuous forward motion of the electrode caused it to contact the substrate again in stage 3 (D4). As it is evidenced from the displacement curve (see Figure 4.8), the displacement of the TiC_p/Ni electrode reached its peak at this stage. Meanwhile, materials transfer occurred between the electrode and substrate by direct contact of molten metal to molten metal. The thin film of molten materials of both the electrode and substrate fused and mixed together through physical contact. The electrode materials were deposited and solidified on the substrate at the points of contact. Moreover, during the materials transfer, part of the molten substrate material (Cu) was adhered and solidified on the electrode surface as shown on Figure 4.7. This is due to molten substrate was ejected to the edge of the crater. Meanwhile, the capacitors discharged the remaining energy and created the second current peak. In the last stage (D5), the TiC_p/Ni electrode was retracted to prevent the local bonding between the Cu substrate and the TiC_p/Ni electrode. Finally, the TiC_p/Ni electrode returned to its original position for subsequent depositions.
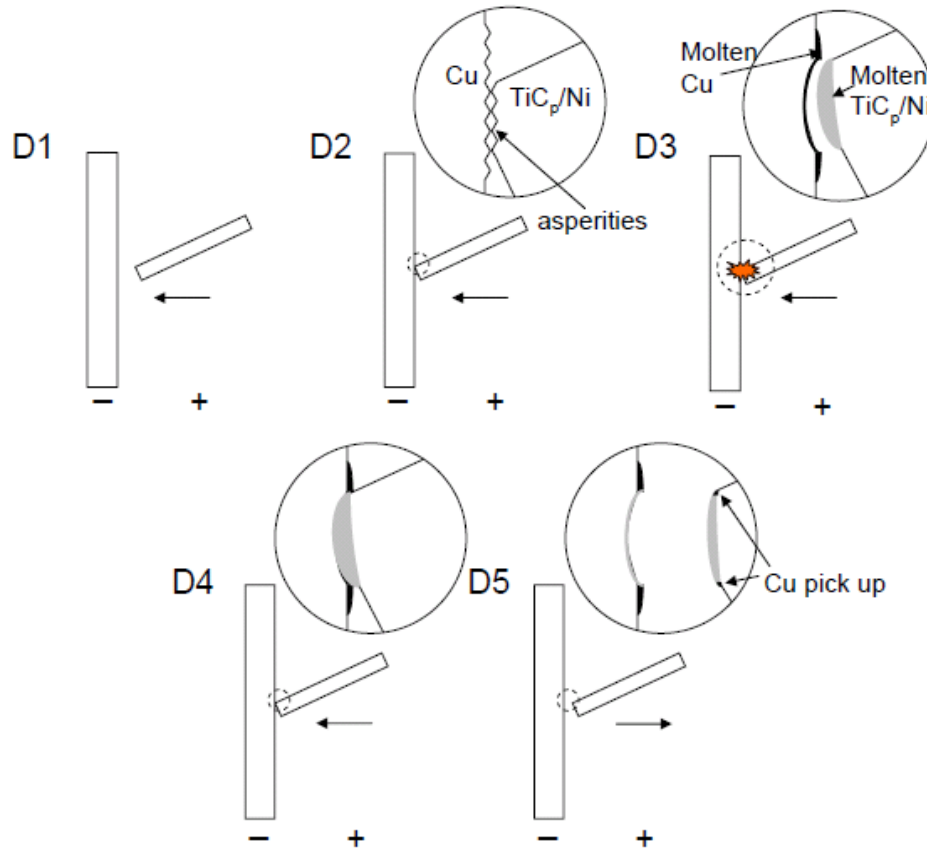
Figure 4.9: Phenomenological model of the formation of single deposition in dynamic mode.

As mentioned previously, Liu *et al* [26] reported that the content of the electrode material was higher at the edge than at the centre of the deposition spot (see Figure 4.6). However, in the present study, the content of the electrode materials was much more concentrated at the centre of the deposition crater. The discrepancy between the literature and present study can be explained by examining the material transfer mechanism. In literature, it was suggested that a molten droplet and molten pool were formed on the electrode and substrate, respectively. The molten droplet detached from the electrode surface and impinged to the molten pool on the substrate by spraying [26, 30]. The deposited electrode materials content was diluted by the molten substrate during the deposition process. This resulted in higher electrode contents at the edge of the deposition spot. However, in the present study, molten droplet was not observed on the electrode surface and the spraying mode of materials transfer did not occur as evidenced in the static mode deposition. According to the above phenomenological model, the materials transfer mechanism between the electrode and the substrate was primarily through direct molten metal to molten

49

metal contact. This is similar to the hypothesis suggested by Galinov *et al* [22]. Galinov *et al* [22] proposed that the molten material on the electrode surface was partly driven away and adhered to the substrate surface. Since the material transfer was through the physical contact between the electrode and the substrate at the centre of the deposition crater, the content of the electrode material was expectedly concentrated at the centre of the deposition spot.

4.3 Comparison of ESD to Other Joining and Welding Processes

In the previous sections, the surface morphology, the materials transfer mechanism and phenomenological model detailing the events taking place during one deposition have been presented and discussed. In the present study, ESD is viewed as a coating process. However, Electro-Spark Deposition (ESD) is often described as a pulsed-arc microwelding process [22, 26, 30]. Therefore, a comparison between ESD and other joining or welding processes was performed.

There are many differences between the ESD and commonly used arc welding processes. For instance, the spark will ignite and extinguish alternately during the ESD process. However, the arc will burn continuously throughout the entire arc welding process [25]. The depositing electrode will be momentarily striking the surface of the substrate in the ESD process, while in the arc welding process, there will be no physical contact between the electrode and the substrate as soon as an arc is ignited. Furthermore, the electrode will be joined and broken away from the substrate alternately due to the electrode motion in the ESD process, while in the arc welding process, the electrode motion is not required.

As a result, it is inappropriate to describe the ESD process as an arc welding process. By examining the voltage and current characteristic and the events taken place during one deposition, the ESD process shows many similarities to the percussion and capacitor discharge welding. These two welding processes belong to the family of resistance welding, in which resistance heating and upset force are often used to join parts without filler metal [33 – 35, 36 – 39].

The principles of the aforementioned welding processes (see Figure 4.10) are similar to the proposed phenomenological model of dynamic mode. The parts to be joined or welded are clamped to the fixtures that are connected to the power source. Then, one of the parts is moved towards to the other, at the local points of contact, resistance heating occurs, the high current density leads to rapid melting and vaporization of the metal at the faying surface, and minute arc is ignited. A narrow opening is generated as the metal melts faster than the moving part towards the other end. The arc is extinguished as the two parts are in contact again. Finally, a weld is made by the application of upset force to bring the molten interfaces in full contact [33 – 35, 36 – 39].
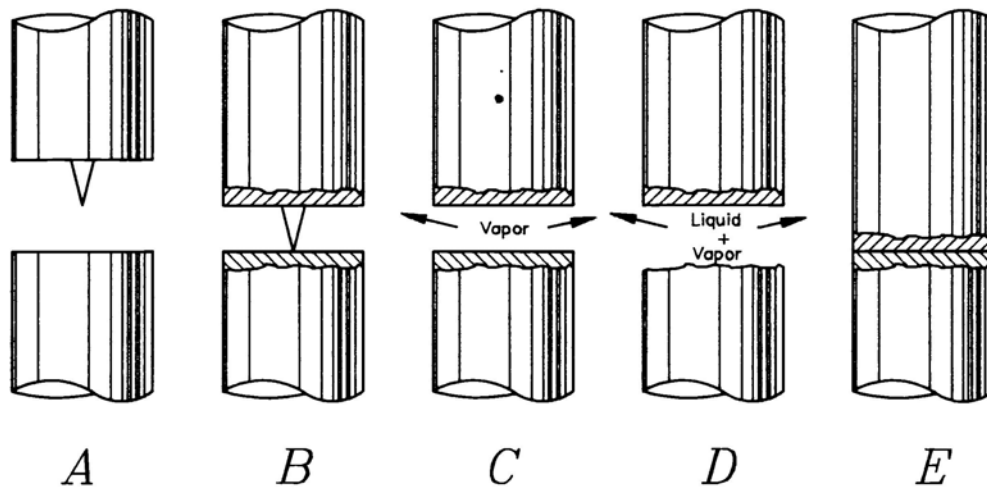
Figure 4.10: Schematic diagram of Capacitor Discharge Welding process. A. cathode positioned above anode; B. arc ignition at the welding top; C. plasma expulsion; D. ejection and condensation of plasma into small metal particles; E. Joint after electrode contact [33].

Another similarity of the ESD process to the aforementioned welding processes is the electrical characteristic. Both percussion and capacitor discharge welding use the capacitors as the power source. A typical current pulse of percussion welding is shown on Figure 4.11, which illustrates the two current peaks profile, and matches with the electrical characteristic in the present study. The similarity in the electrical characteristic is attributed to the principle of the welding process mentioned previously. When the parts to be joined are sufficiently separated, there is no current flow, and then the current increase rapidly upon contact and melting of the materials occurs. The decrease in current flow is associated with the narrow opening as the metal melts faster than the moving part, and finally the materials engage, and shorting occurs with corresponding increase in current flow. However, there is dissimilarity between the ESD process to the percussion and

51

capacitor discharge welding process. Owning to the electrode motion that requires to avoid welding the electrode to the substrate in the ESD process, the electrode will never be joined permanently to the substrate.

Based on the similarities and dissimilarities of the ESD process to the existing welding processes, it can be concluded that the ESD process is more similar to the percussion and capacitor discharge welding process than the arc welding process.
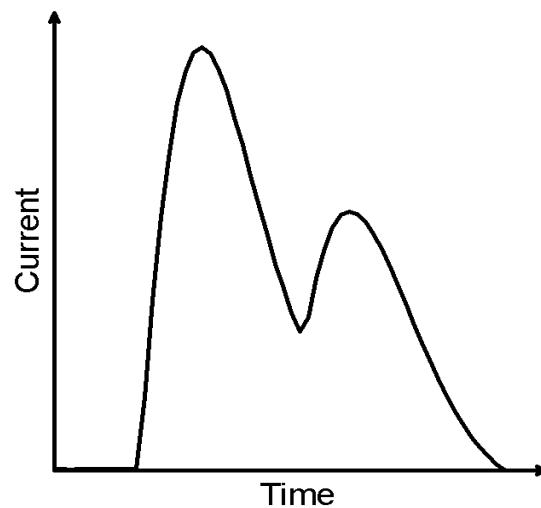
Figure 4.11: Current pulse of percussion welding [19].

4.4   Summary

In this chapter, static and dynamic deposition modes were performed to study the formation of one deposition and the material transfer mechanism during ESD process. Based on the experimental observations of the surface characteristic of one deposition, the electrode surface and the chemical analysis, the coating material was transferred to the substrate through direct molten metal to molten metal contact. A phenomenological model detailing the events taken place during of the formation of one ESD deposition was developed for the each deposition mode. At the end, the proposed model in the present work is used to compare the similar and dissimilar phenomena to the existing welding processes. The ESD process is more similar to the percussion and capacitor discharge welding process than the arc welding process.

52

Chapter 5

5 ESD process characteristic and Coating Evolution

5.1 Process parameter: Effect of Voltage on Electro-Spark Deposition

ESD coatings were deposited using various voltage levels ranging from 25V to 65V to study the effect of voltage on ESD. Since the previous studies only focused on the materials combinations and coating performance, limited work have been done to correlate the applied voltage to the resultant coating characteristic. The average length, width, crater depth, the cross-section of the ESD coating at different voltage levels, the materials transfer trend and efficiency at different voltage levels will be addressed and discussed in this section.

5.1.1 ESD Equipment Characteristic

The ESD circuitry used in this study was designed and built at the UW CAMJ laboratory as described previously in Chapter 3. Figure 5.1 shows the current and voltage as functions of time during single deposition at 25V, 35V, and 45V, respectively. All three current and voltage waveforms profiles show many similarities. The voltage first was decreased sharply to 16V, linearly declined to 13V and finally dropped to 0V. In all cases, two current peaks were observed and the total discharge cycle was approximately 400µs. The characteristic of these electrical discharge profiles was detailed and discussed in Chapter 4.

In the present study, the ESD circuitry was a simple resistor capacitor (RC) circuit, which was driven by a constant voltage source power supply [40]. When discharging the capacitors, the out-flowing current of the capacitor must equal to the in-flowing current as described by Kirchhoff's current law [40]. The governing differential equation of this relationship is:

$$R\frac{dV}{dt} + \frac{V}{C} = 0 \tag{5.1}$$

where, R is the resistance, V is the voltage, C is the capacitance of the capacitor, and t is the discharging time. The solution to the above differential equation is:

$$V = V_0 e^{-t/(RC)} \tag{5.2}$$

where V_0 is the initial voltage of the capacitor prior to discharge and other variables are as previously described. From the above equation, the capacitor's voltage decreases exponentially with time. The rate of discharge is governed by the capacitive time constant, $\tau = RC$. As a result, the discharging time is independent to amount of energy stored in the capacitors. This is in good agreement with the observed data of the present study since the discharge was completed within 400 μs.

(a)

(b)

(c)
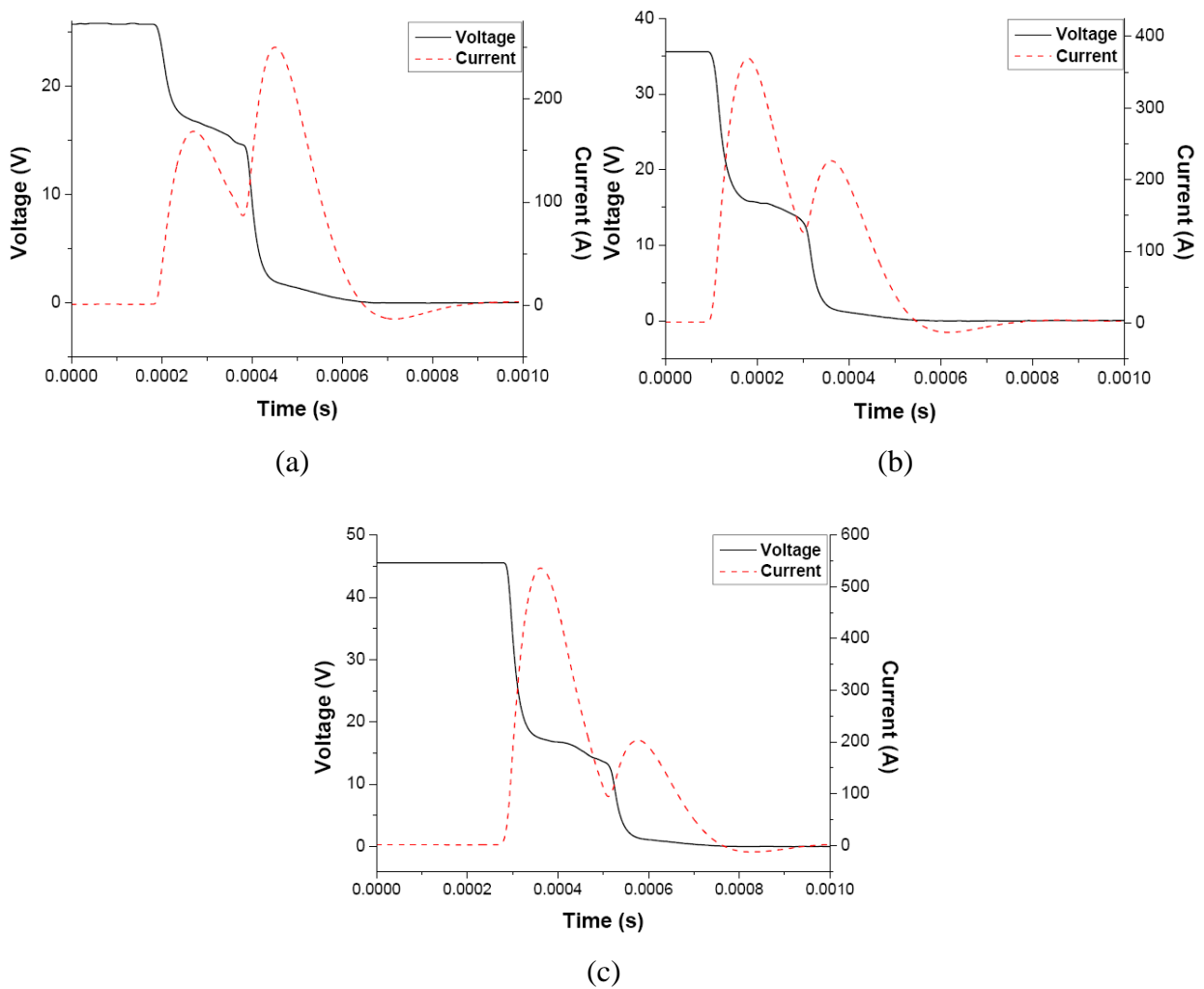
Figure 5.1: Electrical Characteristic of single deposition for a) 25V, b) 35V, c) 45V applied voltage.

Table 5.1 summarizes the electrical characteristic of the ESD single discharge at 25V, 35V and 45V. It should be noted that the electrical characteristic was not available for 65V due to limitations of the signal conditioning box of the DAQ system. The electrical characteristic of the ESD single discharge was represented by the average pulse energy, E_p for five different runs at each of the voltage levels. The pulse energy was calculated from the current and voltage waveform [22, 24], as followed:

$$E_p = \int_0^{t_p} V(t) \cdot I(t) dt \tag{5.3}$$

where $V(t)$ is the time-voltage data during discharge, $I(t)$ is a time-current data during discharge and t_p is the total pulse duration. From the data, as the voltage level increased, the average first current peak amplitude and the average electric pulse energy increased. However, the average second current peak amplitude stayed relatively constant at approximately 234A.

Table 5.1: Summary of the electrical characteristic of single deposition.

Voltage (V)	Avg. 1st Current peak (A)	Avg. 2nd Current peak (A)	Avg. Pulse energy (J)
25	183	243	0.488
35	371	235	0.886
45	541	225	1.449

*Pulse duration at all voltage levels is approx. 400µs

5.1.2 Effect of Voltage on ESD Single Deposition

In this section, the effects of voltage on ESD single deposition will be addressed. The ESD single deposition was performed using the spring-loaded mechanical apparatus at 25V, 35V, 45V, and 65V. As detailed in Chapter 3, the ESD single deposition was performed using the dynamic deposition mode setup.

Figure 5.2 shows the SEM micrograph of the surface morphologies of a single deposit at 25V, 35V, 45V and 65V, respectively. It should be noted that all four micrographs were taken using different magnification in order to capture the entire deposition spot. In general, the surface morphology of a single deposition at different voltage settings contained an elliptical shaped

55

crater at the centre of the deposition spot. The molten materials were expelled and solidified on the periphery of the deposition crater. As the voltage level increased, the size of the deposition spot and the amount of the expelled or ejected molten materials increased as well. Also, the expelled molten materials from the crater were not evenly distributed. The molten materials were mostly expelled along the minor axis direction of the elliptical crater. On the other hand, there was little molten material ejected along the major axis direction of the elliptical crater.
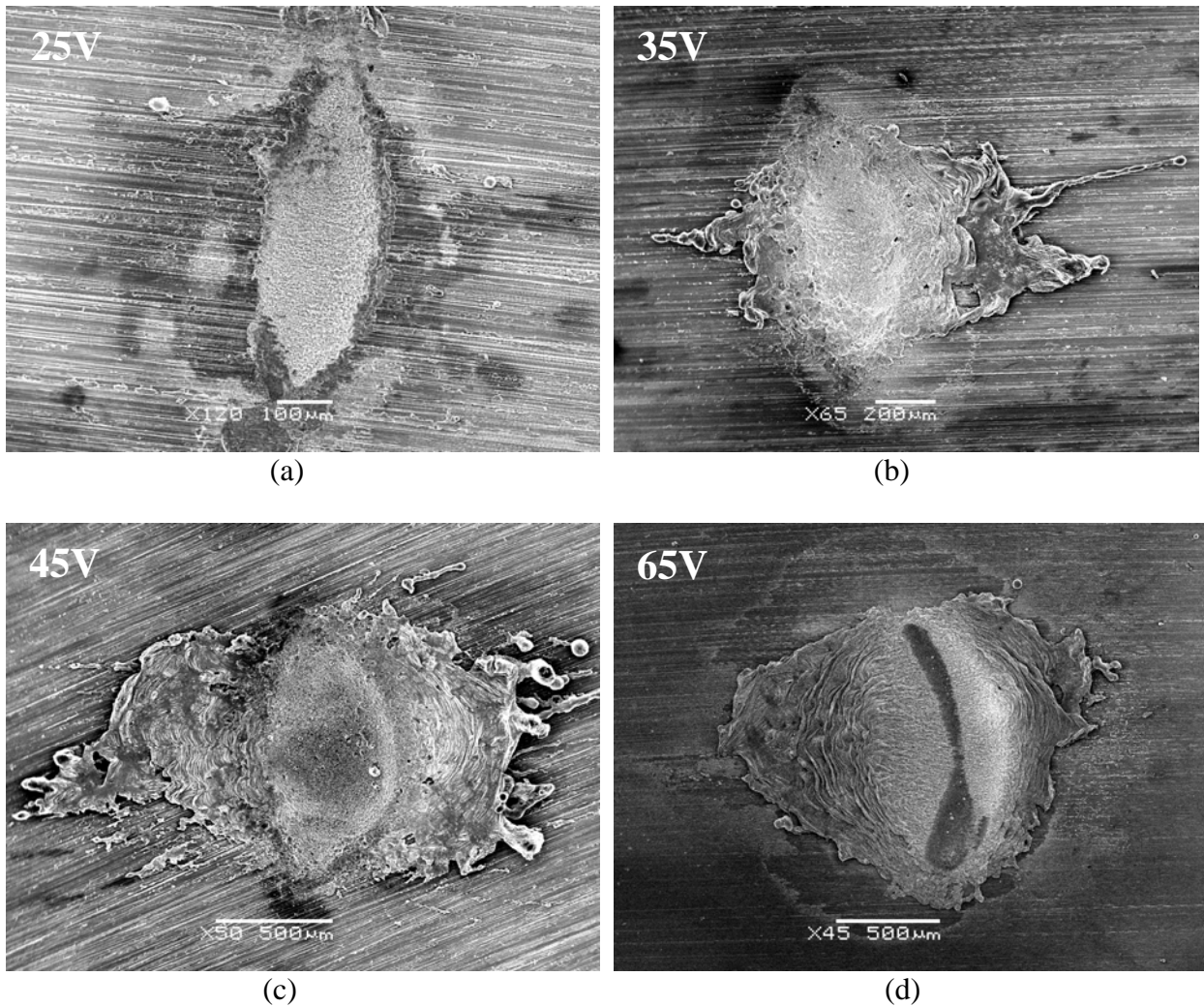
Figure 5.2: SEM micrograph of the surface morphologies of single deposition at a) 25V, b) 35V, c) 45V, d) 65V applied voltage.

The elliptical appearance of the crater was the result of the geometry of the depositing electrode as it contacted the substrate. As mentioned in Chapter 4, the spatter appearance was due to the ejection of the molten substrate. Furthermore, a white region surrounding the crater was the

56

result of cathode pulverization or the surface oxide cleaning action that was often observed in reversed polarity GTAW [26].

The one dimensional contour profiles of the ESD single deposition at 25V, 35V, 45V and 65V are shown in Figure 5.3. Each contour profile was scanned by the optical profiler along the x-direction through the deepest point of the deposition spot. The scanning procedure was as detailed in Chapter 3. In the present study, the original surface of the substrate was used as the zero reference level which was represented by the horizontal dashed line in Figure 5.3. From the contour profiles, as the voltage level increased, the depth and width of the crater increased and more molten metal was thrown further away from the centre of the deposition spot.

In Table 5.1, as the applied voltage increased, the current flow in the system also increased. As mentioned earlier, the heat generated during the ESD process is by resistant heating which is proportional to the current flow ($Q = I^2R$). As a result, the increase in current flow in the system led to the increase in heat input and thus, the amount of the molten substrate and the size of the crater.

In addition, during the deposition process, a spark was ignited. Burleigh and Eagar [41] proposed that the arc force, F, can be mathematically expressed as:-

$$F = \frac{\mu_o I^2}{8\pi}\left(1 + 2\ln\frac{R_2}{R_1}\right)$$ (5.4)

where I is the welding current, μ_0 is the permeability of free space, R_1 is the radius of the arc at the welding electrode and R_2 is the radius of the arc at the substrate. From the above equation, the increase in the deposition current increases the corresponding arc force F. As a result, the molten metal was expelled further away from the crater.
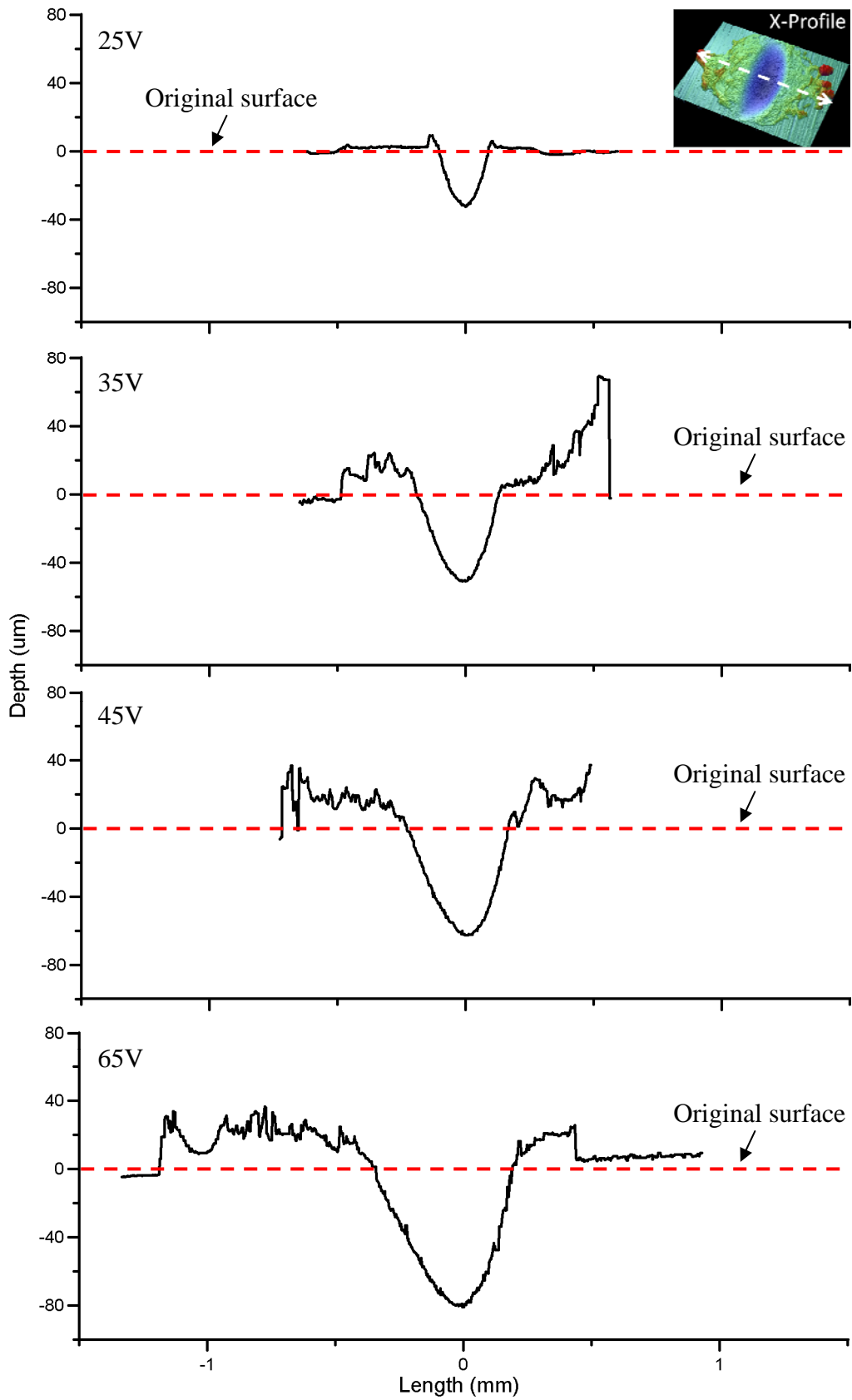
Figure 5.3: One dimensional contour profile (x-direction) of ESD single deposition.

5.1.3 Effect of Voltage on ESD Materials Transfer

Figures 5.4a and 5.4b show the weight gained by the substrate and the weight lost by the TiC_p/Ni depositing electrode during the ESD process at different voltage settings. From the figures, the Cu substrate weight gain increased as the voltage and the numbers of depositions increased. The weight loss data shows the similar trend. The TiC_p/Ni depositing electrode lost more as the voltage and the numbers of depositions increased. Also, the TiC_p/Ni weight loss was always greater than Cu weight gain at all voltage levels. It is because not all the vaporized materials are re-condensed on the surface of the substrate.
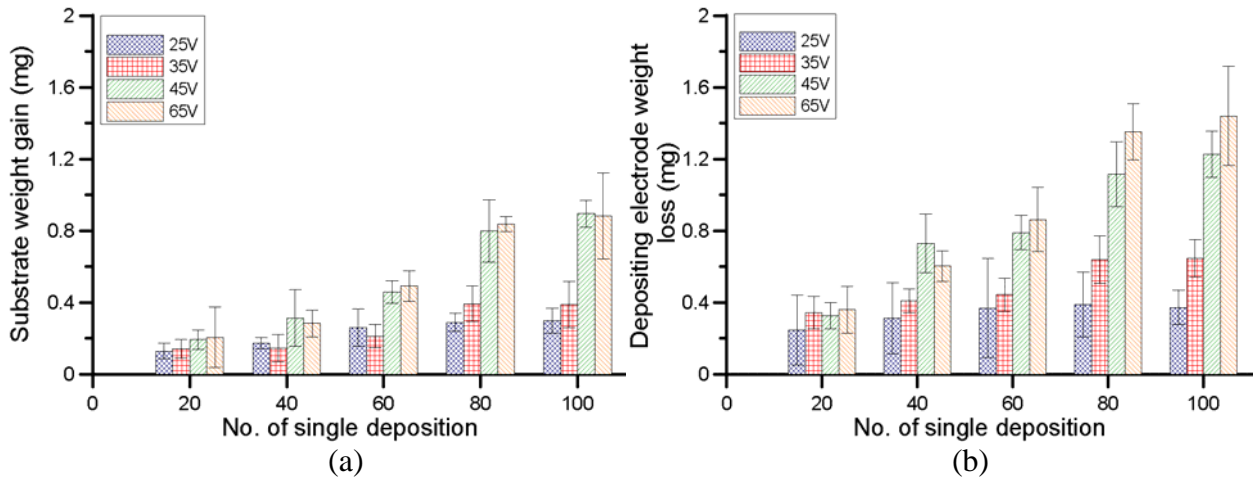
Figure 5.4: The weight gained by the Cu substrate (a) and the weight lost by the TiC_p/Ni depositing electrode (b) during the ESD process.
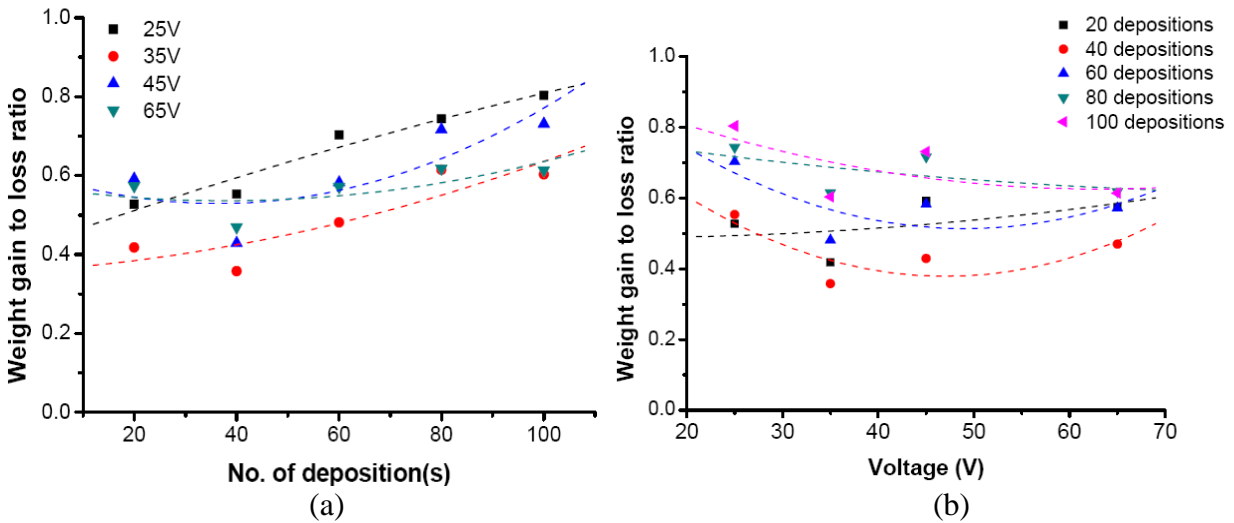
Figure 5.5: Weight gain to loss ratio as a function of a) number of depositions and b) the applied voltage.

Figure 5.5a and 5.5b show ratio between the weight gained to the weight lost as a function of number of depositions and voltage, respectively. This ratio can also be considered as the efficiency of the ESD process. A high ratio implies that more weight was successfully transferred to the substrate to form the coating than the weight lost by both the substrate and the depositing electrode. Figure 5.5a shows that the weight gain to loss ratio increased with the number of depositions for all voltage levels. However, in Figure 5.5b, the weight gain to loss ratio decreased as the applied voltage increased.

In order to understand the effect of voltage on material transfer during the ESD process, the theory of electrode erosion by electrical discharge should be re-visited. Galinov *et al* [22] proposed that the electrode erosion by electrical discharge could be taken place in three distinct phases: solid, liquid or vapour. The solid or vapour phase erosion of the electrode would lead to a net loss while only the liquid phase had a positive net gain on materials transfer during the ESD process. In solid phase erosion, the eroded solid particles by mechanical impact would not adhere to either the electrode or the substrate surfaces. In vapour phase erosion, the vaporized electrode and substrate materials mostly dissipated to the surrounding. Only small amount of the vaporized materials were condensed and re-deposited on the substrate surface [42 – 46].

In liquid phase erosion, a portion of the molten electrode and molten substrate were coupled due to the molten-metal to molten-metal contact and coating was formed on the substrate surface. In this study, the molten-metal to molten-metal contact was clearly illustrated by the comparison between the static and dynamic single deposition testing. As a result, in this study, the main contribution to the Cu substrate weight gain was obtained through the TiC_p/Ni liquid phase erosion. Meanwhile, the TiC_p/Ni electrode weight loss was mostly caused by liquid phase erosion. However, since the electrode weight loss was always much greater than the substrate weight gain, the TiC_p/Ni electrode was also eroded by vapour and perhaps solid phase. In addition, the three different phase erosion could also occur at Cu substrate. The Cu weight gain was the net result of weight gain from the TiC_p/Ni deposit minus the Cu weight loss. Consequently, increasing the applied voltage did not necessary lead to the improvement of the efficiency of the ESD process. It is because increasing the applied voltage did not only increase

60

the TiC_p/Ni erosion, but also increased the Cu substrate erosion. Finally, it leads to the decrease in the efficiency of materials transfer between the TiC_p/Ni electrode and Cu substrate.

5.1.4   Effect of Voltage on ESD Coatings

The ESD coatings at different applied voltages (25V, 35V, 45V, and 65V) were obtained by having ten depositions at the same spot as detailed in Chapter 3. Figure 5.6 shows the SEM micrographs of the cross-section of ESD coating after performing ten depositions at the same location for different applied voltages. It should be noted that the SEM micrographs were taken at different magnifications to obtain the overall cross-sectional view. In each SEM micrograph of Figure 5.6, a continuous and dense coating was observed on the Cu substrate. The increased applied voltage did not affect the overall coating thickness which apparently varied across the entire spot. No delamination was observed between the coating and substrate at the centre of the deposition spot. However, cracks and pores were observed within the coatings. The formation of cracks within the coatings was caused by the repetitive mechanical impact and the thermal stress relief cracking [47].
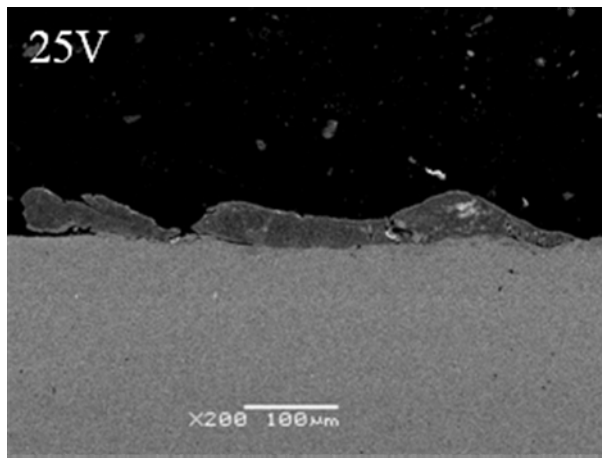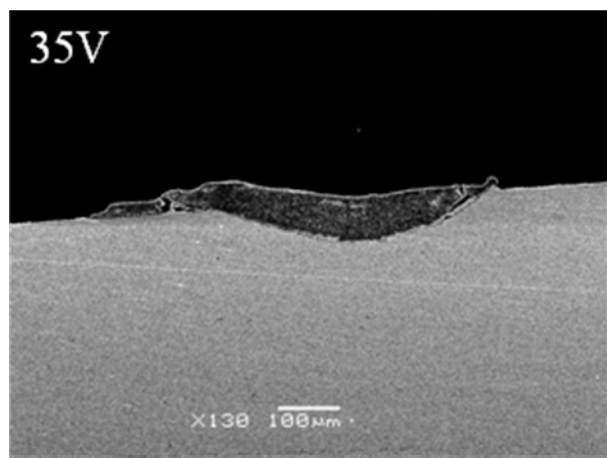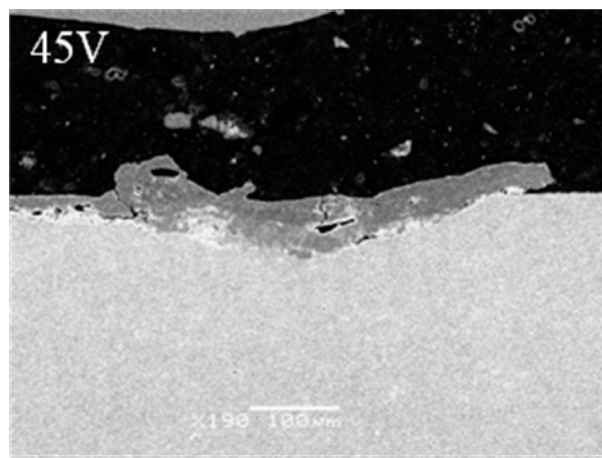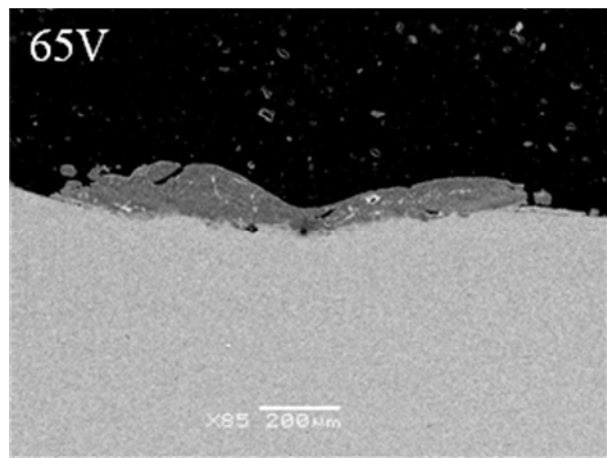
Figure 5.6: SEM micrograph of the cross-section of ESD coating at a) 25V, b) 35V, c) 45V, d) 65V applied voltage.

Figure 5.7a to Figure 5.7h show the edge and the center of the ESD coatings of Figure 5.6 using higher magnification. By comparing these coatings, the cracks were found to be initiated from the edge of the deposition crater and propagated underneath the coating to the Cu substrate. As mentioned previously, there are no gaps or pores observed between the coatings and the substrate at the centre of the deposition spot. It should be noted that the edge of the deposition crater was where all the molten material were expelled to and re-solidified. At 25V (see Figures 5.7a and 5.7b), the crack initiated, but didn't propagate very far into the Cu substrate. When the voltage was set at 35V, the crack reached the centre of the deposition spot (see Figures 5.7c and 5.7d). As the voltage was increased to 45V and later to 65V, the cracks size did not propagate very far from the edge of the crater (see Figures 5.7e to 5.7h).

As discussed previously, ESD is a self-cleaning process in which the surface oxide film was removed by catholic cleaning during electrical discharge. In addition, the spark expelled the molten material outward from the center of the crater, thereby removing the molten contaminants from the bonding surface. Previous studies have shown that surface contaminants and cleanliness of the joining surfaces are crucial to the joint quality and the elimination of the joint defects [22, 24, 26]. As a result, in Figures 5.7b, 5.7d, 5.7f and 5.7h, the TiC$_p$/Ni coating bonded well to the Cu substrate at the centre of the crater. As mentioned previously, cracks were originated from the edge of the crater where the expelled molten materials along with the contaminants were collected. As a result, bonding did not occur easily at the edge of the crater and thus cracking could easily initiate. Furthermore, when the applied voltage was below 35V, the arc force was not high enough to remove and to expel the surface contaminants away from the bonding area. In these low voltage settings, cracks initiated and propagated at the Cu substrate underneath the bonding interface. As the applied voltage increased, the resultant arc force increased. This would expel more contaminant and thus better cleaning at the bonding interface thereby preventing the crack from initiation and propagation.

	Edge	Centre
25V		
35V		
45V		
65V		
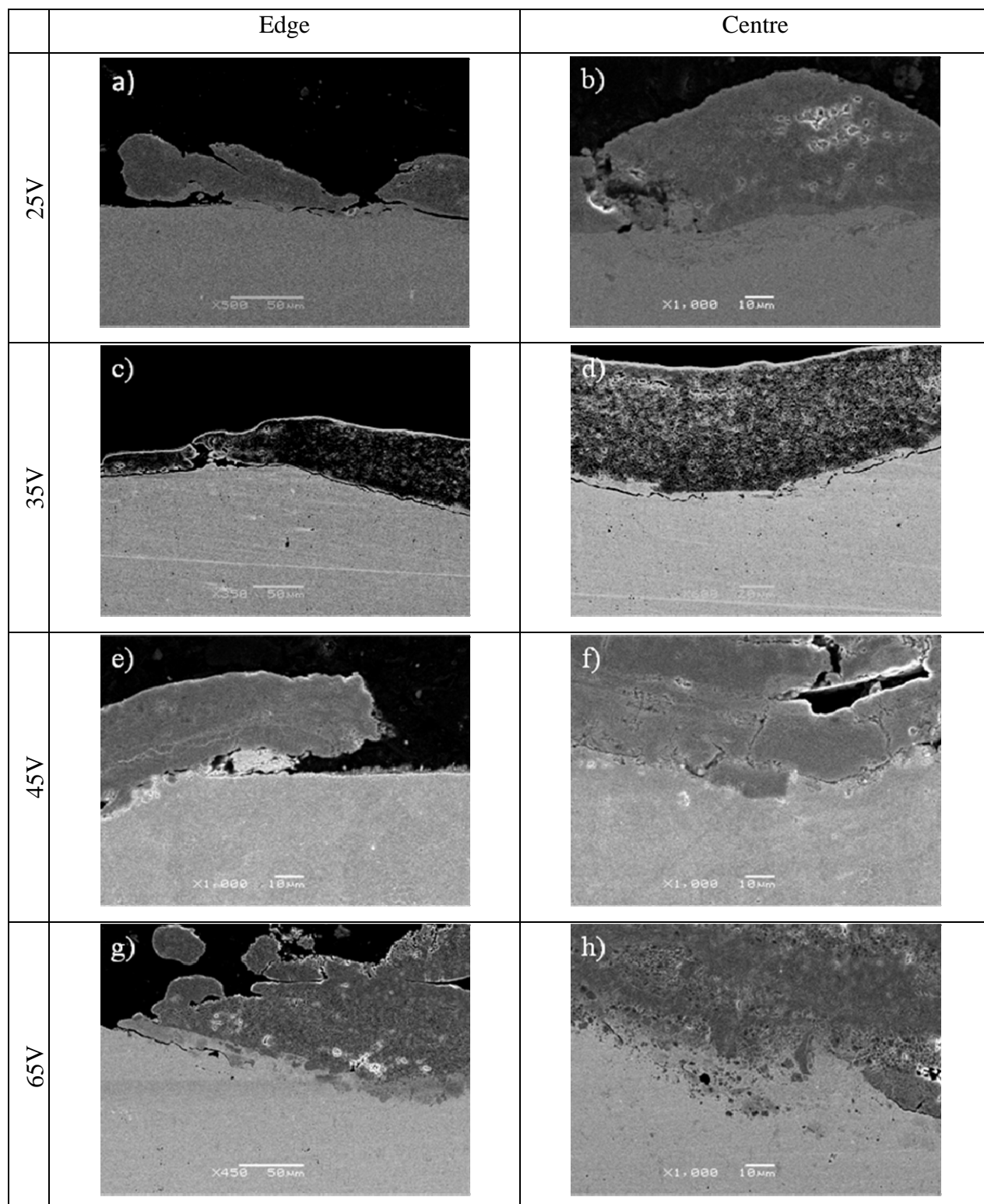
Figure 5.7: SEM micrograph of cross-section of ESD coating at different applied voltage at higher magnification. a-b) 25V, c-d) 35V, e-f) 45V, g-h) 65V.

5.2   Evolution of the ESD Coating by Multi Deposits on the Same Spot

In the previous discussion, this study has been focused on one deposit and the successive build up of ESD coating has never been discussed. In this section, multiple deposits on the same spot of the copper substrate were performed at 35V applied voltage. The spot would eventually have up to 10 single deposits. Through the evolution of the multiple deposits on the same spot, the ESD coating build up was studied.

Figure 5.8 a) to h) show the SEM topography micrograph of the first 8 TiC_p/Ni multi-single depositions on the same spot. Figure 5.8 i) to l) show the topography of the TiC_p/Ni coating after 20, 40, 60, and 80 depositions on the same spot, respectively. As illustrated by the figures, the deposition spot was progressively bigger and more TiC_p/Ni material was deposited on the substrate as the number of depositions increased. As the TiC_p/Ni coating was building up, the surface of the deposition spot was getting rougher. However, the deposited TiC_p/Ni coating was not evenly built across the entire deposition spot. It is also observed on Figure 5.8b that, not much TiC_p/Ni is deposited on the substrate; rather, the deposition spot illustrates the same surface morphology as the single deposition.

As shown from the SEM micrographs, the ESD coating is the build up of the deposits by depositing the TiC/Ni on the previous deposition spot. Initially, the first deposition is identical to the single deposition described in the previous Chapter. In the latter case, a crater was formed at the centre as the surface contaminant was removed from the deposition spot. The surface morphology of the deposition spot changed from the crater to the typical splash appearance of ESD coating [22, 24, 26] as shown on Figure 5.9a after three consecutive deposits. As the coating continued to build up, the coating began to crack and propagate as shown on Figure 5.9b and Figure 5.9c. A dense coating was formed but separated by cracks (see Figure 5.9d) and the splash appearance was no longer observed.
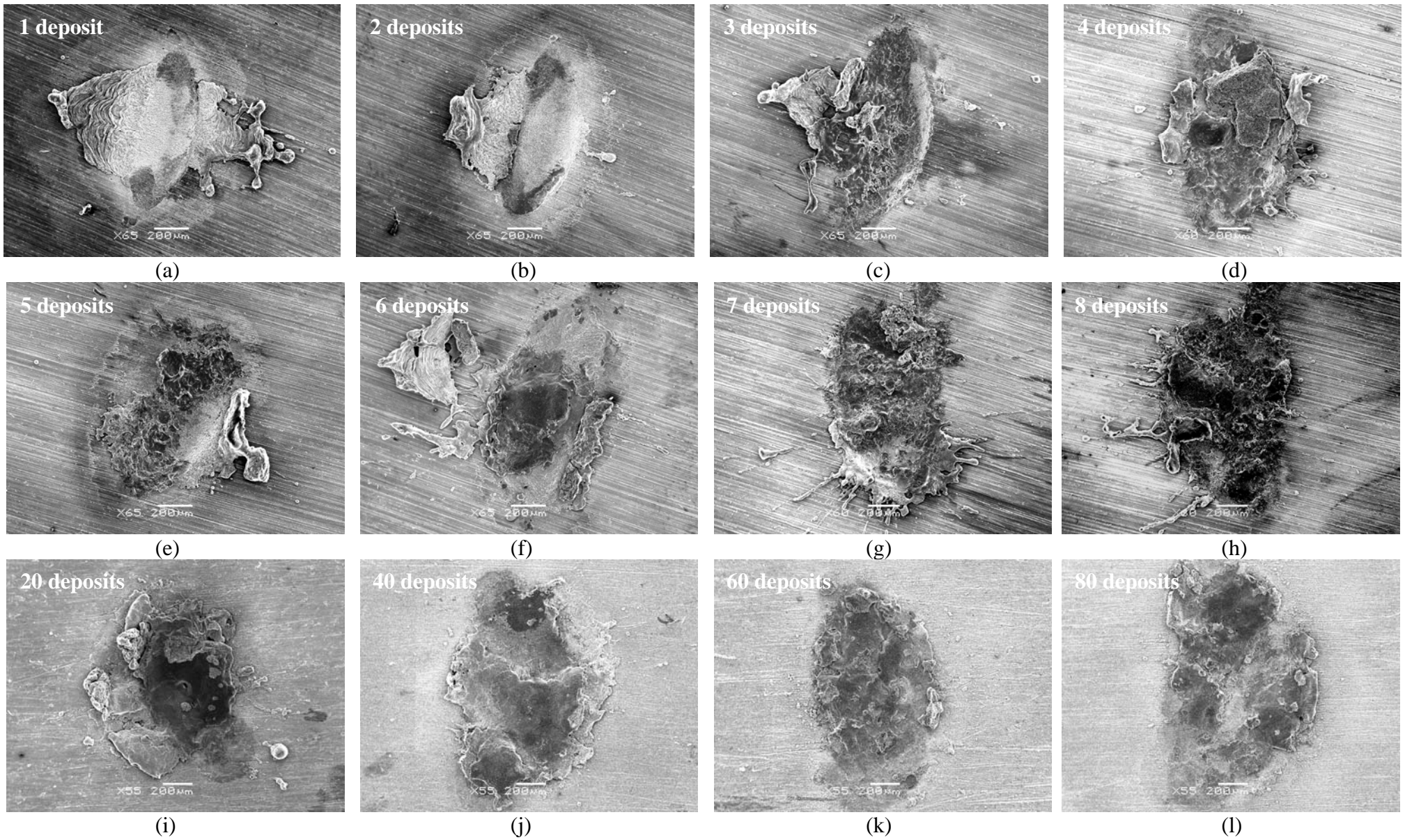
Figure 5.8: SEM micrograph of TiC$_p$/Ni coating after: a) 1, b) 2, c) 3, d) 4, e) 5, f) 6, g) 7, h) 8, i) 20, j) 40, k) 60, and l) 80 deposits.

66

| (a) – 3 deposits | (b) – 4 deposits |
| (c) – 6 deposits | (d) – 60 deposits |
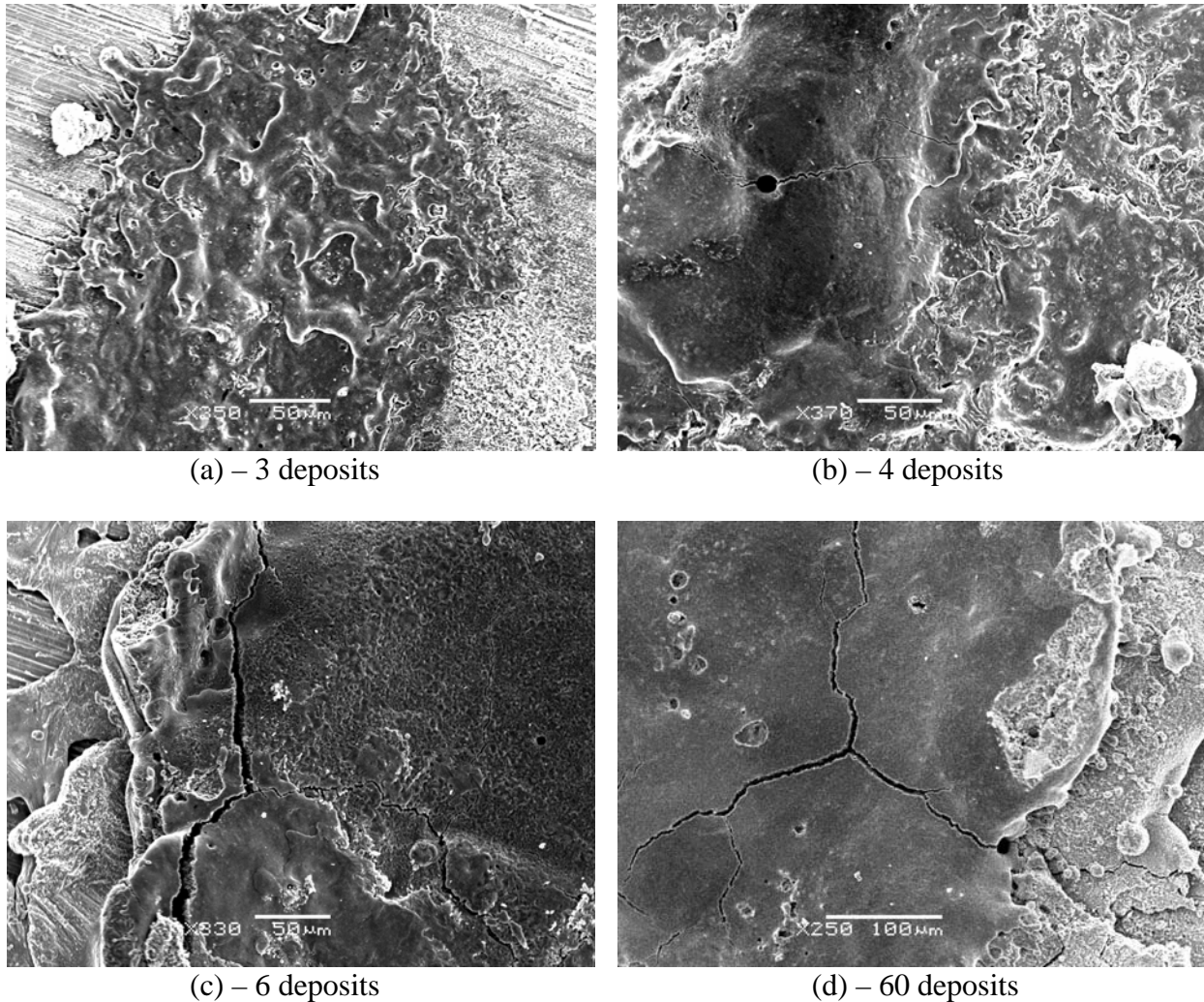
Figure 5.9: SEM micrograph of: a) 3, b) 4, c) 6, d) 60 deposits in higher magnification.

The change of the surface appearance of the coating during the deposition process was caused by the continuous surface melting and surface erosion of both the TiC_p/Ni electrode and the Cu substrate. After the first deposition, the TiC_p/Ni electrode was covered by a thin film of re-solidified TiC_p/Ni, and the deposition spot on the Cu substrate was covered by a thin layer of the mixture of Cu and TiC_p/Ni. As the deposition progressed, TiC_p/Ni was deposited on top of the pre-existing TiC_p/Ni coating. Since the surface erosion of the TiC_p/Ni electrode and coating build up were irregular as shown in Figure 5.10. Local protuberances of deposits are formed on both the depositing electrode and substrate surfaces. These protuberances on both surfaces will serve as the contact points for subsequent depositions [8] resulting in uneven distribution of TiC_p/Ni coating across the deposition spot.

In addition, cracking of the TiC_p/Ni coating was observed as the coating was built up. As mentioned earlier, the formation of cracks was caused by the thermal stress built-up [47]. During the deposition process, the molten TiC_p/Ni was deposited on to the Cu substrate. Since substrate was a greater heat sink due to the high thermal conductivity of copper, the molten TiC_p/Ni rapidly solidified and thus creating residual tensile thermal stress in the coating [47]. As the deposition progressed, the build up of the thermal stress caused more cracks to nucleate and to propagate within the brittle ceramic coating.

(a)   (b)
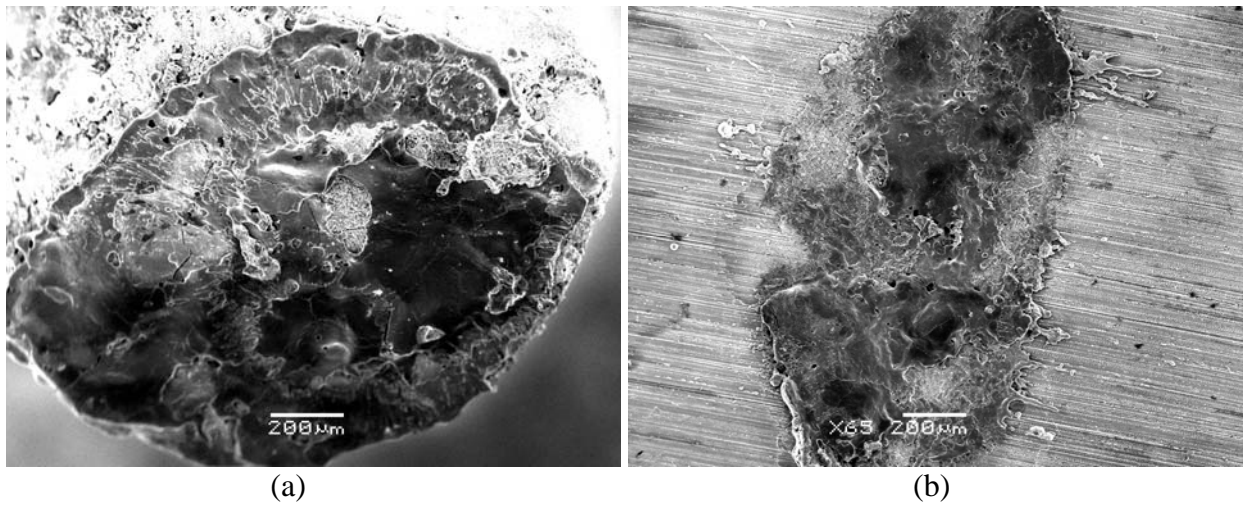
Figure 5.10: SEM micrograph of: a) TiC_p/Ni electrode after 10 deposits, b) TiC_p/Ni coating after 10 deposits.

To further the understanding of the coating formation by the ESD process, TiC_p/Ni and highly pure Ni coatings were also deposited on Ni and Cu substrates respectively. Scanning Electron Microscopy with Energy Dispersive Spectrometer (SEM/EDS) points scan and micro-X-ray Diffraction (XRD) analyses were performed to characterize the coating-substrate interface.
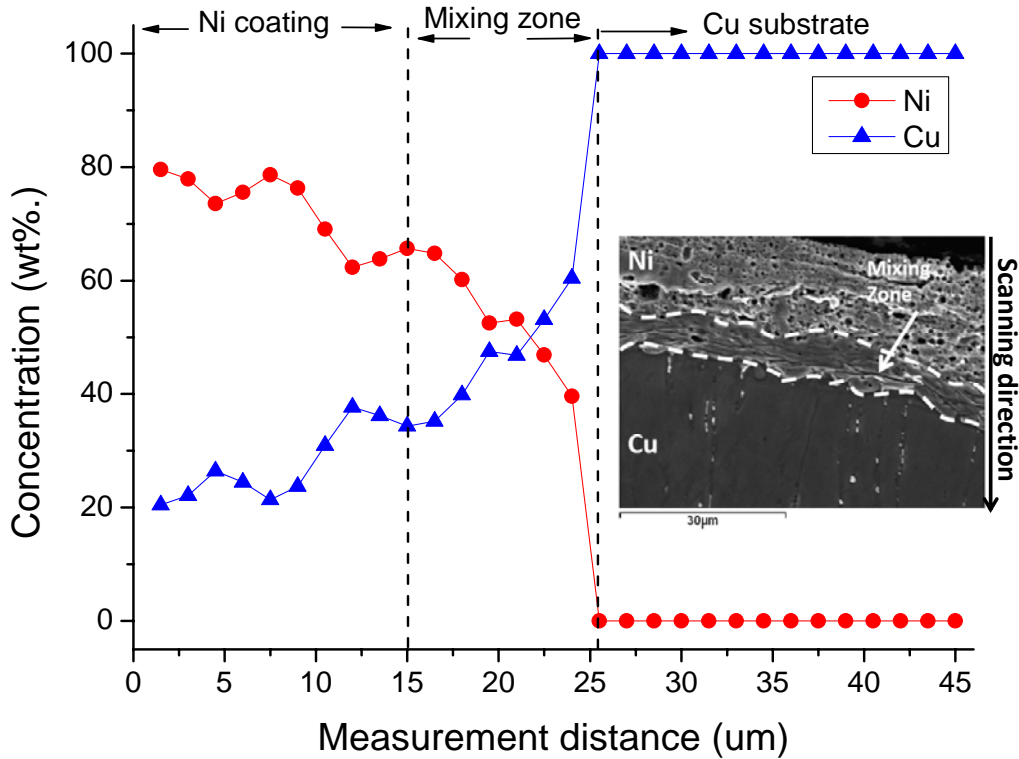
Figure 5.11: Concentration profile of ESD Ni coating on Cu substrate.

The concentration profile of the Ni coating on Cu substrate is presented on Figure 5.11. A strong and continuous interface was observed with the presence of the mixing zone between the Ni coating and Cu substrate. The molten Cu and Ni mixed together to form an intermixing layer during deposition process as predicted by the Cu-Ni binary phase diagram. As illustrated, the Cu mixed much further into the Ni coating than the diffusion of Ni into the Cu substrate. On the Ni coating side, the Cu content varied from 20 to 40 % wt with the Ni content made up the remaining percentage. No nickel was found in the Cu substrate. The formation of the mixing zone between the Ni coating and Cu substrate was the result of the rapid solidification of molten Ni and Cu during the ESD process. Since the Cu substrate was a greater thermal mass, the heat dissipated rapidly causing the molten Ni and Cu to quickly solidify. This result was similar that observed by Dogan *et al* [48], in their study of capacitor discharge of Al-Fe couple. In their study,

Dogan *et al* [48] believes that a mixing zone of Al and Fe formed at the joint interface due to rapid solidification.

Moreover, the Cu-Ni peaks were found on the x-ray diffraction (XRD) spectrum as shown on Figure 5.12, which indicated the Cu-Ni solid solution was formed during coating process. The Cu-Ni solid solution is formed by the intermixing of molten Cu and Ni. As illustrated on the Cu-Ni phase diagram, Cu and Ni are completely soluble to each other at all concentration [49]. The complete solubility of the Cu-Ni system is because of both Cu and Ni have the FCC crystal structure, similar atomic radii (0.128nm for Cu and 0.125nm for Ni respectively) and electronegativity (1.9 for Cu and 1.8 for Ni respectively), and finally the common in valences (+1 for Cu and +2 for Ni respectively) [49]. The presence of the Cu-Ni phase in the Ni coating evidenced the metallurgical bond between the coating and substrate. The metallurgical bonding is attributed to the formation of solid solution.
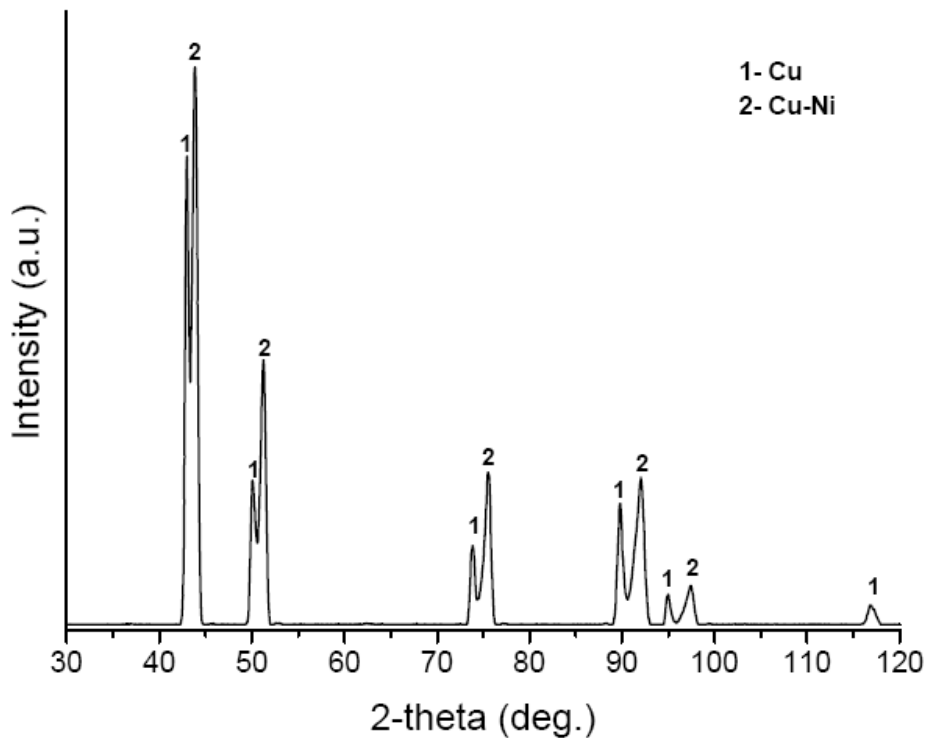
Figure 5.12: XRD pattern of Ni coating on Cu substrate.
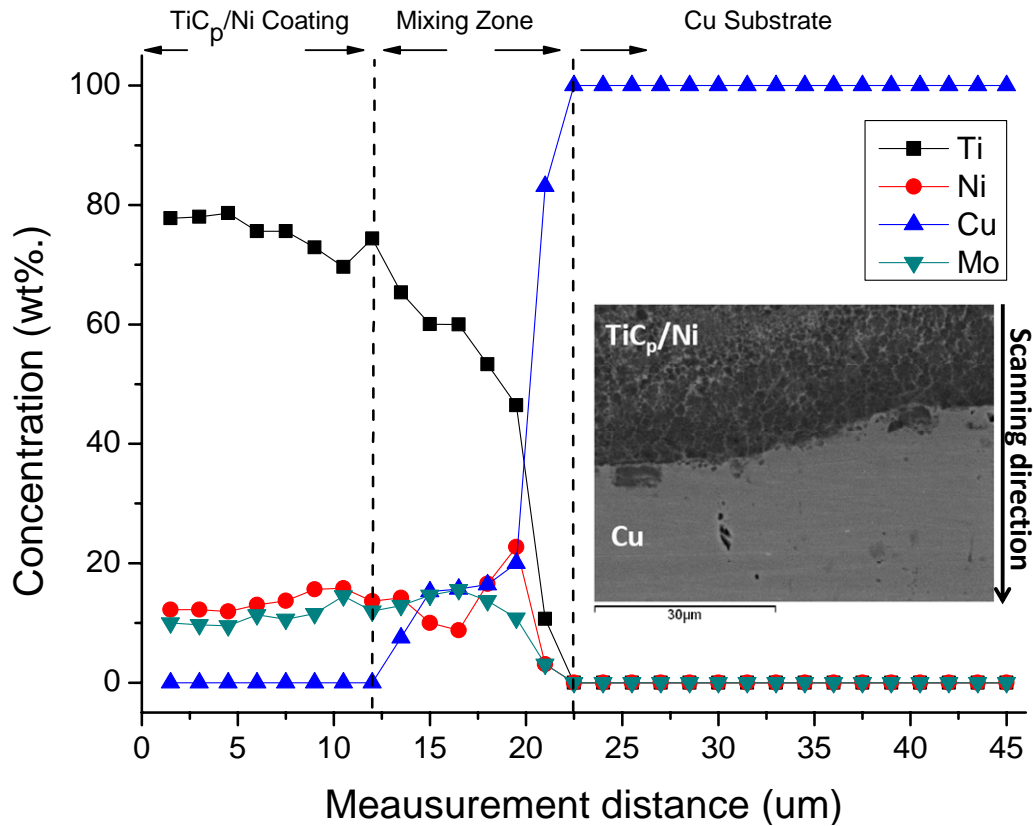
Figure 5.13: Concentration profile of ESD TiC_p/Ni coating on Cu substrate.

Based on the result of the ESD Ni coating on Cu substrate, it is expected that similar phenomenon will be observed for the TiC_p/Ni coating on Cu substrate. Although, an intermixing layer was not found and only a continuous bonded interface was observed between the TiC_p/Ni coating and Cu substrate. A mixing zone is found within the coating close to the bonded interface. As shown on Figure 5.13, the concentration profile of TiC_p/Ni coating on Cu substrate shows that the Ni content remained constant while the Cu content varied from 0 to 20 %wt within the coating close to the bonded interface. This evidence indicates the infiltration of molten Cu into the deposited layer. Note that both Ni and Ti content were not found in the Cu substrate, which is similar to the previous case. Moreover, the Mo content remained constant within the coating and the Ti content decreased from 80 wt-% to 50 wt-% within the transition zone.

TiC_p/Ni coating was deposited on the Ni substrate using the same apparatus and parameters as in the previous cases. From Figure 5.14, a continuous bonding interface was observed similar to the observation from the TiC_p/Ni coating on Cu substrate. In addition, significant amount of Ni from the Ni substrate was mixed in to the coating as the Ni content varied from 16 to 50 wt-%

71

within the mixing zone. The TiC_p/Ni depositing electrode was produced by liquid phase sintering process of TiC particles with Ni and Mo as the binders. The Mo additive is to enhance the wettability of Ni to TiC particles [9]. Since the Ni is used as the binding agent for TiC, it is not available to mix with the molten Cu during the coating process as in the case of Ni coating to Cu substrate.

The presence of Cu and Ni content within the TiC_p/Ni coatings near the bonded interface suggest that both Cu and Ni were mixed into the coating by capillary action during the ESD process as molten metal was more mobile in a metal – ceramic mixture [51]. There was a possibility of the formation of Cu – Ti and Ni – Ti intermetallic phases. In the XRD spectrum of Figure 5.15, the main constitutes of TiC_p/Ni coatings are Cu, Ni, and TiC and there are no peak of any intermetallic phase. Since TiC is the most thermodynamically stable phase in the coating [52], the mixing of Cu and Ni in the TiC/Ni coating is mostly mechanical.
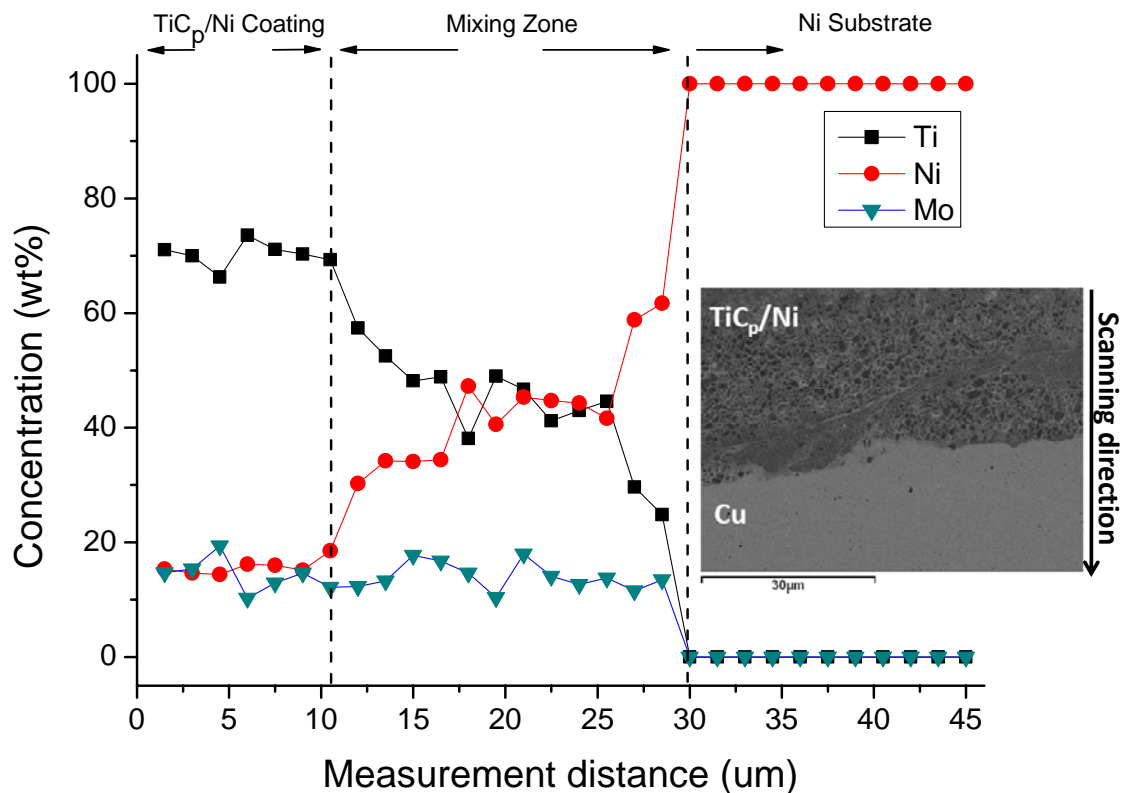
Figure 5.14: Concentration profile of ESD TiC_p/Ni coating on Ni substrate.

72
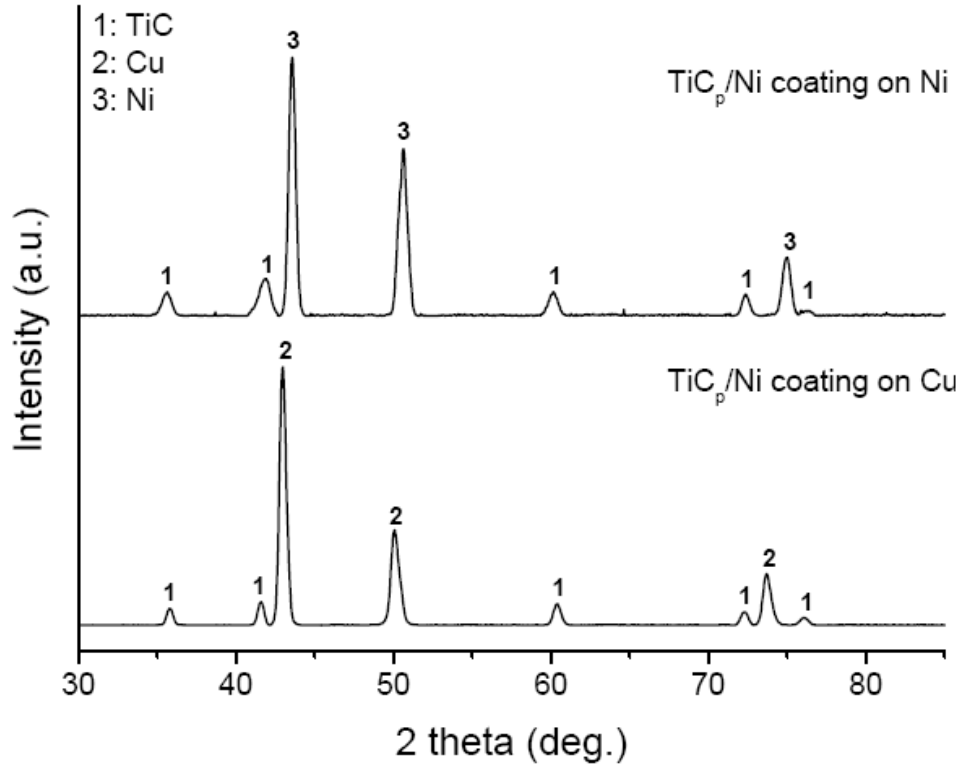
Figure 5.15: XRD pattern of TiC$_p$/Ni coating on Cu substrate and TiC$_p$/Ni coating on Ni substrate.

The continuous bonded interface found in the TiC$_p$/Ni electrode – Cu substrate and TiC$_p$/Ni electrode – Ni substrate systems can be attributed to the used of Cu and Ni as the binding agents to the TiC particles within the coating [52 – 54]. Agarwal et al [53 – 54] have shown that Cu is not a good binder for TiC due to its poor wettability while Ni is an excellent binder to TiC particles. The difference between Cu and Ni as the binding agents for ceramic compound can be explained by the wettability. Wettability of metal on ceramic compound is a function of the electron transfer between atoms of the metal and the compound [55]. Ogwu et al [56 – 57] have shown that the wetting phenomenon between the transition metals (group IV, V, and VI on the periodic table) and their compounds (i.e. borides and carbides) is depended on the unfilled d orbital configuration. An empirical rule was proposed for the choice of metal binders for transition metals based compounds based on the theoretical analysis and experimental results. In order to bind a transition metal or compound with an unfilled d^x shell, a transition metal binder with an unfilled d^y shell would be the most suitable if the following condition is satisfied [56 - 57]:

73

$$x + y = 11 \tag{5.5}$$

where x and y represent the number of electrons in the unfilled d shells.

In the present study, Cu has completely filled d shells with the configuration of $3d^{10}$ and the electron configuration of TiC is $3d^{2.27}$ as reported by Manninen *et al* [56]. Since the empirical rule of Equation 5.5 is not satisfied, Cu is a poor binder for TiC particles. In the case of TiC_p/Ni electrode and Ni substrate system, Ni has the unfilled d shells with the configuration of $3d^8$. This satisfies the empirical rule and as a result, there is good metallurgical bonding (see Figure 5.14). In addition, the theoretical analysis suggests that delamination or interfacial de-cohesion will occur between the TiC_p/Ni coating and Cu substrate since Cu is a poor binder for TiC. However, in the study of TiC_p/Ni coating on Cu substrate, a continuous bonded interface is observed. The variation between the theoretical analysis and the experimental observation can be explained by presence of Ni in the TiC_p/Ni depositing electrode. It is reported by Chrysanthou *et al* [52] and Lu *et al* [59] that the addition of Ni to TiC – Cu system will enhance the wettability of Cu to TiC particles. Thus, a continuous bonding interface was observed for the TiC_p/Ni electrode and Cu substrate.

5.3   Summary

In this Chapter, the effect of voltage on ESD coating, the evolution of ESD coating, and the ESD bonding mechanism have been studied and discussed. In the effect of voltage on ESD coating, the increase in applied voltage improved the surface cleanliness and led to stronger bonding interface. However, the increase in applied voltage will also lead to greater materials loss in the Cu substrate due to greater surface erosion. From the study of multi-single depositions on the same spot, the dense ESD coating is achieved by the build up of countless of single depositions that overlapped each other. Based on the experimental studies, the bonding mechanism of ESD process is material dependence. In the metal – metal system, a metallurgical bond is formed with the evidence of the intermixing layer between the coating and substrate. However, in the ceramic – metal system, the molten metal is mixed into the coating and served as the binding agent to the ceramic particles.

Chapter 6

6 Conclusions and Recommendations

In this chapter, major observations, results, conclusions and recommendations from the current study will be summarized.

6.1 Conclusions

6.1.1 Formation of ESD Single Deposition and Material Transfer

In this study, the formation of one coating deposition on the substrate and material transfer mechanism from the electrode to the substrate during ESD process were investigated. From the experimental observations, a phenomenological model was proposed to detail the events taken place during the ESD process as summarized below:

1) Once the electrode contacted substrate, an electrical spark was formed due to the extremely high current density at the local contact points. The spark melted both the substrate and the electrode.

2) The formation of the crater at the centre of the deposition spot was caused by outward expulsion of the molten substrate material. A very narrow gap was created between the TiC_p/Ni depositing electrode and the Cu substrate. At this stage, material transfer between the depositing electrode and the substrate did not occur.

3) Since the electrode continued to move forward, it came into contact with the substrate a second time. The material transfer between the depositing electrode and the substrate initiated during this second molten metal to molten metal contact. The thin film of molten TiC_p/Ni fused with the melting pool on the Cu substrate, and rapidly solidified to form a coating.

6.1.2 The Effects of Voltage on ESD Coating

The effects of voltage on ESD coating were examined by using single and multi-single depositions on the same location. Some key conclusions include:

1) The size and the depth of the crater increased with higher applied voltages. The high applied voltage would increase both the current density and the arc force. As a result, more of the substrate was melted and ejected away forming a larger deposition crater.

2) The higher applied voltages increased the amount of coating deposited on the substrate. However, it didn't necessarily improve the overall net efficiency of the ESD process. Increase in voltage would also increase the erosion rate of the substrate as more of the molten substrate material ejected away.

3) The ESD is a self-cleaning process as the surface contaminants and oxide layer were ejected away along with the molten substrate material. The increase in applied voltage led to the reduction in crack size at the coating and substrate interface. In fact, the increase in applied voltage improved the bonding between the coating and the substrate by effectively removing the surface contaminant.

6.1.3 ESD Coating Evolution

By having multi-single depositions on the same spot, the build-up of ESD coating was investigated. The major experimental observations and conclusions are:

1) The ESD coating was formed by the build-up from numerous single depositions. After the first deposition, the TiC_p/Ni electrode was covered by a thin film of re-solidified metal. Meanwhile, the crater on the Cu substrate contained a mixed layer of Cu and TiC_p/Ni. As the deposition progressed, TiC_p/Ni deposited on top of the pre-existing TiC_p/Ni coating.

2) The uneven distribution of TiC_p/Ni deposit across the deposition location was caused by the formation of protuberances on both the TiC_p/Ni depositing electrode and disposition surface. These protuberances served as the contact points for subsequent depositions.

The ESD coating bonding interface was investigated by using 3 different material combinations of the coating and substrate material. The material combinations were Ni electrode – Cu substrate, TiC_p/Ni electrode and Ni substrate and TiC_p/Ni electrode and Cu substrate. The major observations and conclusions are:

1) In the Ni electrode – Cu substrate system, the SEM observations and the XRD patterns showed a metallurgical bond between the deposited coating and the substrate. As predicted by the Cu-Ni phase diagram, an intermixing layer of Ni – Cu solid solution was clearly observed.

2) In TiC_p/Ni – Cu and TiC_p/Ni – Ni combinations, there was no intermixing layer between the coating and the substrate. From the XRD pattern, there was no evidence of intermetallic phases. The SEM/EDS analysis showed the mixing of substrate material into the coating. As a result, in these systems, both Cu and Ni were behaved as the binding agent with the TiC ceramic particles.

3) From the present study, the metallurgical bonding between the coating and the substrate is the bonding mechanism of the ESD process. The formation of the metallurgical bond is attributed to either the formation of intermixing layer/solid solution or the usage of substrate material as the binding agent to the depositing material.

6.2 Recommendations

In the present study, the temperature of the TiC_p/Ni electrode increased during consecutive depositions. Preliminary study has found that the amount of depositing material increased as the temperature of the electrode increased. As a result, the temperature build up during the deposition process should be studied to decipher the influences of temperature of depositing electrode on ESD process.

In addition, the effect of percentage of deposition spot overlapping should be studied. Since cracks between the coating and substrate are originated from the edge of the crater. This is where the expelled molten materials along with the contaminants are collected. As a result, by overlapping the deposition spot might help eliminating cracking between the coating and substrate.

References

[1]   M.R. Finlay. "Resistance Spot Welding of Metallic Coated Steels and PVD Coated Electrodes." CRC Australia and WTIA, CRC No. 18, 1996.

[2]   R. Holiday, J.D. Parker, N.T. Williams. "Relative contribution of electrode tip growth mechanism in spot welding zinc coated steels." Welding in the world 37 (1996) pp. 186-193

[3]   Z. Chen, and Y. Zhou, "Surface modification of resistance welding electrode by electro-spark deposited composite coatings: Part II. Metallurgical behavior during welding," Surf. Coat. Technol., 2006, 201, 2419-2430

[4]   Welding Handbook, Vol. 3, 9th ed., American Welding Society, Miami, FL, 2007 pp. 367 – 419.

[5]   Rointan F. Bunshah, "Handbook of Deposition Technologies for Films and Coatings 2nd Edition." Noyes Publications, 1994, pp. 131 – 163.

[6]   K.R. Chan, N. Scotchmer, J. Zhao, and Y. Zhou. "Weldability Improvement Using Coated Electrodes for RSW of HDG Steel." SAE international, 2006

[7]   Z. Chen, and Y. Zhou, "Surface modification of resistance welding electrode by electro-spark deposited composite coatings: Part I. Coating characterization," Surf. Coat. Technol., 2006, 201, 1503-1510

[8]   R.N. Johnson and G.L. Sheldon. "Advances in the electrospark deposition coating process." J. Vac. Sci. Technol. A 4 (6): 2740 – 2746

[9]   ASM handbook – Powder Metal Technologies and Applications, Vol. 7, 10th ed., ASM Int'l, Materials Park, OH, 1993, pp. 978

[10] Welding Handbook, Vol. 3, 9th ed., American Welding Society, Miami, FL, 2007 pp. 598 – 602.

[11] N.C. Welsh, "Frictional Heating and its Influence on the Wear of Steel," J. Appl. Phys. 28, 960 (1957)

[12] N.C. Welsh, "Surface Hardening of Non-ferrous Metals by Spark Discharge," Nature 181, 1004 (1958)

[13] N.C. Welsh, "Spark Hardening of Metals," J. Inst. Met. 88, 103 (1959)

[14] N.C. Welsh and P.E. Watts, "The Wear Resistance of Spark Hardened Surface," Wear 5, 189 (1962)

[15] N.C. Welsh and P.E. Watts, "Spark Hardening of Cutting Tools: Austenite Formation and Edge Erosion," J. Iron and Steel Inst. London 198, 30 (1961)

[16] B.R. Lazarenko and N.I. Lazarenko, Electric Erosion of Materials (Gasenergoizdat, Moscow/Leningrad, 1944), No. 1

[17] A.U. Polyachenko, New methods of Electrical Working of Materials (Mashgiz, Moscow, 1955), p.352

[18] Reynolds, J.L., R. L. Holdren and L. E. Brown., "Electro-Spark Deposition," Advanced Materials and Process 161 no3. March 2003

[19] R.N. Johnson, "ElectroSpark Deposition: Principles and Applications," 45th Annual Technical Conference Proceedings (2002), Society of Vacuum Coaters, 87 – 92

[20] S.W. Banovic, J.N. DuPont, and A.R. Marder, "Iron Aluminide Weld Overlay Coatings for Bolier Tube Protection in Coal-Fried Low No_x Boilers," Proc. 11th Ann. Conf. on Fossil Energy Materials, CONF-9705115, US-DOE, p. 279, 1997

[21] C.A. Schuh, T.G. Nieh and T. Yamasaki, "Hall-Petch breakdown manifested in abrasive wear resistance of nanocrystalline nickel," Scripta Materialia, Vol 46 (10), May 2002, 735 – 740

[22] I.V. Galinov and R. B. Luban, "Mass Transfer Trends during Electro-spark Alloy," Surf. Coat. Technol., 1996, 79, 9-18

[23] R.J. Wang, Y.Y. Qian, and J. Liu, "Structural and interfacial analysis of WC92-Co8 coating deposited on titanium alloy by electrospark deposition," Applied Surface Science 228 (2004) 405 – 409

[24] A. Lesnjak, and J. Tusek, Processes and properties of deposits in electrospark deposition, Science and Technology of Welding and Joining, 7, 6, 2002, 391-396.

[25] Welding Handbook, Vol.2 , 8th ed., American Welding Society, Miami, FL, 1991 pp. 110-155.

[26] J. Liu, R. Wang, and Y. Qian, "Formation of a single-pulse electrospark deposition spot." Surface and Coatings Technology, 200, 2005, 2433-2437.

[27] R.N. Johnson, "Coatings for Fast Breeder Reactor Components," Thin Solid Films, 118, (1), p. 31, 1984

[28] R.N. Johnson, "Alternative Coatings for Wear and Corrosion: the Electrospark Deposition Process," Proc. AESF Conf. for Environmental Excellence. January 2002.

[29] P.Z. Wang, G.S. Pan, Y. Zhou, J.X. Qu, and H.S. Shao, "Accelerated Electrospark Deposition and the Wear Behavior of Coatings," Journal of Materials Engineering and Performance, 6 (6): 780-784 (1997)

[30] R. Wang, Y. Qian, and J. Liu, Interface behavior study of WC92-Co8 coating produced by electrospark deposition, Applied Surface Science, 240, 2005, 42-47.

[31] R.D. Wilson and J. A. Hawk. "Rapid Solidification Joining using the Capacitor Discharge Welding Process." 1994

[32] J.W. Simmons and R.D. Wilson. "Joining of High-Nitrogen Stainless Steel by Capacitor Discharge Welding." Welding Journal 185 – 190; June 1996

[33] R.D. Wilson, J.R. Woodyard, Sr., And J. H. Devletian. "Capacitor Discharge Welding: Analysis through Ultrahigh-Speed Photography." Welding Journal 101-106; March 1993.

[34] B.K. Paul, D.D. Wilson, E.McDowell, and J. Benjarattananon, " Study of weld strength variability for capacitor discharge welding process automation." Science and Technology of welding and joining 2001 vol. 6 no. 2 109-115

[35] J.F. Lancaster, "The Physics of welding." Pergamon Press,. 1984

[36] Welding Handbook, Vol. 3, 9th ed., American Welding Society, Miami, FL, 2007 pp. 74 – 105.

[37] K.N. Petry et al., "Principles and practices in contact welding." Welding Journal 49(2): 117-126; February 1970

[38] W.F. Savage, "Flash welding: the process and application." Welding Journal 41 (3): 227-237; March 1962

[39] J.F. Sullivan, and W.F. Savage, "Effect of phase control during flashing on flash weld defects." Welding Journal 50(5): 213s-221s; May 1971.

[40] K. Cumings, P. W. Laws, E. F. Redish, and P.J. Cooney, Understanding Physics: Capacitance, 799 – 829; John Wiley & Sons, Inc. 2004

[41] T.D. Burleigh and T.W Eagar, "Measurement of the Force Exerted by a Welding Arc," Metall. Trans A, 14 (1983), 1223-1224

[42] A.E. Gitlevich, V.V. Mikhailov, N.Y. Parkansky and V.M. Revutsky, Electrospark Alloying of the Metallic Surfaces, Stiinca, Kishinev, 1985, 196pp.

[43] G.V. Samsonov, A.D. Verkhoturov, G.A. Bovkun and V.S. Sichev, Electrospark Alloying of the Metallic Surfaces, Naukova Dumka, Kiev, 1985, 219pp.

[44] G.A. Krasiuk, Investigation of the powders – electrospark treatment erosion products, Electrospark Treatment of Metals, Academy of Sciences Publication, Moscow, 1963, pp. 126-132.

[45] K.K. Namitokov, Electroerosion Phenomena, Energiya, Moscow, 1978, 456pp.

[46] N. Parkansky, I.I. Beilis, L. Rapoport, R.L. Boxman, S. Goldsmith, and Yu. Rosenberg, "Electrode erosion and coating properties in pulsed air arc deposition of WC-based hard alloys," Surf. Coat. Technol., 105 (1998) 130-134

[47] N. Parkansky, R.L. Boxman, S. Goldsmith, Surf. Coat. Technol. 61 (1993) 268

[48] C.P. Dogan, R.D. Wilson, and J.A. Hawk., "CD Weld Interfacial Structure for Al-Fe Based Couples." Mat. Res. Soc. Symp. Proc. Vol. 314. (1993) pp. 169-175

[49] ASM handbook – Alloy Phase Diagrams, Vol. 3, 10th ed., ASM Int'l, Materials Park, OH, 1993

[50] W.D. Callister, "Fundamentals of Materials Science and Engineering", John Wiley and Sons Ltd, 2004

[51] J. T. Klomp, Designing interfaces for technological applications: ceramic-ceramic and ceramic-metal joining, 127-144; 1989, New York, NY, Elsevier Applied Science

[52] L. Lu, J.Y.H. Fuh, Z.D. Chen, C.C. Leong, Y.S. Wong, Mater, Res, Bull. 35 (2000) 1555.

[53] A. Agarwal, N.B. Dahotre, T.S. Sudarshan, Surf. Eng. 15 (1999) 27.

[54] A. Agarwal, N.B, Dahotre, Mater. Charact. 42 (1999) 31.

[55] G. V. Samsonov, "Surface phenomena in melts and powder metallurgy processes" (Izd-vo AN UkrSSR, Kiev,1960) p. 60.

[56] A.A. Ogwu, T.J, Davies, Mater. Sci. Technol. 9 (1993) 213

[57] A.A. Ogwu, T.J, Davies, Scr. Mater. 40 (1999) 1377

[58] S. Manninen, and T. Paakkari, Bonding in titanium carbide: I. Experimental electron momentum distributions in polycrystalline Ti and TiC, J. Phys. C: Solid State Phys., Vol. 9, 1976.

[59] A. Chrysanthou, and G. Erbaccio, Enhancing the dispersion of TiC in copper, Journal of Materials Science Letters 15 (1996) 774 – 775.

Appendix A

DAQ Programming for ESD Process

In this section, the LabView 8.5 graphical programming that was used to collect during the ESD process and the description to the programming are presented.

LabView Programming

The following graphical programming illustrates how the current, voltage, and displacement data are collected during the ESD process.

1. Two analog channgles are created to to collect current and voltage data, and one digital channel is created to collect displacement data.
2. A count down clock is set to let the user to preapre for the deposition.
3. A sample clock is set to adjust the sampling rate of the DAQ box.
4. The program will start collecting data upon completion of countdown.
5. All data will be converted to appropiate format and outputed as a graph.
6. Meanwhile, the data is written and saved to a text file.

OK message + warnings

Saved Waveform File Name

Write To
Measurement
File

Signals
Comment
Enable
error in (no error)
File Name

Destination Waveform File Name

Path

Displacement

8.   9.

86

Displacement
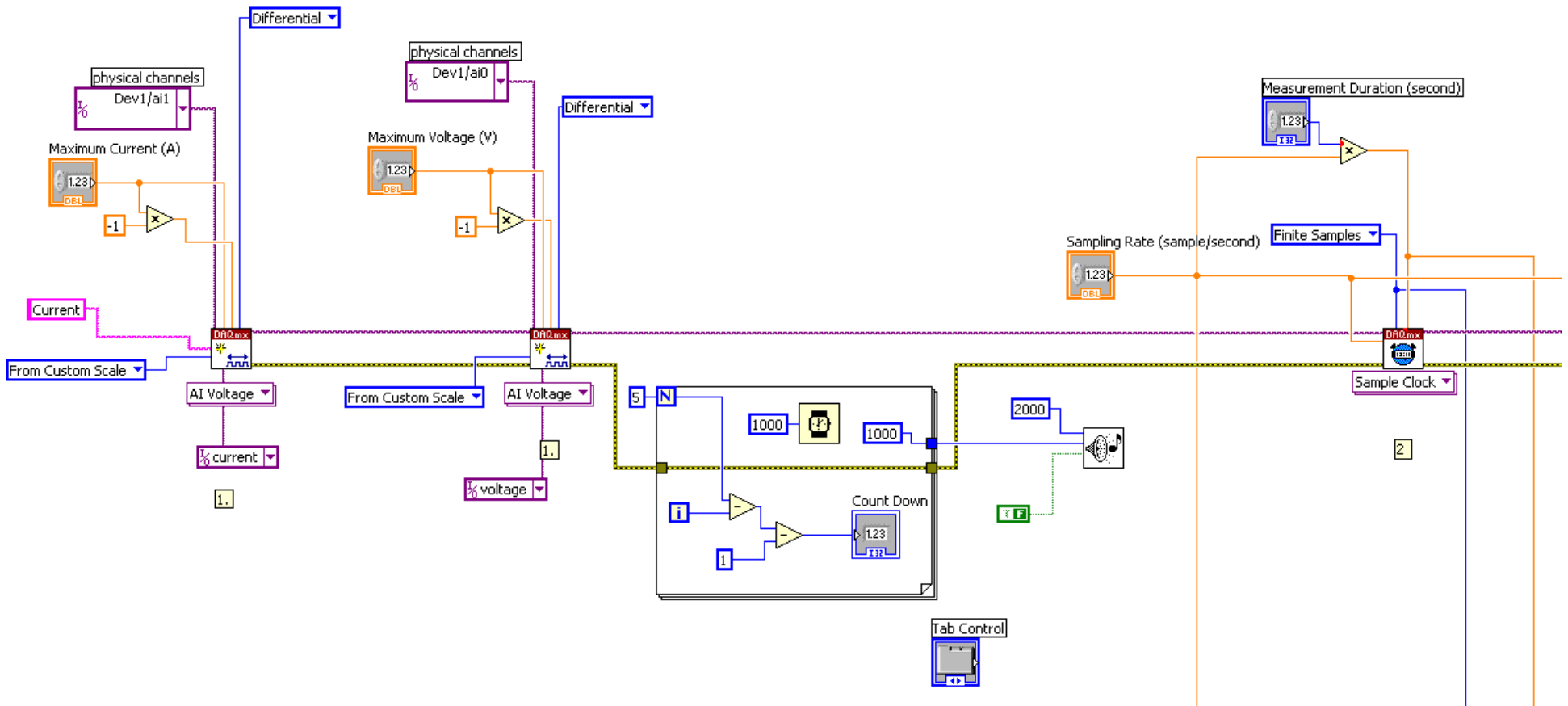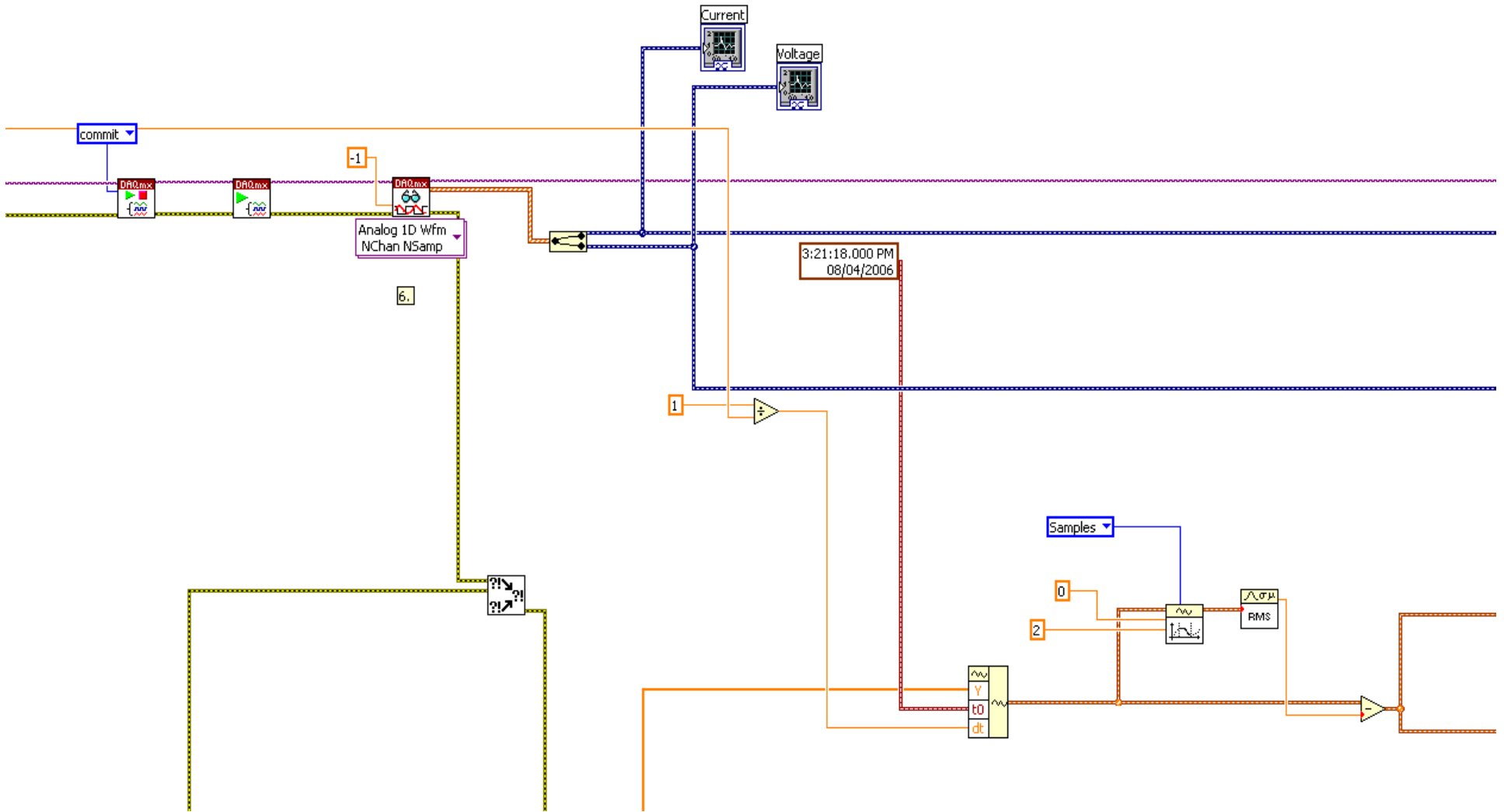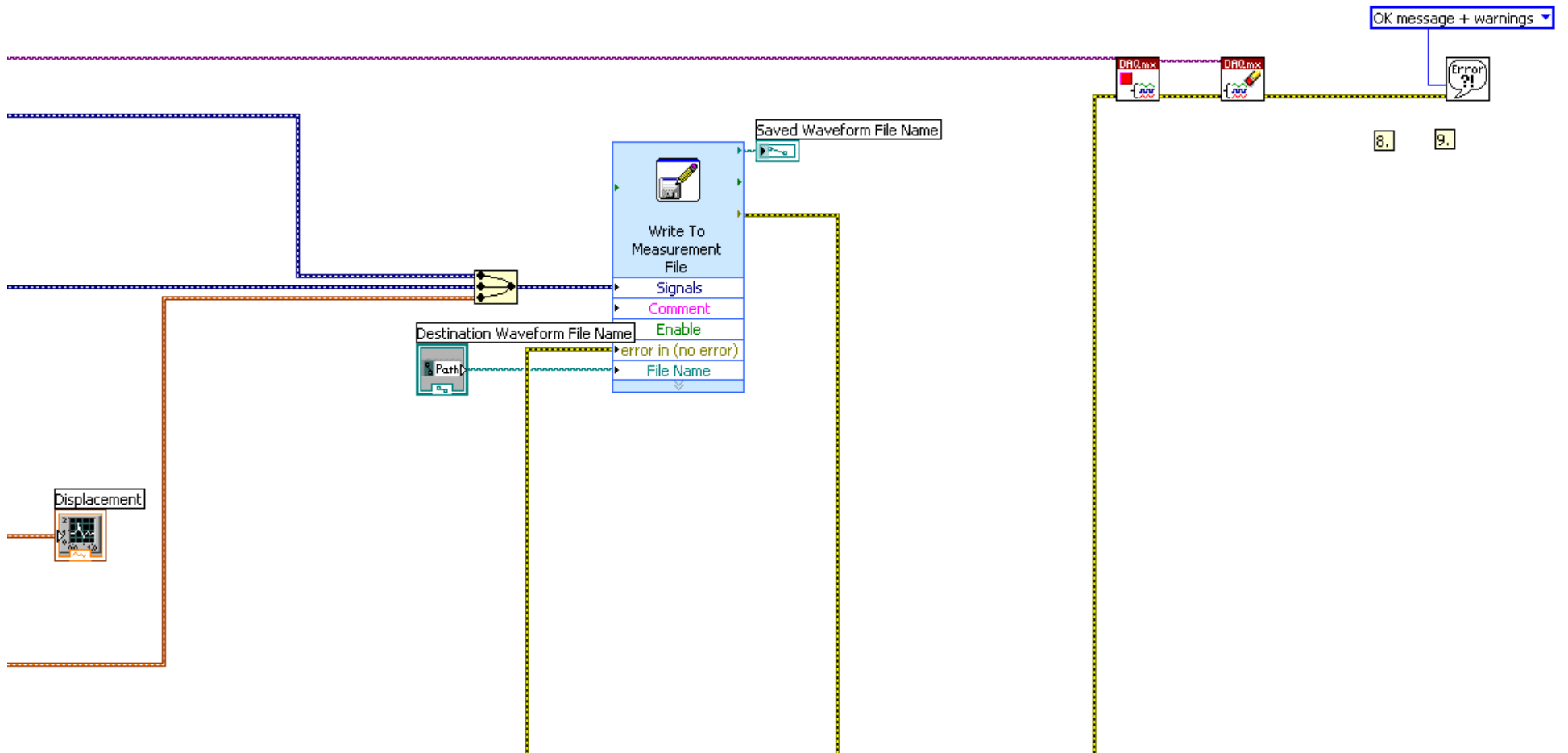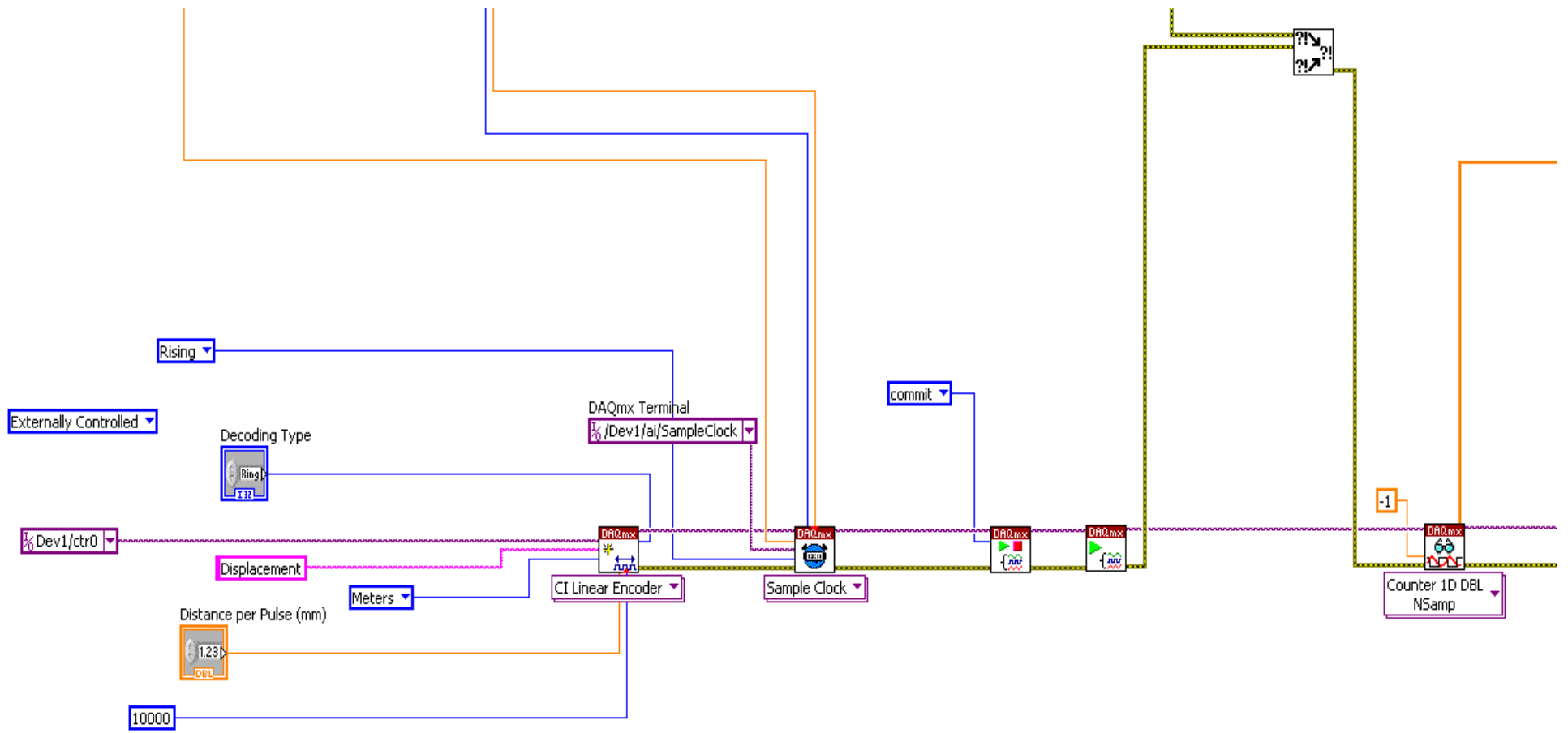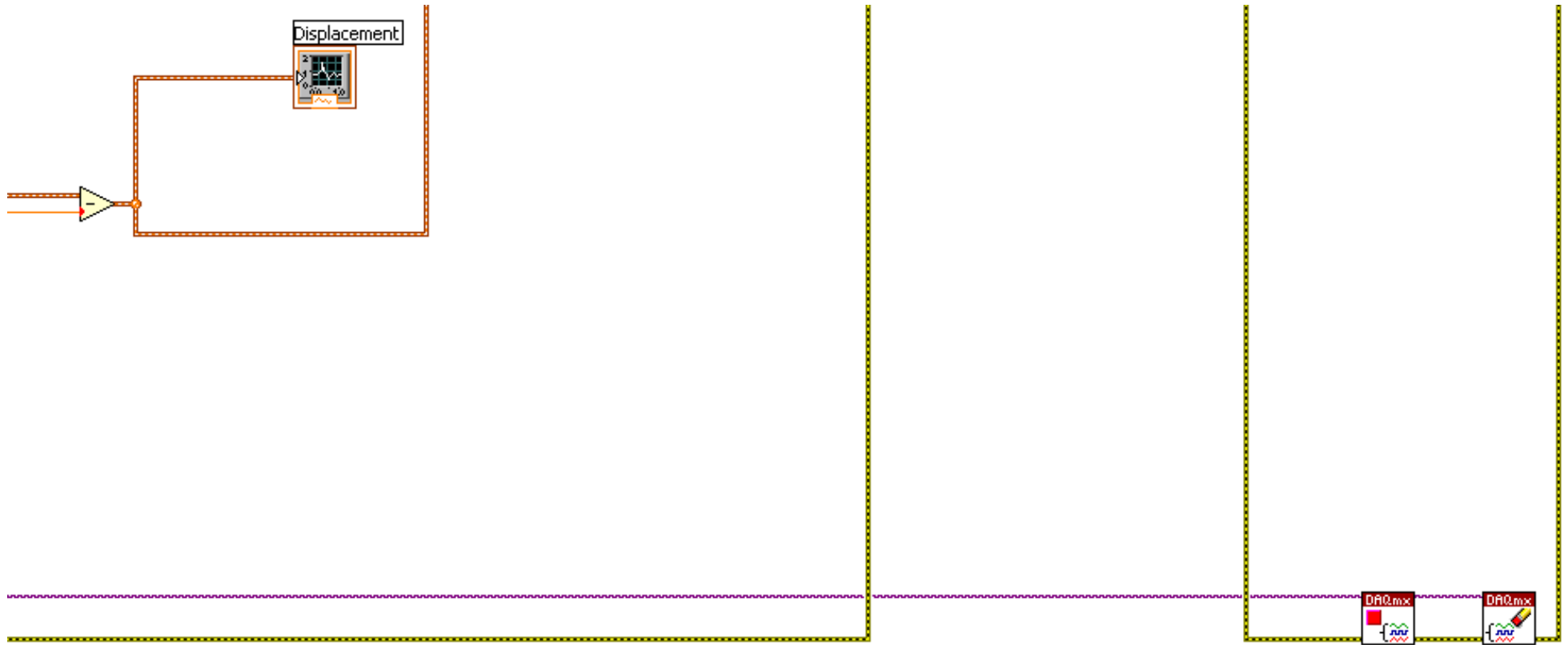
Appendix B

Experimental Data

This section presents the data obtained from the weight quantification study on TiC/Ni electrode and Cu substrate. Experiments were conducted on four different voltage settings, 25V, 35V, 45V, and 65V. In addition, 20, 40, 60, 80, and 100 multi deposits were performed at each of the voltage settings, and the result are shown as follow.

TiC$_p$/Ni Electrode Weight Loss

Table A.1: TiC$_p$/Ni electrode weight loss at 25V

No. of deposits	Before (mg)	After (mg)	Net (mg)	Average	Standard deviation
20	2172.29	2172.06	0.23		
20	2172.5	2172.05	0.45		
20	2172.11	2172.05	0.06	**0.247**	**0.196**
40	1422.53	1422.44	0.09		
40	2173.03	2172.65	0.38		
40	2172.65	2172.18	0.47	**0.313**	**0.199**
60	2172.88	2172.73	0.15		
60	2172.73	2172.05	0.68		
60	2172.57	2172.29	0.28	**0.370**	**0.276**
80	1422.97	1422.53	0.44		
80	1423.26	1423.07	0.19		
80	1423.07	1422.53	0.54	**0.390**	**0.180**
100	1424.09	1423.81	0.28		
100	1423.81	1423.34	0.47		
100	1423.34	1422.97	0.37	**0.373**	**0.095**

Table A.2: TiC$_p$/Ni electrode weight loss at 35V

No. of deposits	Before (mg)	After (mg)	Net (mg)	Average	Standard deviation
20	979.52	979.08	0.44		
20	979.08	978.75	0.33		
20	978.75	978.49	0.26	**0.343**	**0.091**
40	1627.7	1627.3	0.4		
40	1627.5	1627.02	0.48		
40	1627.02	1626.67	0.35	**0.410**	**0.066**
60	1425.39	1424.92	0.47		
60	1424.92	1424.58	0.34		
60	1424.58	1424.06	0.52	**0.443**	**0.093**
80	1446.98	1446.19	0.79		
80	1446.19	1445.6	0.59		
80	1445.6	1445.06	0.54	**0.640**	**0.132**
100	1427.63	1427.01	0.62		
100	1427.01	1426.45	0.56		
100	1426.45	1425.69	0.76	**0.647**	**0.103**

Table A.3: TiC$_p$/Ni weight loss at 45V

No. of deposits	Before (mg)	After (mg)	Net (mg)	Average	Standard deviation
20	2173.95	2173.65	0.3		
20	2173.65	2173.38	0.27		
20	2173.38	2172.97	0.41	**0.327**	**0.074**
40	2178.12	2177.53	0.59		
40	2177.53	2176.62	0.91		
40	2176.62	2175.93	0.69	**0.730**	**0.164**
60	2274.43	2273.63	0.8		
60	2273.63	2272.75	0.88		
60	2272.75	2272.06	0.69	**0.790**	**0.095**
80	2129	2128.07	0.93		
80	2128.37	2127.08	1.29		
80	2126.98	2125.85	1.13	**1.117**	**0.180**
100	2200.72	2199.4	1.32		
100	2199.4	2198.12	1.28		
100	2198.12	2197.04	1.08	**1.227**	**0.129**

Table A.4: TiC$_p$/Ni electrode weight loss at 65V

No. of deposits	Before (mg)	After (mg)	Net (mg)	Average	Standard deviation
20	1431.34	1430.84	0.5		
20	1430.84	1430.6	0.24		
20	1429.6	1429.26	0.34	**0.360**	**0.131**
40	1433.15	1432.45	0.7		
40	1432.45	1431.91	0.54		
40	1431.91	1431.34	0.57	**0.603**	**0.085**
60	1435.74	1434.81	0.93		
60	1434.81	1434.15	0.66		
60	1434.15	1433.15	1	**0.863**	**0.180**
80	1439.8	1438.57	1.23		
80	1438.57	1437.04	1.53		
80	1437.04	1435.74	1.3	**1.353**	**0.157**
100	1445.12	1443.9	1.22		
100	1442.9	1441.15	1.75		
100	1441.15	1439.8	1.35	**1.440**	**0.276**

Cu Substrate Weight Gain

Table A.5: Cu substrate weight gain at 25V

No. of deposits	Before (mg)	After (mg)	Net (mg)	Average	Standard deviation
20	642.45	642.56	0.11		
20	619.36	619.46	0.1		
20	681.59	681.77	0.18	**0.130**	**0.044**
40	648.51	648.69	0.18		
40	644.05	644.25	0.2		
40	669.84	669.98	0.14	**0.173**	**0.031**
60	613.9	614.15	0.25		
60	705.9	706.06	0.16		
60	653.32	653.69	0.37	**0.260**	**0.105**
80	655.29	655.63	0.34		
80	683.18	683.47	0.29		
80	641.45	641.69	0.24	**0.290**	**0.050**
100	670.67	670.92	0.25		
100	696.91	697.18	0.27		
100	627.15	627.53	0.38	**0.300**	**0.070**

Table A.6: Cu substrate weight gain at 35V

No. of deposits	Before (mg)	After (mg)	Net (mg)	Average	Standard deviation
20	423.38	423.58	0.2		
20	438.02	438.12	0.1		
20	432.08	432.21	0.13	**0.143**	**0.051**
40	422.1	422.23	0.13		
40	439.48	439.56	0.08		
40	445.25	445.48	0.23	**0.147**	**0.076**
60	437.3	437.58	0.28		
60	440.46	440.61	0.15		
60	425.73	425.94	0.21	**0.213**	**0.065**
80	831.06	831.24	0.18		
80	905.19	905.53	0.34		
80	876.5	876.86	0.36	**0.293**	**0.099**
100	977.59	977.74	0.15		
100	899.45	899.77	0.32		
100	962.46	962.86	0.4	**0.290**	**0.128**

Table A.7: Cu substrate weight gain at 45V

No. of deposits	Before (mg)	After (mg)	Net (mg)	Average	Standard deviation
20	679.39	679.52	0.13		
20	633.96	634.18	0.22		
20	662.71	662.94	0.23	**0.193**	**0.055**
40	617.08	617.53	0.45		
40	694.17	694.31	0.14		
40	699.37	699.72	0.35	**0.313**	**0.158**
60	662.63	663.16	0.53		
60	706.85	707.26	0.41		
60	696.45	696.89	0.44	**0.460**	**0.062**
80	669.22	670.13	0.91		
80	677.13	677.73	0.6		
80	684.39	685.28	0.89	**0.800**	**0.173**
100	673.42	674.24	0.82		
100	676.48	677.45	0.97		
100	664.61	665.51	0.9	**0.897**	**0.075**

Table A.8: Cu substrate weight gain at 65V

No. of deposits	Before (mg)	After (mg)	Net (mg)	Average	Standard deviation
20	700.98	701.15	0.17		
20	628.57	628.63	0.06		
20	653.93	654.32	0.39	**0.207**	**0.168**
40	666.71	667.02	0.31		
40	676.86	677.06	0.2		
40	659.5	659.84	0.34	**0.283**	**0.074**
60	712.8	713.26	0.46		
60	668.3	668.73	0.43		
60	712.31	712.9	0.59	**0.493**	**0.085**
80	718.7	719.35	0.65		
80	698.13	698.72	0.59		
80	642.02	642.69	0.67	**0.637**	**0.042**
100	653.43	654.18	0.75		
100	667.6	668.76	1.16		
100	668.98	669.72	0.74	**0.883**	**0.240**